OF MICHIGAN
JAN 31 1957
ENGINEERING LIBRARY

Engin
QC
151
.J86
v. 1
no. 2

JOURNAL OF FLUID MECHANICS

VOLUME 1 PART 2

JULY 1956

Printed and Published by

TAYLOR & FRANCIS LTD

RED LION COURT, FLEET STREET, LONDON, E.C.4

The JOURNAL OF FLUID MECHANICS exists for the publication of theoretical and experimental investigations of all aspects of the mechanics of fluids, and is issued in six parts per volume.

Editor:

Dr. G. K. BATCHELOR, Cavendish Laboratory, University of Cambridge, Cambridge, England.

Assistant Editors:

Dr. T. B. BENJAMIN, Dr. I. PROUDMAN.

Associate Editors:

Prof. G. F. CARRIER, Pierce Hall, Harvard University, Cambridge 38, Massachusetts, U.S.A.

Prof. W. C. GRIFFITH, Palmer Physical Laboratory, Princeton University, Princeton, New Jersey, U.S.A.

Prof. M. J. LIGHTHILL, Department of Mathematics, The University, Manchester, England.

Authors wishing to have papers published in the JOURNAL should communicate them to any one of the persons named above, choosing one in their own country where possible.

Authors are urged to ensure that their papers are written clearly and attractively, in order that their work will be readily accessible to readers.

Manuscripts should be typed in double spacing on one side of the paper only, with references listed at the end in alphabetical order of authors. Drawings should be done on a large scale in Indian ink on tracing cloth or drawing paper, captions being typed on a separate sheet. Proofs of papers from overseas will usually be despatched to authors by airmail. Authors are entitled to receive 50 offprints of a paper in the JOURNAL free of charge, and additional offprints can be purchased from the publisher.

PRICE £1 ($3.00) per part

Subscription, £5 10s. 0d. per volume of six parts, post free ($16.50 in U.S.A. and Canada)

Agents for U.S.A. and Canada:

Academic Press Inc., 125 East 23rd Street, New York 10, N.Y., U.S.A.

JOURNAL OF FLUID MECHANICS
Volume 1, Part 2 July 1956

CONTENTS

Experiments on two-dimensional flow over a normal wall
by MIKIO ARIE and HUNTER ROUSE 129

The displacement effect of a sphere in a two-dimensional shear flow
by I. M. HALL 142

The refraction of sea waves in shallow water
by M. S. LONGUET-HIGGINS 163

On steady laminar flow with closed streamlines at large Reynolds number
by G. K. BATCHELOR 177

The law of the wake in the turbulent boundary layer
by DONALD COLES 191

On the flow in channels when rigid obstacles are placed in the stream
by T. BROOKE BENJAMIN 227

Experiments on two-dimensional flow over a normal wall

By MIKIO ARIE
Faculty of Engineering, Hokkaido University

and HUNTER ROUSE
Iowa Institute of Hydraulic Research, State University of Iowa

(*Received 3 January* 1956)

SUMMARY

Measurements of the velocity, pressure, and turbulence behind a series of normal plates in the uniform test section of an air tunnel are described, the oscillation of the wake being prevented in all but one test through use of symmetrically located tail plates. By a combination of experimental and computational techniques, details of the pattern of flow over a wall on a plane boundary in an infinite fluid are closely approximated. A significant difference is indicated between the characteristics of such a flow and those of the flow past an isolated plate with oscillating wake.

INTRODUCTION

For want of experimental information about the characteristics of flow past a sufficiently great variety of boundary shapes, one is forced either to perform specific tests upon each body design that comes into question, or to estimate the expected characteristics from what is known about flow past the individual elements of which the body consists. Under some conditions the latter method is quite effective; often the purely qualitative indication that it provides is far better than none at all, and sometimes the combination of available data with mathematical analysis permits the indication to be of quantitative value as well. Under other conditions the information at hand is merely sufficient to throw serious doubt upon even the qualitative value of such a procedure.

A case in point is the utilization of experimental data for two-dimensional flow past a cylindrical body to predict the conditions of motion that would prevail if a boundary were to exist at the plane of symmetry. Assume, for example, that it was desired to estimate the force exerted by the wind upon a wall, or the effectiveness of such a wall in either shielding something behind it or in promoting the diffusion of some substance in its wake. Drag coefficients and eddy patterns are well known for rectangular plates (Fage & Johansen 1927, Goldstein 1938) but it is also known (Roshko 1955) that interference with an oscillating wake is likely to change the primary nature

of the flow. Just how great this change might be in any particular case can be determined as yet only by experiment.

Whereas the wake behind an immersed body is of basic importance in such professions as aeronautics, ballistics, and marine engineering, it is the wake behind a boundary irregularity, such as the wall, that is of primary interest in hydraulics. Whether the wall typifies roughness elements or part of an orifice or valve makes little difference; and the standing eddy in its wake also has much in common with those which form at any abrupt changes in conduit section. Yet so little is known about their geometrical proportions, about the dynamics of the mean flow within them, and about the generation of turbulence along their borders, that the experimental analysis of such standing eddies has received the attention of the Iowa Institute of Hydraulic Research for nearly a decade. The most recent in this series of investigations has been a study of the wake behind a simple wall (Arie 1955), the purpose of the present paper being to make generally available the most essential of the results.

Flow past a plate that is fully surrounded by fluid differs in several ways from flow past one that is in contact with a continuous boundary. First of all, the former may be considered to lie in the path of essentially irrotational flow, whereas the latter will be immersed in a boundary layer of indefinite thickness. Secondly, as has already been noted, the flow in the wake of an isolated plate is free to oscillate about the plane of symmetry, whereas such oscillation is wholly prevented in the vicinity of a rigid longitudinal boundary. Now the lateral freedom or restraint of the wake marks a dynamically basic distinction between the two cases, whereas the boundary layer is a secondary factor that is not determined by local conditions. Hence, in the experiments under discussion, boundary layer development both upstream and downstream was obviated by placing the plate at the axis, rather than at the floor, of an air tunnel, the lateral boundary restraint at the rear being effected by means of a tail plate which was only slightly longer than the standing eddy.

Whether a plate fully surrounded by the fluid or one in contact with a boundary is simulated in a tunnel, the presence of the test section floor and ceiling will introduce an additional threefold effect. First, these surfaces will correspond geometrically to planes of symmetry between the given plate and standing eddy, on the one hand, and their first images in a series having a finite lateral spacing, on the other; the velocity of the surrounding field being increased thereby. Second, there will be an additional augmentation of velocity as a result of the development of the boundary layer along the tunnel surfaces. Finally, despite the use of a foreshortened downstream boundary, the conversion of energy in the wake of the test plate will produce something akin to a boundary layer effect, which will cause the velocity of the flow outside the wake to become still higher than it would be in an infinite fluid.

Three courses were thus open to the investigator. The pattern of flow could be determined as a function of the relative spacing of a series of plates,

with the double aim of permitting extrapolation to the infinite case and of providing supplementary information about flow between opposite walls in a passage of finite size. Secondly, by means of various experimental artifices, an effort could be made to simulate the infinite case itself without recourse to extrapolation. Finally, the data obtained for any spacing could be recomputed for infinite spacing by means of an analytical approximation. In actuality, these three courses were followed in sequence, the first serving as a guide to the partial refinements of the second, and the final correction proceeding analytically.

Experimental procedure

The air tunnel used for the experiments in question was of the closed circuit type, with a uniform test section 3 feet high, 3 feet wide, and 10 feet long. Air speeds could be varied at will from 10 to 50 feet per second, but for ease in measurement all tests were made in the upper part of this range. The main air speed was indicated by the change in pressure at the bell entrance to the test section; the corresponding pressure-velocity relationship had been determined through test-section traverses with a Prandtl-type Pitot tube, which in turn had been calibrated in the irrotational core of a jet from a 6-inch rounded orifice. No effort was made to reduce the turbulence of the flow, beyond the use of vanes at the turns and a fourfold reduction in cross-sectional area between the plenum chamber and the test section; the root-mean-square velocity fluctuation was about $1\frac{1}{2}\%$ of the mean velocity of flow.

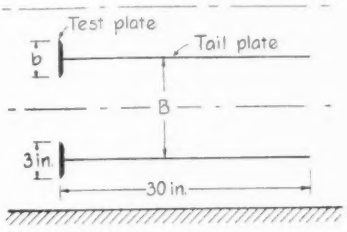

Figure 1. Definition sketch of plate arrangement.

All test plates were introduced into the tunnel approximately midway between the ends of the test section, completely spanning its 3-foot width. They were invariably 3 inches in effective height, 1/4 inch in thickness, and bevelled at an angle of 60° along the edges on the rear side. All but one were of tempered hardboard, the one being of carefully machined brass. Each was guyed with piano wire, at its one-third points, to the floor and ceiling of the tunnel to maintain its alignment and eliminate all possibility of vibration. The tail plates (see figure 1), which were of 1/16-inch sheet aluminium, were attached to the test plates at mid-height, and likewise guyed in place. They extended a distance of 30 inches to the rear, which

had been found by observation to be longer than the eddy by a sufficient amount for the size of the latter to be unaffected by a further lengthening of of the plate. By successively introducing dummy plate assemblies at planes of symmetry on either side of the centrally located test plate, the ratio B/b of spacing to width could be varied through the consecutive values of 12, 6, 3, etc.

Because of the two-dimensional nature of the flow, it was possible to make measurements of the magnitude and direction of the mean velocity at any point by means of one of two alternative Pitot cylinders. Each was constructed of 1/8-inch brass tubing mounted horizontally on a fork-shaped support with bearings 6 inches on centre. One cylinder contained a 0·015-inch hole on each side of a central plug (see figure 2), the two portions

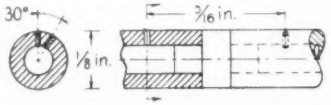

Figure 2. Pitot-cylinder details.

of the tube having been rotated differentially about their common axis till the holes lay at an angle of 30° to each other in the normal plane. A protractor at either bearing permitted the common angular position of the holes to be read to within about 0·2°. The other cylinder differed from the first only in the angle—now 180°—between the holes. After careful calibration of each cylinder, the magnitude of the velocity could be computed from the differential pressure between the respective holes, the 180° cylinder being oriented to yield the maximum reading, and the 30° cylinder being turned so that first one and then the other hole lay directly upstream (in the latter instance the direction of the flow was first determined by noting the angle at which the differential reading was exactly zero). The 30° cylinder was used so long as the velocity gradient was not excessive; since, in zones of high gradient, this cylinder was subject to a pronounced error in both direction and magnitude of the velocity, the 180° cylinder was then employed, and the direction determined by successive steps in plotting the streamlines.

In the zones in which both the inclination and the magnitude of the velocity vector were directly measurable, it was a simple matter to determine and plot, from vertical traverses with the 30° cylinder, the distribution of the longitudinal component of velocity over a series of normal sections. Graphical calculations of the areas $\psi = \int u\,dy$ enclosed by these curves (figure 3), as a function of distance normal to the tail plate, then permitted successive streamlines $\psi = C$ to be located for any selected increment $\Delta\psi$. In those zones for which only the magnitude of the velocity could be measured, this was first assumed to be indicative of the longitudinal component. Evaluation of the streamline location according to the foregoing

method yielded the inclination of the velocity vectors as a first approximation, and a second approximation was usually sufficient to determine the flow pattern with acceptable precision. Figure 4 shows the pattern obtained from the single run made without tail plate for purposes of reference.

This method of determining the flow pattern was followed for $B\ b$ equal to 12 and to 6 without undue experimental difficulty. All attempts to repeat the measurements for $B\ b$ equal to 3 met with no success, however,

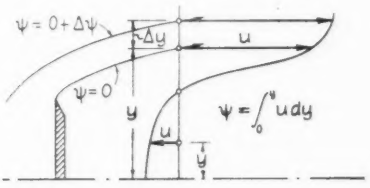

Figure 3. Determination of streamline location.

as the pattern was then not only unsymmetrical about the axis of any plate but unstable as well. This situation is in approximate accord with previous experience, flow through lattice screens being known to become unstable as the solidity ratio approaches the magnitude 0·5. For this reason, no attempt was made to carry the study any farther in the direction of decreasing spacing, which meant that a sufficient number of cases to

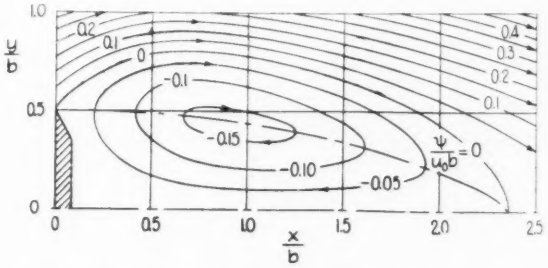

Figure 4. Approximate pattern of mean streamlines for flow without tail plate $B/b = 12$.

permit extrapolation to greater spacing could not thus be realized. A different tack was hence followed in approximating the desired conditions of infinite spacing.

Since the profile of the standing eddy behind the test plate was roughly elliptical in form (figure 5), it was assumed that the streamlines at a considerable distance would approximate those of potential flow past either an ellipse or a Rankine oval of comparable dimensions. The latter being somewhat easier to describe mathematically, the location and strength of

the source and sink were determined so as to yield a profile coinciding most closely with the measured eddy profile for $B/b = 12$. The resulting stream function had the form

$$\psi = -yu_0 + 0{\cdot}56bu_0\left[\tan^{-1}\frac{y}{x-3{\cdot}4b} - \tan^{-1}\frac{y}{x+3{\cdot}4b}\right],$$

the profile of the oval corresponding to $\psi = 0$. From this relationship it was possible to evaluate the coordinates of any desired streamline in the vicinity of the test-section wall; the maximum deviation of the streamline at the approximate lateral distance of 1·5 feet was found to be about 1·5 inches. Because of the boundary layer development along these walls, however, a still further change in their shape would be necessary to eliminate this additional wall effect. The displacement thickness of the boundary layer as a function of distance along this tunnel was hence evaluated by a combination of velocity measurement with extrapolation, in accordance with known boundary layer relationships; its entire variation was found to be slightly less than 1·4 inch over the 10-foot length of test section. False boundaries of hardboard were then introduced along the ceiling and floor of the test section; they were curved according to the stream function of the eddy profile, flared by an amount equal to the displacement thickness of the boundary layer, and smoothly joined to the bell entrance of the test section.

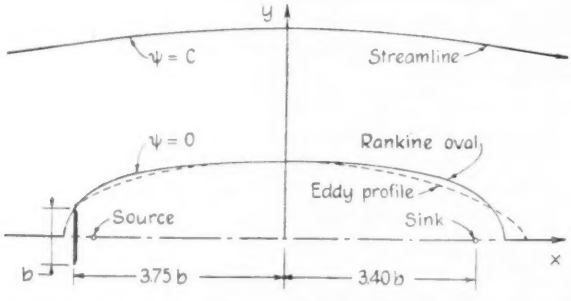

Figure 5. Derivation of stream function for Rankine oval having proportions of standing eddy.

With the falsework in position, the velocity distribution over successive vertical sections throughout the eddy region was again measured with the Pitot cylinder. In addition to such velocity traverses, measurements were also made of the pressure distribution at the same sections, and of the pressure over the faces of the test plate and tail plate. Pressure measurements at the plates themselves required simply the introduction of piezometer orifices along the one side, the velocity measurements being restricted to the same side in order to avoid the disturbing effect of the piezometer connections on the other. The pressure traverses in a plane normal to the two plates involved the use of a third plate, 1/8 inch thick, 5 inches wide (in the

longitudinal direction), and about 18 inches high, sharply bevelled on the leading edge, and having a series of piezometer orifices on one side in a vertical row, which could be placed at any section. Finally, measurements were made with the constant-temperature type of hot-wire anemometer (Hubbard 1954) at the same vertical sections, the wires and circuit being so arranged as to yield the root-mean-square values of the three components of fluctuation and the cross product of the components in the plane normal to the two test plates.

Analysis of measured data

Had the revision in tunnel profile actually been sufficient to simulate infinite-fluid conditions, the experimental results would have yielded directly the patterns of velocity, pressure, and turbulence produced by flow over a normal wall. However, it will be recalled that the boundary profile was determined on the assumption of irrotational flow around a Rankine oval, whereas flow over a wall—though it may be essentially irrotational at the outset—departs from this state more and more with distance downstream, as a result of the pronounced shear and generation of turbulence at the border of the standing eddy. In other words, although a fairly successful effort had been made to compensate for the presence of the eddy and the development of the boundary layer on the tunnel walls, there remained uncompensated the effect of the wake of the plate itself, the importance of which was not at once appreciated. Finally, rather than modify the tunnel profile and repeat the measurements a second time, it was decided to determine by analytical means the magnitude of the corrections still required.

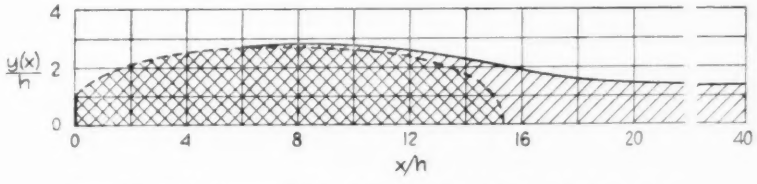

Figure 6. Displacement effect of standing eddy and turbulent wake.

With reference to figure 6 (in which the wall height h is introduced as reference length), the total effect of the wall upon the surrounding flow could be considered equivalent to that of the combination of the Rankine body (shown by double cross-hatching) with an additional tail section (shown by single cross-hatching) corresponding to the displacement thickness of the flow in the wake. The total thickness of the combination was assumed to be given to a first approximation by

$$\delta^* = \int_0^{\delta} \frac{u - u_{\max}}{u_{\max}} dy,$$

the quantity δ representing the value of y, just outside the wake, at which the velocity becomes a maximum.

Just as the profile of the eddy was simulated by the combination of a source and a sink with a uniform flow, the composite profile of the eddy and the tail section (or the profile of either one alone) could be realized by a distribution of sources and sinks, or, more conveniently, by a distribution of doublets (a method analogous to that of Landweber 1951), in place of the single source and sink of the Rankine body. For the case of an infinite fluid the stream function would then have the form

$$\psi = -yu_0 - \int_a^\infty \frac{m(t)\,y}{(x-t)^2+y^2}\,dt,$$

in which $m(t)$ is the doublet strength per unit length as a function of distance t along the line of symmetry and a is the abscissa of the initial point of the distribution which will yield the desired profile for the condition $\psi = 0$. For the case of flow that is confined between parallel walls (i.e., for a series of similar bodies) with the spacing B, on the other hand, the stream function would have to be written as

$$\psi = -yu_0 + \frac{\pi}{B}\int_a^\infty \frac{m(t)\sin 2\pi y/B}{\cosh 2\pi(x-t)/B - \cos 2\pi y/B}\,dt,$$

the doublets being distributed symmetrically along a series of parallel axes midway between the walls.

Because the tunnel boundaries in the present experiments were formed according to the approximate stream function of the eddy alone, the differences between the velocity distributions indicated by the proper space derivatives of these two equations must be due almost entirely to the tail section or wake. Evaluation of the difference, in the form of an approximate correction factor, hence depended upon determination of the doublet distribution $m(t)$ for the tail section alone. Fortunately, the elements shown in figure 6 were sufficiently slender for a considerable simplification (again by analogy with the method of Landweber (1951)) to be made. Thus, upon replacing $m(t)$ by $m(x)$ with $\psi = 0$ in the stream function for the infinite fluid, it could be shown that, with acceptable accuracy,

$$m(x) = -u_0 y(x)\left[\tfrac{1}{2}\pi + \tan^{-1}\frac{x-a}{y}\right]^{-1}.$$

The computed distribution of $m(x)$ for the tail section (and as well for the composite profile, with a value of a that would yield a satisfactory approximation in the vicinity of the plate) was that shown in figure 7. Use of the values indicated by the full curve thus permitted calculation of the factor by which the measured velocity outside the wake should be reduced to correspond with that of the infinite case. (Use of the composite values, it should be noted, will lead to an approximate stream function for the infinite case.)

The magnitude of the resulting corrections may be judged from figure 8 ***a***, in which are superposed the longitudinal components of the measured velocities (the points themselves) and the corrected values (the distribution

curves) at every other measured section. Also shown are the streamlines determined from the corrected distribution curves in the region of the eddy. From these it will be seen that it was actually of little moment whether or not the correction (based upon the assumption of irrotational flow) was made in the rotational region, where the velocity was already quite low. As a matter of fact, the velocity correction was so small in all zones as to have almost no effect upon the flow pattern itself. Its effect upon the pressure distribution, on the other hand, was considerable.

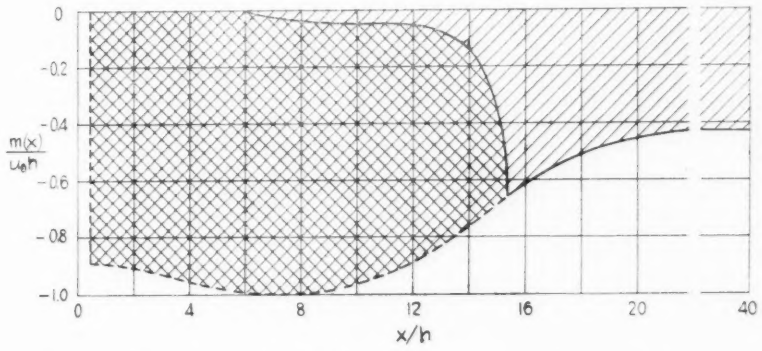

Figure 7. Distribution of doublet strength for eddy and wake displacement of figure 6.

Figure 8 *b* reproduces the actual measurements of the pressure intensity as points and the corrected values as continuous curves plotted to the left of the respective sections (i.e., negatively). Once again the correction was strictly applicable only outside the wake, for it was based upon the assumption of irrotational flow and constancy of the sum $\frac{1}{2}\rho(u^2+v^2)+p$. Unlike the velocity correction, however, that of the pressure could by no means be ignored within the wake, since there it was evidently a maximum. For want of a more precise method of estimating it, the customary boundary layer assumption of negligible pressure change over the distance δ had to be made; in other words, the correction at any point in the eddy was assumed to be the same as that just outside at the same cross-section. That the probable error in this assumption was small may be concluded from the fact that the measurements themselves varied only slightly across the eddy.

With the corrected magnitudes of the velocity and pressure at hand throughout the zone in question, it was a simple matter to compute and plot the distribution of total pressure (i.e., as would be read at the stagnation opening of a Pitot tube) relative to that in the ambient fluid, which is also shown in figure 8 *b*. Comparison of this sequence of curves with the locus of points of maximum velocity will indicate that the latter corresponds rather closely to the approximate limit of the zone of irrotational flow.

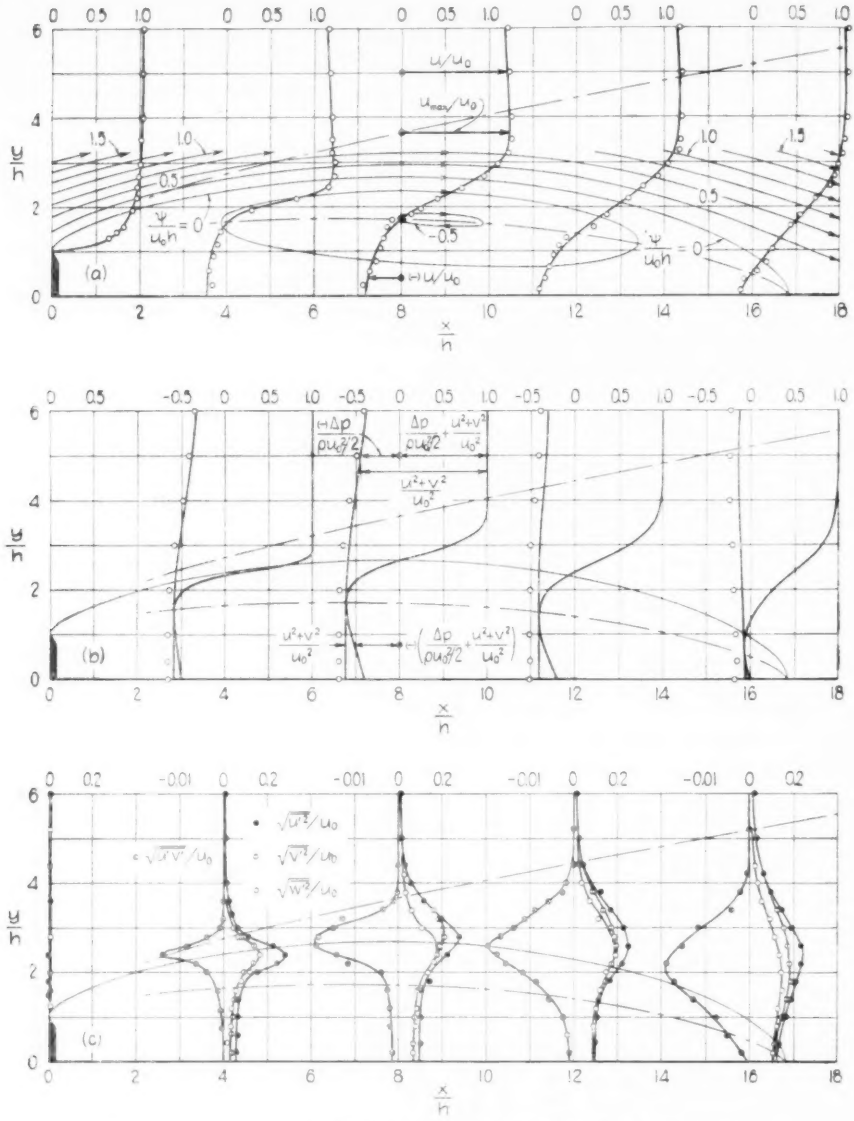

Figure 8. Experimental data and corrected distributions of (*a*) velocity, (*b*) pressure, and (*c*) turbulence, behind test plate.

The summary plots in figure 8*c* of the three components of the turbulent velocity and of the cross product of the two components in the plane of motion (obviously uncorrected for the wake effect) quite logically show

the region of maximum turbulence and maximum shear to coincide at the outset with the mean streamline dividing the main flow from that in the zone of separation, remaining at about twice the wall height as the eddy terminates. Were data for additional characteristics of the turbulence at hand—in particular, the microscale—it would be readily possible to trace the transformation of the energy of the primary or mean flow through its secondary or turbulent stage to its final dissipation as heat (Hsu 1950). For the present, it must suffice to note that in the zone of maximum turbulence level the energy of the secondary motion is some 15% of that of the primary

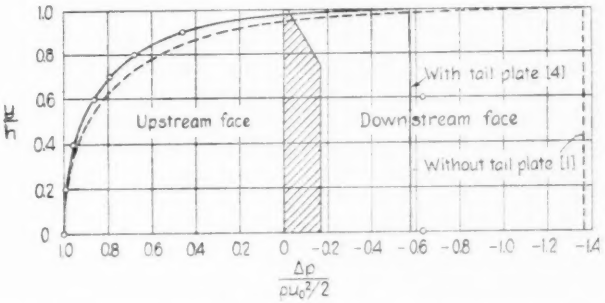

Figure 9. Distribution of pressure on test plate, with and without tail plate.

There remains to be considered here only the evaluation of the force F exerted by the flow upon the wall. From the direct measurements plotted in figure 9, the integral of the variable intensity on the front and the corrected constant intensity on the rear yields for the drag coefficient the magnitude

$$C_D = \frac{F/hL}{\frac{1}{2}\rho u_0^2} = 1{\cdot}38.$$

That this value is in accord with the change in flow pattern that the plate produced was demonstrated by evaluating the momentum equation

$$\int_0^\infty \left(1 - \frac{u^2}{u_0^2}\right) d\left(\frac{y}{h}\right) + \int_0^\infty \frac{p_0 - p}{\rho u_0^2}\, d\left(\frac{y}{h}\right) - \int_0^\infty \frac{\overline{u'^2}}{u_0^2}\, d\left(\frac{y}{h}\right) + \\ + \frac{\nu}{u_0 h} \int_0^\infty \frac{\partial(u/u_0)}{\partial(x/h)}\, d\left(\frac{y}{h}\right) = \frac{F/hL}{\rho u_0^2} = \tfrac{1}{2} C_D$$

between a section far upstream (i.e. where $u\ u_0 = 1$) and an arbitrary section downstream. For the latter the section $x\ h = 4$ was chosen, and the integration was carried out to—in lieu of infinity— the limit $y\ h = 100$ (extrapolation beyond the zone of measurement being facilitated by use of the stream function based upon the distribution of $m(t)$ for the composite profile plotted in figure 7). The successive integrals were found to have

the values $-2{\cdot}29$, $3{\cdot}04$, $0{\cdot}05$, and $0{\cdot}00$, respectively, with the result that $C_D = 1{\cdot}40$, which, as a residual value, is in unexpectedly good agreement with $1{\cdot}38$.

Interpretation of results

One must conclude from this investigation that the use of measurements made on isolated cylindrical bodies to approximate conditions in which the wake is not free to oscillate can result in rather large errors. The actual drag coefficient of the wall ($C_D = 1{\cdot}4$), for example, is only two-thirds that of the isolated plate ($C_D = 2{\cdot}1$), and the relative pressure change Δp $\frac{1}{2}\rho v_0^2$ behind the wall ($-0{\cdot}57$) is less than half the mean value ($-1{\cdot}36$) behind the plate. That this corresponds to a considerable difference in the length of the mean eddy zone (in accordance with the Riabouchinsky and related theories (Birkhoff 1950) that the free-streamline curvature must increase to produce a pressure decrease in a wake or cavity) is verified by the comparative measurements made in the course of the present study, the standing eddy behind the wall being more than three times as long ($l/h = 17$) as the homologous portion of the temporal mean pattern of flow past an isolated plate ($l/h = 2{\cdot}3$).

Such reduction in drag and pressure drop, and such lengthening of the average eddy zone, point to the fact that a major difference between the two cases lies in the considerable amount of mean-flow energy that is required to produce the vortices that are shed alternately into the oscillating wake. At low Reynolds numbers these vortices are known to persist for a considerable distance prior to their disintegration into turbulence; in such circumstances, the wake behind the isolated plate should be narrower than that behind the wall. At high Reynolds numbers, on the other hand, the vortices tend to disintegrate quite rapidly; the rate of lateral spread of the turbulent zone behind the plate then probably exceeds that behind the wall. Since at all Reynolds numbers beyond a few thousand the standing eddy behind the wall appears to maintain an essentially constant form, the same can reasonably be expected of its wake as a whole; and since both the scale and the energy of the turbulence generated at the periphery of the standing eddy are smaller than the corresponding quantities in the oscillating wake, the disturbance caused by the wall should invariably dissipate more rapidly.

How great an effect the existence of boundary shear upstream from the wall (deliberately set aside at the outset because of its undefined magnitude) would actually have upon these characteristics can only be surmised. The complexity of its experimental evaluation is seen from the fact that under even the simplest probable conditions of velocity variation—for example, the semi-logarithmic distribution $u = A + B \log y$—at least two variables must be considered: in brief, a magnitude and a rate of change. Fortunately, a phenomenon analogous to that under discussion is found in flow through a pipe orifice, for which it is both logical and experimentally demonstrable that maintaining a constant mean velocity and varying the transverse distribution by roughening the pipe surface will reduce both the

pressure change and the jet contraction. There is little basic difference between the axisymmetric orifice and the two-dimensional slot, and the slot differs even less from the boundary arrangement investigated in the present study. One may therefore conclude that an increase in the velocity variation over a given vertical distance (say $2h$, the velocity at level h thereby remaining constant) could be expected to cause a decrease in the drag of a wall, in the pressure reduction behind it, and in the size of the standing eddy which it produces. Until the extent of this effect has been determined experimentally, however, the prediction of such related phenomena as cavitation in the eddies formed by boundary projections must continue according to the rule of thumb that the significant velocity is that at a boundary distance equal to the height of the projection.

This investigation was undertaken by the first author under the direction of the second, in part as a thesis project for the degree of Master of Science at the State University of Iowa and in part as a sponsored project under Contract N8onr–500 between the Iowa Institute of Hydraulic Research and the Office of Naval Research. In the course of the hydrodynamic analysis of the flow pattern, considerable assistance was provided by Dr Louis Landweber of the Institute staff.

References

Arie, M. 1955 Flow past a normal plate in contact with a boundary, M. S. thesis, State University of Iowa.

Birkhoff, G. 1950 *Hydrodynamics*. Princeton University Press.

Fage, A. & Johansen, F. C. 1927 On the flow of air behind an inclined flat plate of infinite plan, *Proc. Roy. Soc.* A, **116,** 170.

Goldstein, S. (Ed.) 1938 *Modern Developments in Fluid Dynamics*, vol. 2. Oxford University Press.

Hsu, H. C. 1950 Characteristics of mean flow and turbulence at an abrupt two-dimensional expansion, Ph.D. dissertation, State University of Iowa.

Hubbard, P. G. 1954 Constant-temperature hot-wire anemometry with application to measurement in water, Ph.D. dissertation, State University of Iowa.

Landweber, L. 1951 The axially symmetric potential flow about elongated bodies of revolution, *David Taylor Model Basin, Rep.* no. 761.

Roshko, A. 1955 On the wake and drag of bluff bodies, *J. Aero. Sci.* **22,** 124.

The displacement effect of a sphere in a two-dimensional shear flow

By I. M. HALL
Aerodynamics Division, National Physical Laboratory

(*Received* 22 *December* 1955)

SUMMARY

This paper contains a theoretical investigation of the displacement effect of a pitot tube in a shear flow. Viscosity is neglected throughout so that the vorticity field alone is considered.

It is first shown that a two-dimensional approach does not produce a large enough displacement effect because it does not include the stretching of vortex tubes that takes place around a three-dimensional pitot tube. Then the three-dimensional problem is considered. A solution is obtained in the plane of symmetry for a sphere in a shear flow. This solution is found by making an assumption about the rate of stretching of vortex tubes perpendicular to the plane of symmetry and then considering the shear flow as a small perturbation of a uniform flow. A solution in the plane of symmetry is sufficient to obtain the displacement effect, which is found to be of the same order as the experimental result obtained by Young & Maas (1936) for a conventional pitot tube. The sphere may be considered to represent a conventional pitot tube (of slightly smaller diameter), so it is concluded that a large part of the displacement effect of a pitot tube may be accounted for without the inclusion of viscosity, i.e. by consideration of the vorticity field alone.

To a first approximation, the vorticity in the plane of symmetry is found to depend only on the distance from the centre of the sphere.

An outline of shear flows past some two-dimensional bodies is given in an appendix. The bodies considered are a circular cylinder and a two-dimensional 'pitot-tube' consisting of two parallel semi-infinite plates.

1. INTRODUCTION

Correct interpretation of the pressure measured by a pitot tube in a shear flow is important in the experimental study of boundary layers and wakes, whose velocity profiles are generally obtained from pitot traverses. The problem has been investigated experimentally by Young & Maas (1936) and their approach, outlined below, shows the nature of the problem. The corresponding theoretical problem is then discussed, and an approximate solution is obtained for a spherical 'pitot tube'.

The variation of total pressure across a wake, measured by a pitot tube, is shown in figure 1, together with the hypothetical curve which would be obtained using a tube of zero diameter. In effect, the pitot tube with its axis at B measures the total pressure at A. Hence, if the distance δ were known, the actual distribution could be obtained from the measured one. The distance δ must be a function of the shape of the pitot tube, its diameter D, the velocity and its derivatives, and the kinematic viscosity.

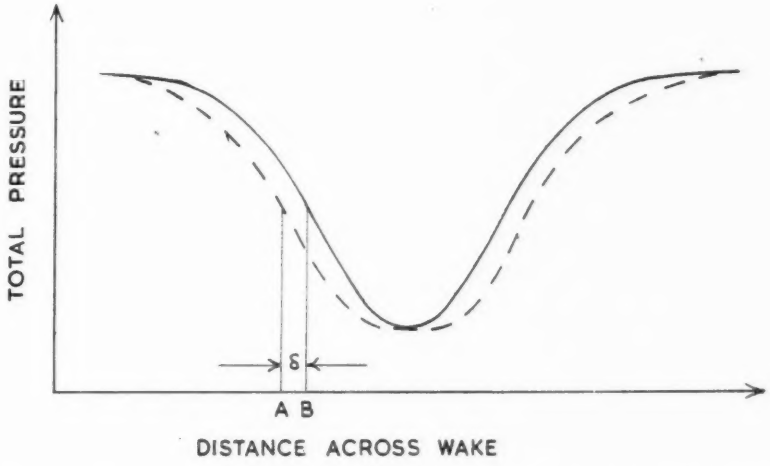

Figure 1. The variation of total pressure across a wake, showing displacement effect due to finite size of pitot tube; ———— measured distribution; – – – – – – actual distribution.

Suppose now that the second and higher derivatives of the velocity are zero, or so small that they can be neglected; i.e. the velocity of the oncoming flow is

$$U + Ay', \tag{1.1}$$

where U is the velocity on the axis of the pitot tube, and y' is a rectangular coordinate perpendicular to the axis. Then, if we consider only geometrically similar tubes, in an inviscid fluid,

$$\delta = \text{function of } D, U, A, \tag{1.2}$$

or, from dimensional considerations,

$$\frac{\delta}{D} = \text{function of } K, \tag{1.3}$$

where

$$K = \frac{AD}{2U}. \tag{1.4}$$

Using flat-nosed pitot tubes with internal diameters approximately equal to 0·6 of their external diameters, Young & Maas found that

$$\frac{\delta}{D} = 0{\cdot}18 \operatorname{sgn} K \tag{1.5}$$

i.e. the displacement is towards the region of higher velocity. This result contains a difficulty at $K = 0$, where there is a discontinuity in the displacement effect. This is not physically plausible since it implies that there is a discontinuous change in the flow pattern when the pitot tube is moved a small distance from a point of zero shear. However, the result obtained by Young & Maas is not necessarily valid near $K = 0$. Their values of δ/D show increasing scatter as K decreases, and no values were obtained for K less than 0·025. Also, when K is small, it is probably not always justified to neglect second and higher derivatives of the velocity. Therefore, it is likely that the actual variation of δ/D with K is rapid, but finite, when K is very small, and that δ/D tends towards some value, constant for a particular pitot tube geometry (0·18 for the shape of tube used by Young & Maas), at larger values of K. During recent work at Cambridge University, further experimental values have been obtained for the displacement effect which are in fair agreement with the Young & Maas result.

So far, no theoretical treatment of a pitot tube in a shear flow has been made. Two classes of problems have been solved in which the oncoming flow has a uniform rate of shear:

(*a*) those in which the body is cylindrical and the whole flow is two-dimensional (Lamb 1932, p. 233, Lighthill, Reichardt 1954, Tsien 1943); some of these solutions are outlined in an appendix;

(*b*) those in which the body is cylindrical with generators perpendicular to the oncoming vorticity (Hawthorne 1954, Squire & Winter 1951).

Other solutions involving bodies in non-uniform streams have been obtained, but these are not relevant to the pitot tube problem (e.g. Nagamatsu 1951, Hawthorne & Martin 1955).

In the completely two-dimensional problem, the displacement effect can be found easily, but it is considerably smaller than the experimental values obtained with an axially-symmetric pitot tube. This is not necessarily due to the omission of viscosity (Reichardt's experiments show very good agreement with inviscid theory) but is probably due to an essential difference between the vorticity fields in shear flows past two and three-dimensional bodies. Thus, consider a vortex tube moving towards the pitot tube. At a large distance upstream, the vorticity is everywhere perpendicular to both the velocity and the direction of the shear, so that a vortex tube is initially a cylinder with its generators perpendicular to the stream direction. When the flow is completely two-dimensional, the generators remain perpendicular to the stream, so that the cross-section of a vortex tube is deformed but its area is unaltered. Hence the vorticity is constant along any streamline. In front of a three-dimensional object, however, there is a retardation of the fluid, while at large lateral distances the flow is almost

unaffected by the body. Therefore, the vortex tube must be stretched so that there is a decrease in cross-sectional area (by continuity) and hence an increase in vorticity (by Kelvin's theorem). The net result is an accumulation of vorticity in front of the body and, in consequence, larger streamline curvatures than occur in the two-dimensional case. This makes possible a much larger displacement effect. For example, it is shown in this paper that, when the vorticity of the oncoming flow is small, a sphere produces, according to certain approximate assumptions, a displacement approximately five times as large as that produced by a cylinder of the same radius.

Another feature introduced by the stretching of the vortex tubes around a three-dimensional object is a streamwise component of vorticity. In the plane of symmetry, the velocity field of this component seems to be predominantly downwards, which would tend to increase the displacement effect. This feature is not accounted for explicity in the analysis of this paper, and would have to be taken into account in any attempt to improve the present theory.

The three-dimensional problem is much more difficult, because the full equations are complicated and non-linear. However, the streamline reaching the stagnation point must always lie in the plane of symmetry, $z = 0$, so that a solution in this plane is sufficient to determine the displacement effect. The flow pattern in this plane is not independent of the rest of the flow pattern, but it can be shown to depend on one quantity only, namely $(\partial w/\partial z)_{z=0}$, where w is the velocity in the z-direction. As a first attack on the problem, the equations of motion in the plane of symmetry are solved below by assigning an approximate value to $(\partial w/\partial z)_{z=0}$. Consider again a vortex tube moving towards the body. It is clear that the behaviour of the flow pattern in the plane of symmetry is governed by the rate of stretching of the vortex tube perpendicular to this plane. This quantity is the relevant component of the rate of strain tensor, i.e. $\partial w/\partial z$. Therefore, it is necessary to know $(\partial w/\partial z)_{z=0}$ in order to solve the problem in the plane of symmetry. This is not possible without a full solution of the three-dimensional problem, so an approximate value is sought. Since the vorticity in the plane of symmetry is in the z-direction, it seems reasonable to assume that, in this plane, $\partial w/\partial z$ is independent of the vorticity. On this assumption, $(\partial w/\partial z)_{z=0}$ must take its value in the irrotational flow.

At this stage the problem is still non-linear: in fact, it involves the solution of three simultaneous partial differential equations. However, in practice the oncoming shear is often small, which suggests that linearization may be effected by considering the shear flow as a perturbation of the uniform flow. Since small shear corresponds to small K, a solution is sought in the form of a series in ascending powers of K. To be able to use this approach, it is necessary to know the solution when K is zero. This solution is not available for a pitot tube of conventional shape but only for bodies with closed, rounded noses. Therefore, since the solution for a sphere in a uniform flow is simple and well known (e.g. Milne-Thomson 1949, p. 413), an attempt has been made to obtain a solution for a sphere in a shear flow.

If the sphere itself were used as a pitot tube, by making a small pressure hole on the axis, the definition of δ as the displacement of the stagnation streamline would not have the desired physical meaning. The pressure measured would be the static pressure at the orifice, which is less than the total pressure on the stagnation streamline. However, a pitot tube of this type would be unsatisfactory because of its sensitivity to yaw. Instead, one may think of the sphere as replacing a conventional pitot tube of slightly smaller outside diameter, so that the streamline reaching the stagnation point is the same as the one reaching the stagnation point inside the pitot tube. Then the displacement effect of the sphere is defined in the same way as for an open body; i.e. the asymptotic distance of the stagnation streamline from the axis. The above argument is illustrated by the two-dimensional case (see the appendix) in which the displacement effects of a cylinder and a parallel plate pitot tube are equal when the diameter of the cylinder is $\sqrt{2}$ times the spacing of the plates.

By expanding the full equations of motion in powers of K, it can be shown that the assumption for $(\partial w/\partial z)_{z=0}$ gives the vorticity correct to the first order in K, but omits an irrotational contribution to the velocity components. Unfortunately, this cannot be remedied without solving the problem for the entire three-dimensional flow pattern*. However, in order to obtain other than a linear variation for the displacement effect, results have been obtained up to the order of K^3 using the above assumption for $(\partial w/\partial z)_{z=0}$. The cubic term produces a maximum value of δ/D which is of the same order as the asymptotic values found experimentally and which occurs within the possible working range of values of K.

The result for the first approximation to the vorticity is of some interest since it shows that it is a function of the distance from the centre of the sphere only, and that it has a square root infinity on the surface. In fact, the first approximation is $(1-r^{-3})^{-1/2}$ times the oncoming vorticity, where r is the distance from the centre of the sphere divided by its radius.

The mathematical formulation of the problem, using the above assumptions, is given in § 2, and the equations are solved in § 3. The solution is summarized in § 4, and the velocity components are obtained. In § 5, differential equations for the streamlines are found and solved for the stagnation streamline. Outlines of some two-dimensional solutions are given in an appendix.

2. Mathematical formulation of the problem

Consider a cylindrical coordinate system r', θ, z' with its origin at the centre of a sphere of radius a. The undisturbed flow is independent of z', so that $z'=0$ is the plane of symmetry of the flow pattern, and is in the direction $\theta=\pi$ (figure 2). Non-dimensional coordinates r, z, are defined as r'/a, z'/a.

* Since this work was completed, Lighthill has solved the first order problem over the entire flow field. He obtains the same order of magnitude for the displacement effect and for the downwash velocity ahead of the sphere. This increases one's confidence in the cubic term obtained in this paper.

In the plane of symmetry, the vorticity components are $(0, 0, \zeta)$ and the velocity is $(u, v, 0)$ where u and v are even functions of z. Therefore, in this plane, Helmholtz's equations of motion reduce to

$$u\frac{\partial\zeta}{\partial r}+v\frac{\partial\zeta}{r\partial\theta}=\zeta\left(\frac{\partial w}{\partial z}\right)_{z=0}, \tag{2.1}$$

where

$$\frac{1}{r}\frac{\partial(rv)}{\partial r}-\frac{\partial u}{r\partial\theta}=a\zeta. \tag{2.2}$$

The equation of continuity is

$$\frac{1}{r}\frac{\partial(ru)}{\partial r}+\frac{\partial v}{r\partial\theta}=-\left(\frac{\partial w}{\partial z}\right)_{z=0}. \tag{2.3}$$

Equations (2.1) to (2.3) are the same as those for a two-dimensional rotational flow except for the additional terms containing $(\partial w/\partial z)_{z=0}$. If a value is inserted for $(\partial w/\partial z)_{z=0}$, the problem is reduced, in effect, to a two-dimensional

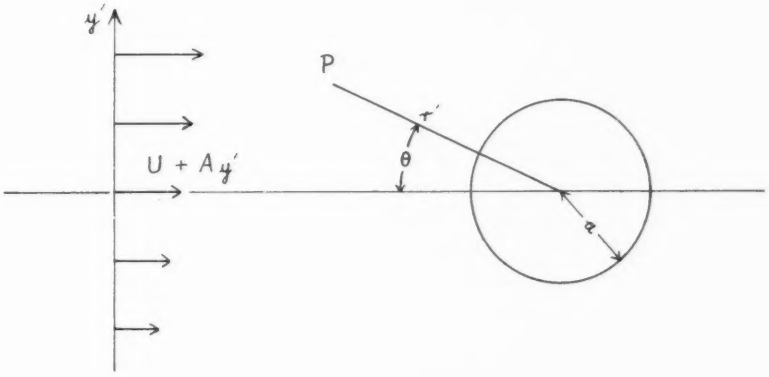

Figure 2. The plane of symmetry of the flow pattern.

one, and the above equations are sufficient to determine u, v, and ζ, provided that the boundary conditions are suitable. In § 1, it was shown that a good approximation to $(\partial w/\partial z)_{z=0}$ is its value in the irrotational flow. Therefore (Milne-Thomson 1949),

$$\left(\frac{\partial w}{\partial z}\right)_{z=0}=\frac{3U\cos\theta}{2r^4}. \tag{2.4}$$

By means of the transformation

$$\left.\begin{aligned} u&=U\frac{\partial\phi}{\partial r}+Aa\frac{\partial\psi}{r\partial\theta}=U\left(\frac{\partial\phi}{\partial r}+K\frac{\partial\psi}{r\partial\theta}\right),\\ v&=U\frac{\partial\phi}{r\partial\theta}-Aa\frac{\partial\psi}{\partial r}=U\left(\frac{\partial\phi}{r\partial\theta}-K\frac{\partial\psi}{\partial r}\right),\end{aligned}\right\} \tag{2.5}$$

equations (2.2) and (2.3) become

$$\nabla^2\phi = -\frac{3\cos\theta}{2r^4}, \tag{2.6}$$

$$\nabla^2\psi = -\frac{\zeta}{A}, \tag{2.7}$$

where

$$\nabla^2 = \frac{1}{r}\frac{\partial}{\partial r}\left(r\frac{\partial}{\partial r}\right) + \frac{1}{r^2}\frac{\partial^2}{\partial\theta^2}. \tag{2.8}$$

The oncoming flow is parallel and has uniform rate of shear. Hence, the boundary conditions are

$$\begin{aligned} &(a)\ \text{at } r = \infty, && \zeta = A, \\ & && -u = U\cos\theta + Aar\sin\theta\cos\theta, \\ & && v = U\sin\theta + Aar\sin^2\theta, \\ &(b)\ \text{at } r = 1, && u = 0. \end{aligned}$$

However, when A is zero, the solution is known (Milne-Thomson 1949, p. 413). Thus, ϕ satisfies the equations

$$\left.\begin{aligned} \frac{\partial\phi}{\partial r} &= -\cos\theta\left(1-\frac{1}{r^3}\right), \\ \frac{\partial\phi}{r\partial\theta} &= \sin\theta\left(1+\frac{1}{2r^3}\right). \end{aligned}\right\} \tag{2.9}$$

But this solution for ϕ satisfies (2.6) when A is not zero.* Hence the problem is reduced to that of solving (2.1) and (2.7) with boundary conditions

$$\left.\begin{aligned} &(a)\ \text{at } r = \infty, && \zeta = A, \\ & && \psi = -\tfrac{1}{2}r^2\sin^2\theta, \\ &(b)\ \text{at } r = 1, && \psi = \text{constant}. \end{aligned}\right\} \tag{2.10}$$

The solution is obtained by inserting expansions for ζ and ψ in powers of K. These are

$$\left.\begin{aligned} \psi &= \psi_0 + K\psi_1 + K^2\psi_2 + \ldots, \\ \frac{\zeta}{A} &= \zeta_0 + K\zeta_1 + K^2\zeta_2 + \ldots. \end{aligned}\right\} \tag{2.11}$$

On substituting (2.11) in (2.1) and (2.7) two series of differential equations are obtained. These are

$$\frac{\partial\phi}{\partial r}\frac{\partial\zeta_n}{\partial r} + \frac{\partial\phi}{r\partial\theta}\frac{\partial\zeta_n}{r\partial\theta} = \frac{3\cos\theta}{2r^4}\zeta_n + g_n(\psi_0, \ldots \psi_{n-1}, \zeta_0, \ldots \zeta_{n-1}), \tag{2.12}$$

$$\nabla^2\psi_n = -\zeta_n, \tag{2.13}$$

* It would not do so if the term of order K in $(\partial\zeta/\partial z)_{z=0}$ were included.

where the functions g_n are given by

$$\left.\begin{aligned} g_0 &= 0, \\ g_n &= \sum_{i-j=n-1} \left(\frac{\partial \psi_i}{\partial r} \frac{\partial \zeta_j}{r \partial \theta} - \frac{\partial \psi_j}{r \partial \theta} \frac{\partial \zeta_i}{\partial r} \right). \end{aligned}\right\} \tag{2.14}$$

The boundary conditions are

$$\left.\begin{aligned} &(a) \text{ at } r = \infty, \quad \zeta_0 = 1, \quad \psi_0 = -\tfrac{1}{2} r^2 \sin^2\theta, \\ &\qquad\qquad \zeta_n = 0, \quad \psi_n = 0, \quad (n \neq 0), \\ &(b) \text{ at } r = 1, \quad \psi_n = \text{constant}. \end{aligned}\right\} \tag{2.15}$$

In § 3, equations (2.12) and (2.13) are solved for $n = 0$, 1, and 2. First, equation (2.12) with $n = 0$ is solved to obtain the first approximation to the vorticity. This is substituted in (2.13) to obtain the first approximation to ψ. Then, substituting back in (2.12) with $n = 1$, the second approximation to the vorticity is found. This is inserted in (2.13), and so on. Physically, this corresponds to finding first the vorticity field obtained by convecting initially constant vorticity along the irrotational streamlines, and then the velocity perturbations caused by this vorticity field. On substituting back into (2.12), the vorticity field that is convected along the perturbed streamlines is found. Then the further velocity perturbation is obtained, and the process is continued until the desired approximation is reached.

3. Solution of the differential equations

The general solutions of equations (2.12) and (2.13) are found below and then the special solutions satisfying the boundary conditions (2.15) are determined.

Substituting from (2.9), equation (2.12) is

$$-\cos\theta \left(1 - \frac{1}{r^3}\right) \frac{\partial \zeta_n}{\partial r} + \sin\theta \left(1 + \frac{1}{2r^3}\right) \frac{\partial \zeta_n}{r \partial \theta} = \frac{3\cos\theta}{2r^4} \zeta_n + g_n. \tag{3.1}$$

The general solution of (3.1) is the sum of a particular integral, which depends on g_n, and the complementary function η, which is the solution of

$$-\cos\theta \left(1 - \frac{1}{r^3}\right) \frac{\partial \eta}{\partial r} + \sin\theta \left(1 + \frac{1}{2r^3}\right) \frac{\partial \eta}{r \partial \theta} = \frac{3\cos\theta}{2r^4} \eta. \tag{3.2}$$

Changing the independent variables from r, θ to r, χ, (3.2) becomes

$$\begin{aligned} -\cos\theta \left(1 - \frac{1}{r^3}\right) \left(\frac{\partial \eta}{\partial r}\right)_\chi + \Bigg\{ &-\cos\theta \left(1 - \frac{1}{r^3}\right) \frac{\partial \chi}{\partial r} + \\ &+ \sin\theta \left(1 + \frac{1}{2r^3}\right) \frac{\partial \chi}{r \partial \theta} \Bigg\} \left(\frac{\partial \eta}{\partial \chi}\right)_r = \frac{3\cos\theta}{2r^4} \eta. \end{aligned} \tag{3.3}$$

Therefore, if χ is an integral of

$$\frac{dr}{-\cos\theta(1-r^{-3})} = \frac{r d\theta}{\sin\theta(1+\frac{1}{2}r^{-3})}, \tag{3.4}$$

e.g.

$$\chi = \left(\frac{r^3-1}{r}\right)^{1/2}\sin\theta, \tag{3.5}$$

equation (3.3) reduces to

$$-\left(1-\frac{1}{r^3}\right)\left(\frac{\partial\eta}{\partial r}\right)_{\chi} = \frac{3}{2r^4}\eta, \tag{3.6}$$

whose solution is

$$\eta = j(\chi)\left(\frac{r^3}{r^3-1}\right)^{1/2}, \tag{3.7}$$

where j is an arbitrary function, determined by the boundary condition.

Equation (2.13) is

$$\nabla^2\psi_n = -\zeta_n. \tag{3.8}$$

This is a Poisson-type equation whose general solution is the sum of a particular integral, depending on ζ_n, and the complementary function, which is independent of ζ_n. The latter is a solution of Laplace's equation in two dimensions, and is

$$\tfrac{1}{2}a_0 + \sum_{1}^{\infty}[(a_n r^n + b_n r^{-n})\cos n\theta + (c_n r^n + d_n r^{-n})\sin n\theta], \tag{3.9}$$

where a_n, b_n, c_n, d_n are constants determined by the boundary conditions.

First approximation to the vorticity

g_0 is zero. Therefore, when $n = 0$, the solution of (3.1) is the complementary function alone, given by (3.7), i.e.

$$\zeta_0 = j(\chi)\left(\frac{r^3}{r^3-1}\right)^{1/2}. \tag{3.10}$$

Since $\zeta_0 = 1$ at $r = \infty$,

$$j(\chi) = 1. \tag{3.11}$$

Therefore,

$$\zeta_0 = \left(\frac{r^3}{r^3-1}\right)^{1/2}. \tag{3.12}$$

This equation shows that, to a first approximation, ζ is independent of θ. This is because, for the particular case of irrotational flow past a sphere, u and $(\partial w/\partial z)_{z=0}$ have the same variation with θ. This can only occur when the body can be represented by a doublet at the origin, since this is the only case in which the velocity potential is the product of two terms, one of which is a function of θ only and the other is independent of θ.

Equation (3.12) also shows that the vorticity becomes infinite on the sphere. This is to be expected from the previous considerations regarding the stretching of a vortex tube. In fact, the vorticity must become infinite on any body with a stagnation point.

First approximation to ψ

Substituting (3.12) in (3.8) gives

$$\frac{1}{r}\frac{\partial}{\partial r}\left(r\frac{\partial\psi_0}{\partial r}\right)+\frac{1}{r^2}\frac{\partial^2\psi_0}{\partial\theta^2} = -\left(\frac{r^3}{r^3-1}\right)^{1/2}. \tag{3.13}$$

A particular integral is Ψ, where

$$\frac{1}{r}\frac{d}{dr}\left(r\frac{d\Psi}{dr}\right) = -\left(\frac{r^3}{r^3-1}\right)^{1/2}. \tag{3.14}$$

Hence,

$$r\frac{d\Psi}{dr} = -\int^{r} x^{5/2}(x^3-1)^{-1/2}\,dx. \tag{3.15}$$

To ensure convergence of the integral as $r\to\infty$, (3.15) is rewritten as

$$r\frac{d\Psi}{dr} = -\tfrac{1}{2}r^2+\int_{r}^{\infty}\{x^{5/2}(x^3-1)^{-1/2}-x\}\,dx. \tag{3.16}$$

Integrating again,

$$\Psi = -\tfrac{1}{4}r^2-Q, \tag{3.17}$$

where

$$Q = \int_{r}^{\infty}\frac{ds}{s}\int_{s}^{\infty}\{x^{5/2}(x^3-1)^{-1/2}-x\}\,dx, \tag{3.18}$$

or, reversing the order of integration,

$$Q = \int_{r}^{\infty}\{x^{5/2}(x^3-1)^{-1/2}-x\}\log\left(\frac{x}{r}\right)dx \tag{3.19}$$

$$\sim \tfrac{1}{2}r^{-1} \quad \text{as } r\to\infty. \tag{3.20}$$

The solution of (3.13) is the sum of Ψ and the complementary function (3.9). Hence, applying the boundary conditions (2.15),

$$\psi_0 = \frac{1}{4}\left(r^2-\frac{1}{r^2}\right)\cos 2\theta-\tfrac{1}{4}r^2-Q. \tag{3.21}$$

Second approximation to ζ

Substituting (3.12) and (3.21) in (2.14) gives

$$g_1 = g_1'(r)\sin\theta\cos\theta, \tag{3.22}$$

where

$$g_1' = -\tfrac{3}{2}r^{-5/2}(r^4-1)(r^3-1)^{-3/2}. \tag{3.23}$$

Therefore, when $n=1$, a particular integral of (3.1) is $Z(r)\sin\theta$, where

$$\frac{dZ}{dr}-\frac{Z}{r} = -\left(1-\frac{1}{r^3}\right)^{-1}g_1', \tag{3.24}$$

i.e.

$$Z = -\frac{3r}{2}\int_{r}^{\infty}x^{-1/2}(x^4-1)(x^3-1)^{-5/2}\,dx \tag{3.25}$$

$$\sim -\tfrac{1}{2}r^{-2} \quad \text{as } r\to\infty. \tag{3.26}$$

The solution of (3.1) is

$$\zeta_1 = j(\chi)\left(\frac{r^3}{r^3-1}\right)^{1/2} + Z(r)\sin\theta, \tag{3.27}$$

where χ is given by (3.5). Then, since $\zeta_1 = 0$ at $r = \infty$,

$$j(\chi) = 0, \tag{3.28}$$

and

$$\zeta_1 = Z(r)\sin\theta. \tag{3.29}$$

Second approximation to ψ

Substituting (3.29) in (3.8) gives

$$\frac{1}{r}\frac{\partial}{\partial r}\left(r\frac{\partial\psi_1}{\partial r}\right) + \frac{1}{r^2}\frac{\partial^2\psi_1}{\partial\theta^2} = -Z(r)\sin\theta. \tag{3.30}$$

A particular integral is $R(r)\sin\theta$, where

$$\frac{1}{r}\frac{d}{dr}\left(r\frac{dR}{dr}\right) - \frac{R}{r^2} = -Z. \tag{3.31}$$

It is convenient, both for algebraic manipulation and for computation, to consider the integrals R_1 and R_2, where

$$R_1 = r\frac{dR}{dr} - R = -\frac{1}{r}\int^r x^2 Z(x)\,dx \tag{3.32}$$

$$R_2 = r\frac{dR}{dr} + R = -r\int^r Z(x)\,dx. \tag{3.33}$$

The double integrals on the right hand sides of (3.32) and (3.33) can be reduced to single integrals. Integrating by parts, (3.32) becomes

$$R_1 = -\tfrac{1}{4}r^2 Z + \frac{1}{4r}\int^r x^4\frac{d}{dx}\left(\frac{Z}{x}\right)dx, \tag{3.34}$$

where $d(Z/x)/dx$ is known from (3.24). From (3.26),

$$\frac{d}{dx}\left(\frac{Z}{x}\right) \sim \tfrac{3}{2}x^{-4} \quad \text{as } x \to \infty. \tag{3.35}$$

Therefore, subtracting 3/2 from the integrand to ensure convergence, and adding $3r/2$ outside the integral,

$$\frac{1}{4r}\int^r x^4\frac{d}{dx}\left(\frac{Z}{x}\right)dx = \frac{3}{8} - \frac{H}{4r}, \tag{3.36}$$

where

$$H = \frac{3}{2}\int_r^\infty \{x^{7/2}(x^4-1)(x^3-1)^{-5/2} - 1\}\,dx. \tag{3.37}$$

Similarly,

$$R_2 = -\tfrac{1}{2}r^2 Z - \tfrac{1}{4}rG, \tag{3.38}$$

where

$$G = \frac{3}{2}\int_r^\infty x^{3/2}(x^4-1)(x^3-1)^{-5/2}\,dx. \tag{3.39}$$

As $r \to \infty$,

$$G \sim \tfrac{3}{2}r^{-1}, \tag{3.40}$$

$$H \sim \tfrac{15}{8}r^{-2}. \tag{3.41}$$

Therefore, as $r \to \infty$,

$$R = \frac{R_2 - R_1}{2} \sim -\tfrac{1}{2}. \tag{3.42}$$

The function ψ_1 is the sum of $R\sin\theta$ and the complementary function (3.9). Since ψ must be constant on $r = 1$,

$$\psi_1 = \left\{R - \frac{R(1)}{r}\right\}\sin\theta + \tfrac{1}{2}a_0 + \sum_1^{\infty}\{a_n(r^n - r^{-n})\cos n\theta + c_n(r^n - r^{-n})\sin n\theta\}. \tag{3.43}$$

This solution cannot satisfy the boundary condition at infinity for any values of a_n, c_n. However, the part of the flow pattern in which deviations from the upstream conditions would be expected to be important is a strip

$$|y| = |r\sin\theta| < k, \tag{3.44}$$

where k is finite. In principle, the complete flow pattern could be obtained by joining three solutions; the present one in the strip $|y| < k$, and two solutions for $|y| > k$ which would have to be found by another method. However, since the outer flows would be very nearly parallel, and would have little effect on the inner flow near $y = 0$, if k were taken to be large enough, it should be sufficient to satisfy the boundary condition at infinity in the strip $|y| < k$ only. In this strip, the boundary condition is satisfied if a_n, c_n are zero for all n, i.e. if

$$\psi_1 = \left\{R - \frac{R(1)}{r}\right\}\sin\theta \tag{3.45}$$

$$\sim -\frac{y}{2r} \quad \text{as } r \to \infty.$$

Third approximation to ζ

The equation for g_2 may be written in the form

$$g_2 = g_2'(r)\cos\theta + g_2''(r)\sin^2\theta\cos\theta, \tag{3.46}$$

where

$$g_2 = \tfrac{1}{2}r^{-4}Z - r^{-1}Z\frac{dQ}{dr} + \tfrac{3}{2}r^{-1/2}(r^3 - 1)^{-3/2}, \tag{3.47}$$

$$g_2'' = \left(r - \frac{1}{r^3}\right)\frac{dZ}{dr} - \left(r + \frac{1}{r^3}\right)\frac{Z}{r}.$$

When $n = 2$, a particular integral of (3.1) is

$$X(r) + Y(r)\sin^2\theta,$$

where

$$-\left(1 - \frac{1}{r^3}\right)\frac{dX}{dr} = \frac{3}{2r^4}X + g_2', \tag{3.48}$$

$$-\left(1-\frac{1}{r^3}\right)\frac{dY}{dr}+2\left(1+\frac{1}{2r^3}\right)\frac{Y}{r}=\frac{3}{2r^4}Y+g_2''. \tag{3.49}$$

Hence, solving these equations,

$$X=\left(\frac{r^3}{r^3-1}\right)^{1/2}X_1(r), \tag{3.50}$$

$$Y=r^{1/2}(r^3-1)^{1/2}Y_1(r), \tag{3.51}$$

where

$$X_1=\int_r^\infty\left(\frac{x^3}{x^3-1}\right)^{1/2}g_2'(x)\,dx, \tag{3.52}$$

$$Y_1=\int_r^\infty x^{5/2}(x^3-1)^{-3/2}g''(x)\,dx. \tag{3.53}$$

As $r\to\infty$,

$$X\sim-\tfrac{1}{4}r^{-4}, \tag{3.54}$$

$$Y\sim\tfrac{1}{2}r^{-1}. \tag{3.55}$$

Therefore, the solution of (3.1) for ζ_2, satisfying $\zeta_2=0$ at $r=\infty$, is

$$\zeta_2=X(r)+Y(r)\sin^2\theta. \tag{3.56}$$

Third approximation to ψ

Substituting (3.56) in (3.8) gives

$$\frac{1}{r}\frac{\partial}{\partial r}\left(r\frac{\partial\psi_2}{\partial r}\right)+\frac{1}{r^2}\frac{\partial^2\psi_2}{\partial\theta^2}=-X-\tfrac{1}{2}Y+\tfrac{1}{2}Y\cos 2\theta. \tag{3.57}$$

A particular integral is

$$S(r)+T(r)\cos 2\theta,$$

where

$$\frac{1}{r}\frac{d}{dr}\left(r\frac{dS}{dr}\right)=-X-\tfrac{1}{2}Y, \tag{3.58}$$

$$\frac{1}{r}\frac{d}{dr}\left(r\frac{dT}{dr}\right)-\frac{4T}{r^2}=\tfrac{1}{2}Y. \tag{3.59}$$

Integration of (3.58) gives, after manipulation similar to the previous cases,

$$S=-\tfrac{1}{4}r-\int_r^\infty\{(X+\tfrac{1}{2}Y)x+\tfrac{1}{4}\}\log\left(\frac{x}{r}\right)dx. \tag{3.60}$$

The integration of (3.59) is carried out in the same manner as the integration of (3.31). Two integrals, T_1 and T_2, are defined by

$$\left.\begin{aligned}T_1&=r\frac{dT}{dr}-2T,\\ T_2&=r\frac{dT}{dr}+2T.\end{aligned}\right\} \tag{3.61}$$

These are found to be

$$T_1=\tfrac{1}{12}r+\tfrac{3}{8}r^{-2}\log r-r^{-2}\int_r^\infty\{\tfrac{1}{2}x^3Y-\tfrac{1}{4}x-\tfrac{3}{8}x^{-1}\}\,dx, \tag{3.62}$$

$$T_2=-\tfrac{1}{2}r^2\int_r^\infty x^{-1}Y\,dx \tag{3.63}$$

$$\sim-\tfrac{1}{4}r\quad\text{as } r\to\infty.$$

Hence, as $r \to \infty$,

$$T = \frac{T_2 - T_1}{4} \sim -\tfrac{1}{12}r. \tag{3.64}$$

Again, it is not possible to satisfy the boundary condition at infinity for all values of θ. However, the solution satisfying the condition $\psi_2 = 0$ at infinity in the strip $|y| < k$, as well as the condition $\psi_2 = \text{constant}$ on $r = 1$, is

$$\psi_2 = S + \left\{T - \frac{T(1)}{r^2}\right\}\cos 2\theta + \frac{1}{3}\left(r - \frac{1}{r}\right)\cos\theta \tag{3.65}$$

$$\sim \frac{y^4}{r^3} \quad \text{as } r \to \infty.$$

4. The velocity field

The results of § 3 are summarised below:

$$\frac{\zeta}{A} = \zeta_{00} + K\zeta_{11}\sin\theta + K^2\zeta_{20} + K^2\zeta_{22}\cos 2\theta + O(K^3), \tag{4.1}$$

$$\psi = \Psi_{00} + \Psi_{02}\cos 2\theta + K\Psi_{11}\sin\theta + K^2\Psi_{20} + K^2\Psi_{21}\cos\theta + K^2\Psi_{22}\cos 2\theta + O(K^3), \tag{4.2}$$

where

$$\left.\begin{aligned} &\zeta_{00} = \left(1 - \frac{1}{r^2}\right)^{-1/2}, && \zeta_{11} = Z, \\ &\zeta_{20} = X + \tfrac{1}{2}Y, && \zeta_{22} = -\tfrac{1}{2}Y, \\ &\Psi_{00} = -\tfrac{1}{4}r^2 - Q, && \Psi_{02} = \frac{1}{4}\left(r^2 - \frac{1}{r^2}\right), \\ &\Psi_{11} = R - \frac{R(1)}{r}, && \Psi_{20} = S, \\ &\Psi_{21} = \frac{1}{3}\left(r - \frac{1}{r}\right), && \Psi_{22} = T - \frac{T(1)}{r^2}. \end{aligned}\right\} \tag{4.3}$$

The integrals Q, R, S, etc. have been evaluated and are given in table 1.

$1/r$	Q	$-R$	$-S$	T	$-X$	Y	$-Z$
0·0	0·0000	0·5000	∞	∞	0·0000	0·0000	0·0000
0·1	0·0500	0·4099	2·2005	0·8358	0·0000	0·0501	0·0050
0·2	0·1003	0·4994	1·2540	0·4329	0·0003	0·1011	0·0202
0·3	0·1502	0·4980	0·8373	0·2908	0·0014	0·1556	0·0464
0·4	0·2006	0·4953	0·6320	0·2274	0·0047	0·2177	0·0859
0·5	0·2515	0·4909	0·5108	0·1917	0·0125	0·2947	0·1436
0·6	0·3032	0·4841	0·4319	0·1691	0·0341	0·3999	0·2295
0·7	0·3562	0·4745	0·3773	0·1532	0·0821	0·5617	0·3659
0·8	0·4114	0·4609	0·3378	0·1401	0·2038	0·8573	0·6133
0·9	0·4701	0·4413	0·3081	0·1268	0·6450	1·6112	1·2219
1·0	0·5377	0·4089	0·2818	0·1077	∞	∞	∞

Table 1

The velocity components u and v are obtained from (2.5), (2.9) and (4.2), in the forms

$$\frac{u}{U} = -(1-r^{-3})\cos\theta - 2Kr^{-1}\Psi_{02}\sin 2\theta + K^2 r^{-1}\Psi_{11}\cos\theta - \\ - K^3\{r^{-1}\Psi_{21}\sin\theta + 2r^{-1}\Psi_{22}\sin 2\theta\} + O(K^4), \quad (4.4)$$

$$\frac{v}{U} = (1+\tfrac{1}{2}r^{-3})\sin\theta - K\left\{\frac{d\Psi_{00}}{dr} + \frac{d\Psi_{02}}{dr}\cos 2\theta\right\} - \\ - K^2\frac{d\Psi_{11}}{dr}\sin\theta - K^3\left\{\frac{d\Psi_{20}}{dr} + \frac{d\Psi_{21}}{dr}\cos\theta + \frac{d\Psi_{22}}{dr}\cos 2\theta\right\} + O(K^4). \quad (4.5)$$

The velocity is always finite, and this suggests that the series (4.4) and (4.5) converge when K is small enough.

The position of the stagnation point is easily found from (4.5). On $r = 1$

$$\frac{v}{U} = 1{\cdot}5000\sin\theta - K\{0{\cdot}3505 + \cos 2\theta\} + 0{\cdot}9667K^2\sin\theta + \\ + K^3\{0{\cdot}5262 - 0{\cdot}6667\cos\theta + 0{\cdot}5524\cos 2\theta\} + O(K^4). \quad (4.6)$$

Put
$$y = r\sin\theta. \quad (4.7)$$

Then, if y_s is the value of y at the stagnation point,

$$y_s = Ky_{1s} + K^3 y_{3s} + O(K^5), \quad (4.8)$$

and equation (4.6) gives

$$0 = K(1{\cdot}5000y_{1s} - 1{\cdot}3505) + \\ + K^3(1{\cdot}5000y_{3s} + 2{\cdot}0000y_{1s} + 0{\cdot}9667y_{1s} + 0{\cdot}4119) + O(K^5), \quad (4.9)$$

whence
$$\left.\begin{aligned} y_{1s} &= \ \ 0{\cdot}9004, \\ y_{3s} &= -1{\cdot}9357. \end{aligned}\right\} \quad (4.10)$$

5. Streamlines and displacement effect

The streamlines are integrals of the equation

$$\frac{dr}{u} = \frac{rd\theta}{v}. \quad (5.1)$$

Substituting from (2.5), this can be written

$$K\left(\frac{\partial\psi}{\partial r}dr + \frac{\partial\psi}{\partial\theta}d\theta\right) = \frac{\partial\phi}{r\partial\theta}dr - \frac{\partial\phi}{dr}r\,d\theta, \quad (5.2)$$

or, using (2.9),

$$K\,d\psi = \frac{1}{2r\sin\theta}\,d\left\{\left(1-\frac{1}{r^3}\right)r^2\sin^2\theta\right\} \tag{5.3}$$

$$= \frac{1}{2y}\,dP,$$

where

$$P = \left(1-\frac{1}{r^3}\right)y^2 = py^2. \tag{5.4}$$

Using y and r as independent variables, (5.3) can be written

$$K\frac{\partial\psi}{\partial r}\,dr + K\frac{\partial\psi}{\partial y}\,dy = \frac{1}{2y}\frac{\partial P}{\partial r}\,dr + \frac{1}{2y}\frac{\partial P}{\partial y}\,dy, \tag{5.5}$$

i.e.

$$\left\{K\frac{\partial\psi}{\partial y} - \frac{1}{2y}\frac{\partial P}{\partial y}\right\}\frac{dy}{dr} + \left\{K\frac{\partial\psi}{\partial r} - \frac{1}{2y}\frac{\partial P}{\partial r}\right\} = 0, \tag{5.6}$$

which is a differential equation for y as a function of r along a streamline. Now, ψ can be expanded in the form

$$\psi = \psi_{00} + \psi_{02}\,y^2 + K\psi_{11}\,y + \dots, \tag{5.7}$$

where the ψ_{ij}'s can be found by comparison with (4.2). Then, assuming that on a streamline

$$y = y_0(r) + Ky_1(r) + \dots, \tag{5.8}$$

a series of linear differential equations for $y_i(r)$ is obtained. These equations are

$$p\frac{dy_i}{dr} + \frac{1}{2}\frac{dp}{dr}y_i = n_i(r, y_0, \dots, y_{i-1}), \tag{5.9}$$

where

$$\left.\begin{aligned} &n_0 = 0,\\ &n_1 = \frac{\partial\psi_{00}}{\partial r} + \frac{\partial\psi_{02}}{\partial r}y_0^2 + 2\psi_{02}\,y_0\frac{dy_0}{dr},\\ &\dots\dots\dots\dots\dots\dots \end{aligned}\right\} \tag{5.10}$$

The solutions of (5.9) are

$$y_0 = C_0\,p^{-1/2}, \tag{5.11}$$

$$y_i = -p^{-1/2}\int_r^\infty p^{-1/2}n_i\,dr + C_i\,p^{-1/2}. \tag{5.12}$$

It can be seen that (5.11) is the equation for the streamlines in the irrotational flow, as would be expected from (5.8).

The streamline reaching the stagnation point is of particular interest since it gives the displacement effect. On this streamline,

$$y_0 = y_2 = y_4 = \ldots = 0. \tag{5.13}$$

Hence

$$\left.\begin{aligned} n_1 &= \frac{\partial \psi_{00}}{\partial r}, \\ n_3 &= \frac{\partial \psi_{02}}{\partial r} y_1^2 + \frac{\partial \psi_{11}}{\partial r} y_1 + \frac{\partial \psi_{20}}{\partial r} + (2\psi_{02} y_1 + \psi_{11}) \frac{dy_1}{dr}, \\ &\ldots\ldots\ldots\ldots\ldots\ldots \end{aligned}\right\} \tag{5.14}$$

Since y_i must be finite when $r = 1$, the coefficient of $p^{-1/2}$ in (5.12) must be zero, i.e.

$$C_i = \int_1^\infty p^{-1/2} n_i \, dr. \tag{5.15}$$

Hence

$$y_i = p^{-1/2} \int_1^r p^{-1/2} n_i \, dr. \tag{5.16}$$

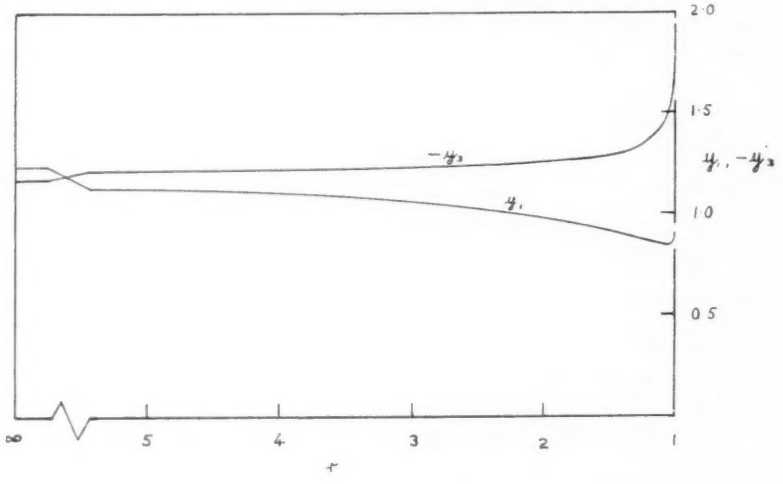

Figure 3. The stagnation steamline, $y(r) = Ky_1(r) + K^3 y_3(r) + O(K^5)$.

Using (5.14), the functions y_i may now be evaluated. The results for y_1 and y_3 are shown graphically in figure 3.

The displacement, δ, of the stagnation streamline at infinity is given by

$$\begin{aligned} \frac{\delta}{a} &= Ky_1(\infty) + K^3 y_3(\infty) + O(K^5) \\ &= 1{\cdot}2400K - 1{\cdot}1752K^3 + O(K^5). \end{aligned} \tag{5.17}$$

The variation of $\delta/2a$ with K is shown in figure 4. It can be seen that the displacement effect found in this investigation is of the same order of magnitude as the experimental result of Young & Maas. The gradient of $\delta/2a$ with K, when K is small, is somewhat less than would be desired for

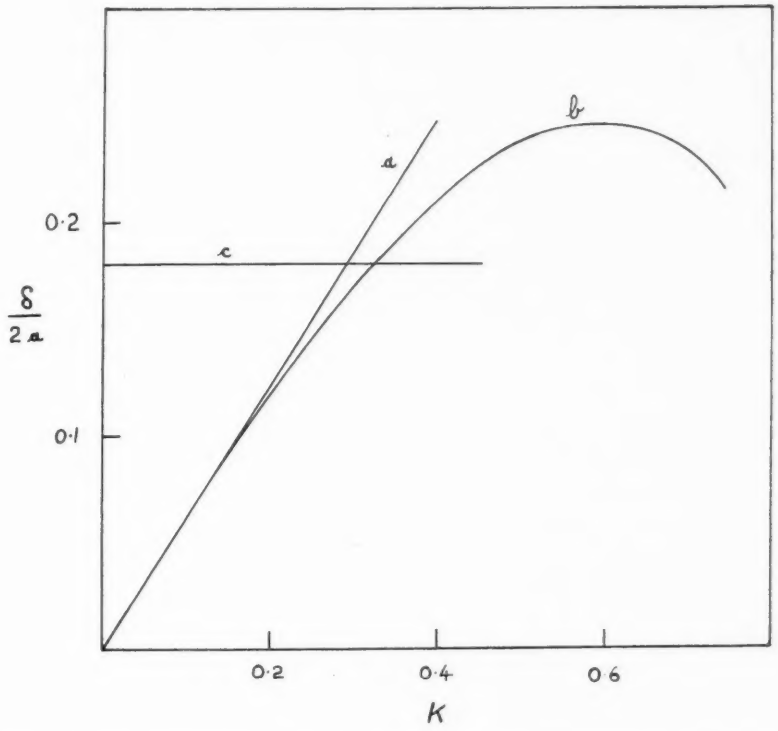

Figure 4. The displacement effect of a sphere: (*a*) first approximation neglecting $O(K^3)$; (*b*) next approximation neglecting $O(K^5)$; (*c*) experiment, flat-nosed pitot tube.

good agreement with experiment. However, as indicated in § 1, the displacement effect of a sphere is probably the same as that of a pitot tube of smaller diameter. Therefore, the initial gradient of $\delta/2a$ would be expected to be larger for a conventional pitot tube than for a sphere.

It may be concluded from the above results that the major part of the displacement effect of a pitot tube in a shear flow may be accounted for without the inclusion of viscosity; i.e. the vorticity field is of prime importance.

This work was done while the author was at the Fluid Motion Laboratory, University of Manchester. The author wishes to thank Professor M. J. Lighthill for suggesting the problem and for his continued interest and advice during the preparation of this paper.

Appendix. Shear flow past two-dimensional bodies

The flow pattern around a two dimensional body in a flow with constant rate of shear A is defined by a stream function ψ which is a solution of

$$\nabla^2\psi = -A, \tag{A. 1}$$

subject to the condition that ψ is constant on the surface of the body (e.g. Milne-Thomson 1949, p. 108). Since ψ is constant on any streamline the displacement δ of the stagnation streamline is obtained directly from the value of ψ on the surface of the body.

Solutions of (A. 1), and hence δ, are given below for a circular cylinder and for a parallel plate pitot tube.

(*a*) *The circular cylinder*

The centre of a circular cylinder of radius a is taken as the origin of coordinates r, θ, and the undisturbed flow has velocity $U + Ar\sin\theta$ in the direction $\theta = \pi$. The stream function for this flow is (Lamb 1932, Tsien 1943, Reichardt 1954)

$$\psi = -\tfrac{1}{4}A(r^2 - a^2) + \tfrac{1}{4}A\left(r^2 - \frac{a^4}{r^2}\right)\cos 2\theta - U\left(r - \frac{a^2}{r}\right)\sin\theta. \tag{A. 2}$$

Since ψ is zero on the cylinder, the displacement δ is the value of $r\sin\theta$ for which ψ is zero at infinity, so that

$$\tfrac{1}{4}Aa^2 - \tfrac{1}{2}A\delta^2 - U\delta = 0. \tag{A. 3}$$

Hence

$$\frac{\delta}{a} = K^{-1}\{-1 + \sqrt{(1 + \tfrac{1}{2}K^2)}\} \tag{A. 4}$$

$$\sim \tfrac{1}{4}K \quad \text{as } K \to 0. \tag{A. 5}$$

The negative square root has been discarded in (A. 4) because δ must be zero when K is zero. The variation of $\delta/2a$ with K is shown in figure 5.

An interesting deduction about the stagnation streamline can be made from (A. 2). The term $-\tfrac{1}{4}Aa^4r^{-2}\cos 2\theta$ represents the effects of the image vorticity inside the cylinder, which tends to deflect the oncoming flow downwards. But the doublet term $Ua^2r^{-1}\sin\theta$ tends to deflect the flow away from the axis. Hence, the stagnation streamline is the one on which these effects balance, i.e. the one on which

$$\frac{Ua^2}{r}\sin\theta - \frac{Aa^4}{4r^2}\cos 2\theta = 0. \tag{A. 6}$$

Therefore, if θ is always small on the stagnation streamline, the latter is straight and parallel to the axis at a distance $r\sin\theta$ from it, where

$$\frac{a}{r}\sin\theta = \tfrac{1}{4}K, \tag{A. 7}$$

in agreement with (A. 5). This result can also be obtained mathematically from (A. 2).

(*b*) *The parallel-plate pitot tube*

This idealized pitot tube consists of two semi-infinite flat plates at $y = \pm c$, stretching from $x = 0$ to $x = \infty$, with no net mass flow between the plates (cf. Lamb 1932, p. 75). The undisturbed flow has velocity in the positive x-direction.

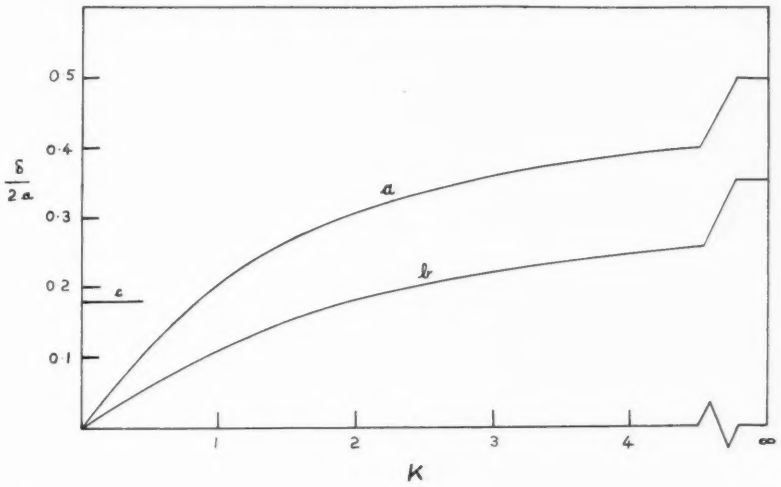

Figure 5. The displacement effect of two-dimensional bodies: (*a*) parallel plate pitot tube, distance $2a$ apart; (*b*) circular cylinder; (*c*) experimental result for flat-nosed axially symmetric pitot tube.

Let the stream function be ψ_0 when A is zero, where ψ_0 is zero on the surface of the body. At infinity, $\psi_0 \sim Uy$. Then, in the general case, the stream function is

$$\psi = \psi_0 + \tfrac{1}{2}A. \tag{A. 8}$$

The displacement δ must satisfy the equation

$$U\delta + \tfrac{1}{2}A(\delta^2 - c^2) = 0, \tag{A. 9}$$

whence

$$\frac{\delta}{c} = K^{-1}\{-1 + \sqrt{(1+K^2)}\} \tag{A. 10}$$

$$\sim \tfrac{1}{2}K \quad \text{as } K \to 0. \tag{A. 11}$$

Comparison of (A. 9) with (A. 3) shows that, for identical oncoming flows, the displacement effect of the cylinder is equal to that of the parallel plate pitot tube when

$$c = \frac{a}{\sqrt{2}}, \tag{A. 12}$$

i.e. when the diameter of the cylinder is $\sqrt{2}$ times the spacing of the plates.

Figure 5 shows that $\delta/2c$ always increases with K and only reaches 0·18 when $K = 0{\cdot}83$. Since the highest value of K used in the experiments of Young & Maas was 0·3, this solution does not afford an explanation of the displacement effect.

The above analysis is only slightly modified when the two-dimensional pitot tube is of arbitrary shape, provided that it consists of two parallel plates at infinity. These are at a distance $2c$ apart as before. In this case, the stream function is

$$\psi = \psi_0 + \tfrac{1}{2}Ay^2 + \psi_1, \tag{A. 13}$$

where ψ_0 is the stream function when A is zero, and ψ_1 is an irrotational stream function included to satisfy the boundary conditions. But, on the body, ψ_1 can differ from $-\frac{1}{2}Ac^2$ over a finite region only. Hence it must always take this value on the body, and the displacement effect is the same as before.

References

Hawthorne, W. R. 1954 *J. Aero. Sci.* **21,** 588.

Hawthorne, W. R. & Martin, M. E. 1955 *Proc. Roy. Soc.* A, **232,** 184.

Lamb, H. 1932 *Hydrodynamics*, 6th Ed. Cambridge University Press.

Lighthill, M. J. (Unpublished) To appear in *Aerofoil Theory* (Ed. B. Thwaites).

Milne-Thomson, L. M. 1949 *Theoretical Hydrodynamics*, 2nd Ed. London: Macmillan.

Nagamatsu, H. T. 1951 *J. Math. Phys.* **30,** 131.

Reichardt, H. 1954 *Mitt. a.d. Max Planck Inst. f. Stromungf.* 9.

Squire, H. & Winter, K. G. 1951 *J. Aero. Sci.* **18,** 271.

Tsien, H. S. 1943 *Quart. Appl. Math.* **1,** 130.

Young, A .D. & Maas, J. N. 1936 *Aero. Res. Counc., Lond., Rep.* & *Mem.* no. 1770.

The refraction of sea waves in shallow water

By M. S. LONGUET-HIGGINS
National Institute of Oceanography, Wormley

(*Received* 2 *December* 1955)

SUMMARY

This paper considers the changes that occur in the character of short-crested sea waves when they are refracted by a shallowing depth of water. Besides a change in mean wavelength and direction there is also a change (usually an increase) in the mean length of the crests. If the waves approach obliquely they become skew, that is, the crests become staggered one behind another.

When a short-crested sea is superposed on a long-crested swell, refraction tends to amplify the longer waves more than the shorter ones. This also produces an increase in the mean length of the crests.

Numerical examples are given.

INTRODUCTION

It is often noticed that sea waves tend to become more regular as they approach a coast, and that the length of the crests perpendicular to the direction of propagation appears to increase. Jeffreys (1924) considered two possible explanations: (1) non-linear effects reduce the short-crested waves by breaking, while the long-crested waves, being of smaller amplitude, do not break until later; (2) the reduction in depth has a greater magnifying effect on the long-crested waves than on the short-crested waves of the same period. On the basis of theoretical analysis, Jeffreys decided in favour of the first alternative.

There are other possible causes, however. The most important of these, now to be considered, is the refraction of the waves on entering shallow water.

It is well known that when waves enter shallow water their velocity and wavelength decrease; also, if they approach obliquely, the direction of the crests changes so as to become nearly parallel to the shore. But in general the crest-length also changes. If the water surface were a simple sine-wave, the waves would be infinitely long-crested and would remain so after refraction. But in fact the sea surface must be thought of as the sum of a whole spectrum of harmonic components having different wavelengths and directions; the 'long-crestedness' depends on the angular deviation of the wave components from the mean direction: the smaller the deviation, the greater is the ratio of mean crest-length to mean wavelength. Refraction thus affects the crest-length in the following two ways.

(1) Wave components of the same wavelength and different direction are 'collimated' so as to become more nearly parallel to the coast and to one another; this tends to diminish the angular deviation of the wave components and to make the waves more long-crested (§ 2 (*a*)).

(2) Wave components in the same direction but of different wavelength are refracted through different angles and so separated (as in the separation of white light by a prism); this tends to increase the angular deviation of the wave components and to make the waves more short-crested (§ 2 (*b*)).

The two effects (collimation and separation) are illustrated in § 2 by considering a sea made up of just two harmonic components. The full representation of the sea surface, which requires a continuous spectrum of harmonic components, is discussed in § 3. In general, the mean wavelength, mean crest-length, etc., must be defined statistically (see Longuet-Higgins 1956 a*). The changes in these quantities are deduced in § 4 and § 5, and a numerical example is given in § 6.

One of the more interesting consequences of refraction is that waves which were originally symmetrical about their mean direction become skew, i.e. the principal direction of the wave envelope is in a different direction to that of the crests. The waves then tend to line up in an échelon pattern, each wave crest being displaced (on the average) sideways relative to the preceding crest.

The change in the amplitude of the waves is also studied, and it is shown that the increase in amplitude may itself be considered as a result of refraction.

Finally, in § 7, we consider what happens when two distinct bands of swell, of different wavelength, are present in the spectrum. For example, swell from a distant storm may be present simultaneously with shorter waves due to local winds. In general, the longer waves are amplified more than the shorter waves, and so, since the longer waves are usually also more long-crested, there is an increase in the average crest-length. We calculate the extent of this increase and give a numerical example.

1. Refraction of a simple wave train

Consider a single, infinitely long-crested train of waves of wavelength $\lambda = 2\pi/w$ and period $\tau = 2\pi/\sigma$ approaching a straight coast at an angle θ to the normal (see figure 1 (*a*)). If the depth of water varies gradually the wavelength will be related to the local depth h by the equation (see Lamb 1932, ch. 9)

$$w \tanh wh = \frac{\sigma^2}{g} = w', \tag{1.1}$$

where g denotes gravity and a prime ($'$) denotes the value in deep water. The direction θ will depend on the wavelength according to Snell's law:

$$\frac{\sin\theta}{\sin\theta'} = \frac{\lambda}{\lambda'} = \frac{w'}{w}, \tag{1.2}$$

which may also be written

$$w \sin\theta = w' \sin\theta' = \text{constant}, \tag{1.3}$$

that is, the wave-number parallel to the coast is a constant.

* This paper will subsequently be referred to as I.

We shall find it useful to represent the waves by a point P in a wave-number diagram as in figure 1(*b*): the direction of OP is opposite to the direction of propagation of the waves, and the length of OP is w, the wave-number in the direction of propagation. It may easily be shown that the wave-number in any other direction is the projection of OP in that direction; in particular the coordinates

$$(u, v) = (w\cos\theta, w\sin\theta) \tag{1.4}$$

are the wave-numbers perpendicular and parallel to the coast.

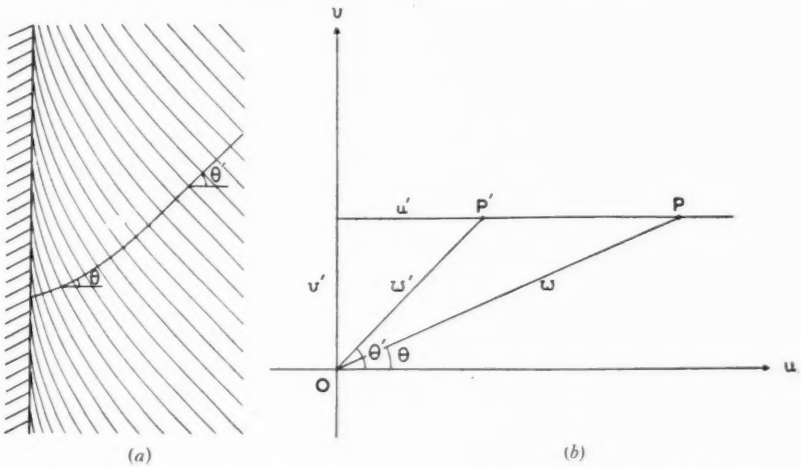

(*a*) (*b*)

Figure 1. (*a*) A regular, long-crested train of waves approaching a straight coast; (*b*) its representation in the wave-number diagram.

Let $P' = (u', v')$, represent the wave train in deep water, and $P = (u, v)$ the refracted waves. Then, by (1.1),

$$\frac{OP}{OP'} = \frac{w}{w'} = \coth wh > 1, \tag{1.5}$$

and, by (1.3)

$$v = v', \tag{1.6}$$

so that the effect of refraction is to displace the representative point P *away from the origin and parallel to the axis of u.*

2. Two long-crested wave trains

Two effects of refraction can be simply seen by considering the sum of a pair of long-crested wave trains in the following two cases.

(*a*) *Wave trains having the same wave-number w and slightly different directions* θ *and* $\theta + \delta\theta$

The sum of two such trains is a short-crested pattern whose wave-number is w in a direction perpendicular to the crests and $w\delta\theta$ along the crests (see figure 2(*a*)). The ratio of the wavelength to the crest-length is $\delta\theta$. Let

the two wave trains be represented by points P_1 and P_2 in the wave-number diagram (figure 2(*b*)). Then $OP_1 = OP_2 = w$ and $\angle P_1OP_2 = \delta\theta$. Also $P_1P_2 = w\,\delta\theta$, the wave-number along the crests. Now refraction displaces P_1 and P_2 parallel to the u-axis, and

$$\frac{P_1P_2}{P_1'P_2'} = \frac{\delta v \sec\theta}{\delta v \sec\theta'} = \frac{\cos\theta'}{\cos\theta} < 1, \tag{2.1}$$

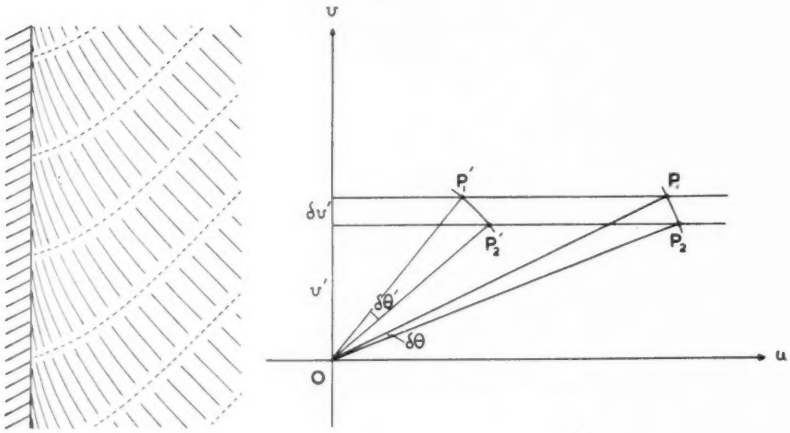

(*a*) (*b*)

Figure 2. (*a*) The pattern of crests formed by two wave trains of equal wavelength and slightly different direction ; (*b*) their representation in the wave-number diagram.

since $\theta < \theta'$. Therefore, refraction increases the length of the crests, though the wavelength is diminished. The angle between the component wave trains, which is equal to P_1P_2/OP_1, is also diminished.

(*b*) *Wave trains having the same direction* θ *but different wave-numbers* w *and* $w + \delta w$

The sum of two such waves is a pattern which is long-crested but of varying amplitude, the waves coming in 'groups' of length $\pi/\delta w$. In the wave-number diagram the unrefracted waves are represented by two points P_1' and P_2' on the same line through the origin (figure 3 (*b*)) and with $P_1'P_2' = \delta w'$. However, (if P_1 and P_2 represent the refracted waves) P_1P_2 does not in general pass through O; for in that case we should have $\delta w/w = \delta v/v = \delta w'/w'$ and so $\delta w'/\delta w = w'/w$, whereas in fact we have, on differentiating equation (1.1),

$$\frac{\delta w'}{\delta w} = \tanh wh + wh\,\mathrm{sech}^2 wh > \tanh wh = \frac{w'}{w}. \tag{2.2}$$

Hence P_1P_2 subtends a positive angle at the origin, and the refracted wave trains have differing directions. Thus the refracted pattern is short-crested, i.e. the crest-length is reduced.

Since the refracted waves are also of different wavelength, the resulting pattern is 'staggered' (see I). A similar effect has been pointed out by Stoneley (1935) in connection with seismic waves refracted at a discontinuity.

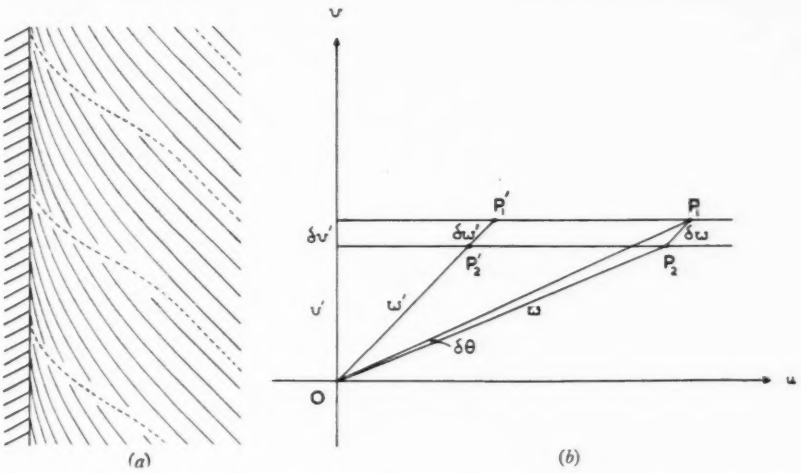

Figure 3. (*a*) The pattern of crests formed by two wave trains initially in the same direction and of slightly different wavelength ; (*b*) their representation in the wave-number diagram.

3. General representation

To describe actual, irregular sea waves we use the representation described in I. It is assumed that the waves in any given locality are statistically uniform, and that they contain wave components of every possible wavelength and direction. Corresponding to each wave number (u, v) we define the energy density $E(u, v)$ such that $E\,dudv$ is the energy associated with wave-numbers in a small region $dudv$ of the (u, v)-plane. Thus the total energy per unit of the sea surface, for example, is given by

$$\mu = \int_{-\infty}^{\infty}\int_{-\infty}^{\infty} E(u, v)\,dudv. \tag{3.1}$$

Many of the frequency characteristics of the sea surface may be derived in terms of E (see I). Here we shall make the assumption that the spectrum is narrow, i.e. that the energy E is mainly clustered near the mean wave-number $(\bar{u}, \bar{v})$, defined by

$$\int_{-\infty}^{\infty}\int_{-\infty}^{\infty} (u-\bar{u})\,E\,dudv = \int_{-\infty}^{\infty}\int_{-\infty}^{\infty} (v-\bar{v})\,E\,dudv = 0. \tag{3.2}$$

The waves are then more or less long-crested, having a mean wave-number $\bar{w}$ in the direction $\bar{\theta}$ perpendicular to the crests, where

$$(\bar{u}, \bar{v}) = (\bar{w}\cos\bar{\theta}, \bar{w}\sin\bar{\theta}) \tag{3.3}$$

(see figure 4). Let coordinates (ξ, η) be taken with origin at the mean point and with ξ and η measured along and perpendicular to $\mathrm{O\overline{P}}$, so that, approximately,

$$\left.\begin{aligned} \xi &= w - \overline{w} = \delta w, \\ \eta &= \overline{w}(\theta - \bar{\theta}) = \overline{w}\,\delta\theta, \end{aligned}\right\} \tag{3.4}$$

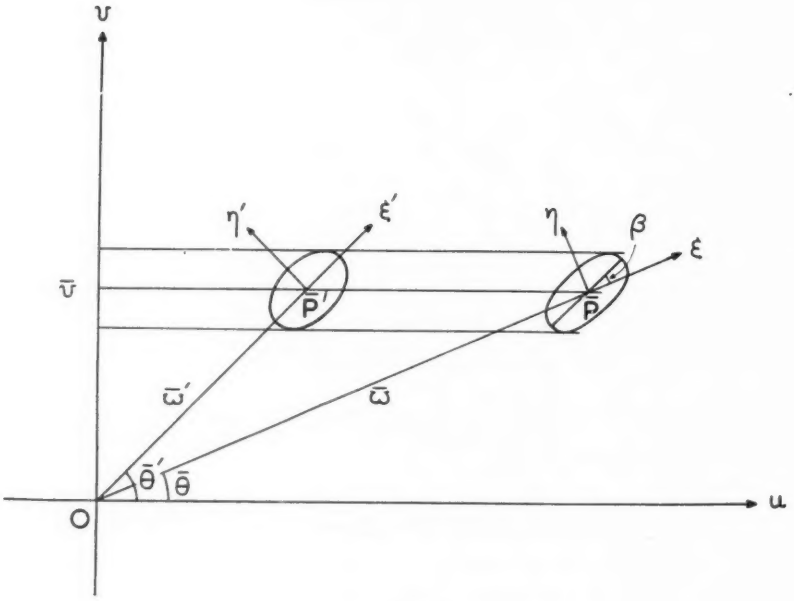

Figure 4. The effect of refraction on a continuous spectrum.

say. We define the moments

$$\left.\begin{aligned} \mu_{20} &= \int_{-\infty}^{\infty}\int_{-\infty}^{\infty} \xi^2 E\, d\xi d\eta, \\ \mu_{11} &= \int_{-\infty}^{\infty}\int_{-\infty}^{\infty} \xi\eta E\, d\xi d\eta, \\ \mu_{02} &= \int_{-\infty}^{\infty}\int_{-\infty}^{\infty} \eta^2 E\, d\xi d\eta, \end{aligned}\right\} \tag{3.5}$$

an interpretation of which is as follows (see I). First,

$$\mu_{20} = \mu\overline{w}^2\nu^2, \tag{3.6}$$

where ν is the r.m.s. proportional spread in wave-number in a direction perpendicular to the crests; ν is inversely proportional to the average number of waves in a 'group'. Secondly,

$$\mu_{02} = \mu\overline{w}^2\gamma^2, \tag{3.7}$$

where γ is the r.m.s. angular deviation of the waves from their mean direction; it may be shown that

$$\gamma = \frac{N_{\min}}{N_{\max}}, \tag{3.8}$$

where $N_{\max}$ is the average number of times per unit distance that the surface crosses a line at mean level perpendicular to the crests, and $N_{\min}$ is the corresponding number for a line parallel to the crests. Thus if $\bar{\lambda}$ is the mean wavelength and $\bar{\kappa}$ the mean crest-length,

$$\bar{\lambda} = 2/N_{\max}, \quad \bar{\kappa} = 2/N_{\min}, \quad \gamma = \bar{\lambda}/\bar{\kappa}. \tag{3.9}$$

Thirdly,

$$\mu_{11} = \mu\overline{w}^2(\nu^2-\gamma^2)q, \tag{3.10}$$

where q is a measure of the *skewness* of the waves; it may be shown that

$$q = \tfrac{1}{2}\tan 2\beta, \tag{3.11}$$

where β is the angle between the mean direction of the waves and the principal direction of their *envelope* (see I).

4. Changes due to refraction

If the wave amplitude is sufficiently small, the energy corresponding to each wave-number is refracted independently. Further, it is assumed that the energy reflected from the coast is negligible. Under these conditions, it may be shown (see Longuet-Higgins 1956 b) that if $E'(u, v)$ denotes the energy density before refraction and $E(u, v)$ the energy density after refraction, then E is related simply to E' by

$$E(u, v) = E'(u', v'), \tag{4.1}$$

where (u, v) is related to (u', v') as in § 1. Hence a contour of energy density $E' =$ constant is transformed into a contour $E =$ constant (see figure 4), though the area enclosed by the contour may be changed, as also may be its shape.

We shall consider how the parameters μ, ν, γ, q defined above will change on refraction of the waves. Let (ξ', η') be coordinates defined for the unrefracted waves similarly to (ξ', η') for the refracted waves (equations (3.4)). Now, to the first order of small quantities,

$$\delta w = \frac{dw}{dw'}\,\delta w', \tag{4.2}$$

where from (1.1)

$$\frac{dw}{dw'} = \frac{1}{\tanh wh + wh\,\mathrm{sech}^2 wh}. \tag{4.3}$$

Also, on differentiating (1.2) logarithmically, we have

$$\frac{\delta\theta}{\tan\theta} - \frac{\delta\theta'}{\tan\theta'} = \delta w - \delta w', \tag{4.4}$$

and so, using (4.2) and (1.2),

$$w\,\delta\theta = \left(\frac{w}{w'} - \frac{dw}{dw'}\right)\tan\theta\,\delta w' + \frac{w}{w'}\,\frac{\tan\theta}{\tan\theta'}\,w'\,\delta\theta'. \tag{4.5}$$

Equations (4.2) and (4.5) may be written

$$\left.\begin{aligned} \xi &= \alpha_{11}\xi' + \alpha_{12}\eta', \\ \eta &= \alpha_{21}\xi' + \alpha_{22}\eta', \end{aligned}\right\} \tag{4.6}$$

where

$$\left.\begin{aligned} \alpha_{11} &= \frac{\partial\xi}{\partial\xi'} = \frac{dw}{dw'}, & \alpha_{12} &= \frac{\partial\xi}{\partial\eta'} = 0, \\ \alpha_{21} &= \frac{\partial\eta}{\partial\xi'} = \left(\frac{w}{w'} - \frac{dw}{dw'}\right)\tan\theta, & \alpha_{22} &= \frac{\partial\eta}{\partial\eta'} = \frac{w}{w'}\,\frac{\tan\theta}{\tan\theta'}. \end{aligned}\right\} \tag{4.7}$$

Therefore,

$$\frac{\partial(\xi,\eta)}{\partial(\xi',\eta')} = \alpha_{11}\alpha_{22}. \tag{4.8}$$

Over the narrow region of integration, $\alpha_{11}, \alpha_{12}, \alpha_{21}, \alpha_{22}$ may be treated as constants. Hence, on changing the variable in (3.1) and remembering (4.1), we have

$$\mu = \alpha_{11}\alpha_{22}\mu'; \tag{4.9}$$

similarly, from (3.5) we find

$$\left.\begin{aligned} \mu_{20} &= \alpha_{11}\alpha_{22}(\alpha_{11}^2\mu'_{20}), \\ \mu_{11} &= \alpha_{11}\alpha_{22}(\alpha_{11}\alpha_{21}\mu'_{20} + \alpha_{11}\alpha_{22}\mu'_{11}), \\ \mu_{02} &= \alpha_{11}\alpha_{22}(\alpha_{21}^2\mu'_{20} + 2\alpha_{21}\alpha_{22}\mu'_{11} + \alpha_{22}^2\mu'_{02}), \end{aligned}\right\} \tag{4.10}$$

where μ' is the initial value of μ, and so on. Thus ν, q, γ are transformed as follows:

$$\left.\begin{aligned} \nu^2 &= \frac{w'^2}{w^2}\alpha_{11}^2\nu'^2, \\ (\nu^2-\gamma^2)q &= \frac{w'^2}{w^2}[\alpha_{11}\alpha_{21}\nu'^2 + \alpha_{11}\alpha_{22}(\nu'^2-\gamma'^2)q'], \\ \gamma^2 &= \frac{w'^2}{w^2}[\alpha_{21}^2\nu'^2 + 2\alpha_{21}\alpha_{22}(\nu'^2-\gamma'^2)q' + \alpha_{22}^2\gamma'^2], \end{aligned}\right\} \tag{4.11}$$

(the bar in $\overline{w}$ has been dropped). We may assume that q', the skewness of the unrefracted waves, is zero. Then, on inserting the values of $\alpha_{11}, \alpha_{12}, \alpha_{22}$ in (4.11), we have

$$\left.\begin{aligned} \nu^2 &= r^2\nu'^2 \\ (\nu^2-\gamma^2)q &= r(1-r)\tan\theta\,\nu'^2 \\ \gamma^2 &= (1-r)^2\tan^2\theta\,\nu'^2 + \frac{\tan^2\theta}{\tan^2\theta'}\,\gamma'^2 \end{aligned}\right\} \tag{4.12}$$

where

$$r = \frac{w'}{w}\,\frac{dw}{dw'} \tag{4.13}$$

and θ is given by Snell's law (1.2).

5. Discussion

The first of equations (4.12) gives

$$\nu = r\nu', \tag{5.1}$$

that is to say, the average number of waves in a group is divided by r on refraction. Now, from (4.13), the factor r may be written

$$r = \frac{\sigma/w}{d\sigma/dw} \div \frac{\sigma'/w'}{d\sigma'/dw'} \tag{5.2}$$

since, if the frequencies are preserved, $\sigma = \sigma'$. But σ/w and $d\sigma/dw$ are the phase-velocity and group-velocity respectively, whose ratio varies from 2 in deep water to 1 in shallow water (see Lamb 1932, ch. 9). Thus in shallow water $r = 1/2$, and hence the number of waves in a group is doubled when the waves reach shallow water. (This effect was noticed by Barber (1950) in the case when the waves approach the shore normally.) However, if the waves were recorded in time at a fixed point, the groups in the record would appear to have the same average number of waves, regardless of the depth of water.

Equations (4.12) show that ν and q depend only on ν', the initial spread in wave-number, but that γ has a contribution from both ν' and γ'. By setting $\gamma' = 0$ and $\nu' = 0$ in turn, we see that γ may be either greater or less than γ'.

The average length of the crests is given by

$$\bar{\kappa} = \bar{\lambda}/\gamma = 2\pi/\gamma w. \tag{5.3}$$

So from the third of equations (4.12) we have

$$\frac{1}{\bar{\kappa}^2} = \frac{1}{4\pi^2}(1-r^2)w^2\nu'^2\tan^2\theta + \frac{\cos^2\theta'}{\cos^2\theta}\frac{1}{\bar{\kappa}'^2}, \tag{5.4}$$

which shows that the mean crest-length, also, may be either increased or decreased by refraction.

A particularly simple case is when θ' is small, or when the wave crests are nearly parallel to the coast. Then from (1.3),

$$w\theta = w'\theta', \tag{5.5}$$

approximately, and from (4.12) and (5.4),

$$\gamma^2 = \frac{w'^2}{w^2}\gamma'^2, \quad \bar{\kappa} = \bar{\kappa}' \tag{5.6}$$

(assuming $\nu'\theta' \ll \gamma'$). Thus the average crest-length remains unchanged, although the average wavelength and the angular deviation are both diminished.

The wave amplitude

The change in amplitude of the waves may be found as follows. If a denotes the r.m.s. wave amplitude, the mean energy per unit area of the sea surface is $\frac{1}{2}\rho g a^2$. But this is equal to μ, by definition. Therefore, from (4.9),

$$\frac{a^2}{a'^2} = \frac{\mu}{\mu'} = \alpha_{11}\,\alpha_{22} = \frac{dw}{dw'}\frac{\cos\theta'}{\cos\theta} \tag{5.7}$$

and

$$a = a'\left(\frac{dw}{dw'}\frac{\cos\theta'}{\cos\theta}\right)^{1/2}. \tag{5.8}$$

Equation (5.7) is a generalization of the well-known formula (Burnside 1914) for the change in amplitude of waves approaching a coast normally; on setting $\theta = \theta' = 0$, we obtain Burnside's equation (ii). Since, in general $\cos\theta > \cos\theta'$, we deduce that waves approaching a coast obliquely are amplified less than those approaching normally.

To facilitate numerical calculation, we have plotted in figure 5 graphs of

$$\frac{w'}{w} = \tanh wh \tag{5.9}$$

and

$$r = (1 + 2wh \operatorname{cosech} 2wh)^{-1} \tag{5.10}$$

as functions of $w'h = \sigma^2 h/g$. The amplitude function

$$\left(\frac{dw}{dw'}\right)^{1/2} = (rw/w')^{1/2} \tag{5.11}$$

is also shown. When $w'h$ is large, these all tend to unity.

When $w'h$ is small, we have

$$\frac{w'}{w} \sim (w'h)^{1/2}, \qquad \nu \sim \tfrac{1}{2}, \qquad \left(\frac{dw}{dw'}\right)^{1/2} \sim \frac{(w'h)^{-1/4}}{\sqrt{2}} \tag{5.12}$$

(as was first shown by Green, 1838). However, the present linear approximation is only valid so long as

$$a \ll \tfrac{4}{3} w^2 h^3 \tag{5.13}$$

(Stokes 1847, Ursell 1953), which implies that

$$a' \ll \frac{4\sqrt{2}}{3} (w'h)^{5/4} h \frac{\cos\theta}{\cos\theta'}. \tag{5.14}$$

If this condition is not satisfied, the waves will depart from the sinusoidal form, and may become solitary waves or may break.

6. Numerical example

Suppose that waves of mean period 10 sec approach the shore initially at an angle of 60° to the normal:

$$\sigma = \frac{2\pi}{10} \text{sec}^{-1}, \qquad w' = \frac{\sigma^2}{g} = 0{\cdot}012 \text{ ft}^{-1}, \qquad \theta' = 60°.$$

When the waves have reached water of depth $h = 20$ ft we have $w'h = 0{\cdot}25$ and so, from figure 5,

$$\frac{w'}{w} = 0{\cdot}48, \qquad r = 0{\cdot}54, \qquad \left(\frac{dw}{dw'}\right)^{1/2} = 1{\cdot}07.$$

The angle θ between the wave crests and the shore is given by

$$\sin\theta = 0{\cdot}48 \sin 60° = 0{\cdot}42, \qquad \theta = 24°.$$

Let the initial spread in wave-number be one-quarter of the mean wave-number, and the initial spread in direction be 15°:

$$\nu' = 0{\cdot}25, \qquad \gamma' = 0{\cdot}26.$$

Then, assuming that $q' = 0$, we have from (4.12)

$$\nu = 0{\cdot}135, \qquad \gamma = 0{\cdot}088, \qquad q = 0{\cdot}68.$$

Therefore, the angular spread is reduced by a factor $\gamma/\gamma' = 0{\cdot}30$.

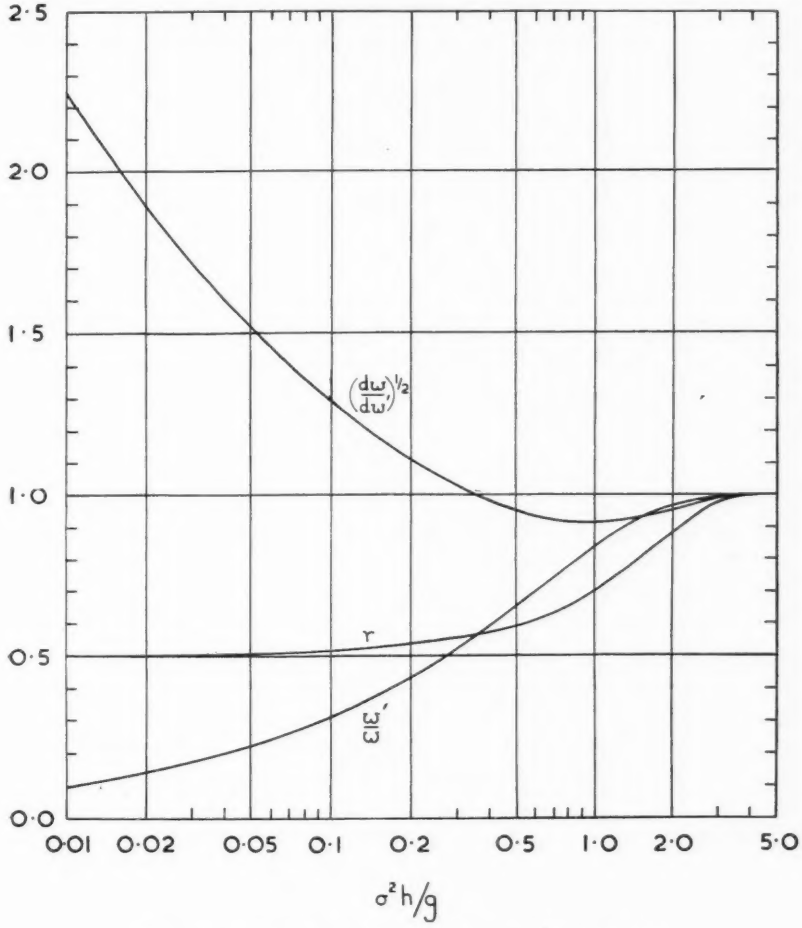

Figure 5. Graphs of the functions w'/w, r and $(dw/dw')^{1/2}$.

Taking account of the reduction in mean wavelength ($w'/w = 0{\cdot}48$), we see that the mean length of the crests is multiplied by 1·6, i.e. increased by 60%.

From (3.10), we find for the angle of skewness

$$\beta = 27°,$$

and from (5.8),

$$a = 0{\cdot}79a'.$$

Thus the r.m.s. wave amplitude is reduced by 21%, although if the waves approached the coast normally it would be increased by 7%.

Equation (5.14) shows that, for the analysis to be valid, the amplitude a' in deep water must be small compared with 11 ft.

7. A MIXED SPECTRUM

So far we have supposed that the distribution of energy is narrowly restricted in wave-number and direction. It is interesting, however, to consider the changes due to refraction when the sea consists of a long-crested swell superposed on short-crested local waves. Under these conditions, the swell may be expected to be amplified more than the local waves, producing an increase in the length of the crests.

Let the energy function E consist of two parts, E_1 and E_2, which represent respectively a narrow band of swell, of total energy μ_1 and a local, fairly short-crested, sea of total energy μ_2.

For simplicity, we suppose that both systems of waves are approaching the coast normally.

The average number of zero-crossings along a line parallel to the crests will be denoted simply by N (so that $N = N_{\min}$). It can be shown (see I) that

$$\mu N^2 = \frac{1}{\pi^2}\int_{-\infty}^{\infty}\int_{-\infty}^{\infty}\eta^2 E\, d\xi d\eta. \tag{7.1}$$

So, if N_1 and N_2 denote the corresponding numbers for the two component systems,

$$\left.\begin{aligned}\mu N^2 &= \mu_1 N_1^2 + \mu_2 N_2^2,\\ \mu &= \mu_1 + \mu_2,\end{aligned}\right\} \tag{7.2}$$

giving

$$N^2 = \frac{\mu_1 N_1^2 + \mu_2 N_2^2}{\mu_1 + \mu_2}, \tag{7.3}$$

or, if a_1, a_2 are the corresponding r.m.s. wave amplitudes,

$$N^2 = \frac{a_1^2 N_1^2 + a_2^2 N_2^2}{a_1^2 + a_2^2}. \tag{7.4}$$

The amplitudes and wave-numbers are transformed (approximately) as follows:

$$\left.\begin{aligned}N_1 &= N_2', \qquad a_1 = \left(\frac{dw_1}{dw_1'}\right)^{1/2} a_1',\\ N_2 &= N_2', \qquad a_2 = \left(\frac{dw_2}{dw_2'}\right)^{1/2} a_2',\end{aligned}\right\} \tag{7.5}$$

where w_1, w_1', w_2, w_2' are the values of w and w' for the two groups. These relations enable us to determine N in terms of the initial values of a_1, a_2, N_1 and N_2.

For example, suppose that the mean periods of the two bands are 12 sec and 6 sec, respectively, and their r.m.s. angular widths are 10° and 20°. Then we have

$$w_1' = 8{\cdot}5 \times 10^{-3}\,\text{ft}^{-1}, \qquad N' = 4{\cdot}7 \times 10^{-4}\,\text{ft}^{-1},$$
$$w_2' = 3{\cdot}4 \times 10^{-2}\,\text{ft}^{-1}, \qquad N_2' = 3{\cdot}8 \times 10^{-3}\,\text{ft}^{-1},$$

and, if the wave amplitudes are initially equal, the crest-length is given by

$$N'^2 = \tfrac{1}{2}(N_1^2 + N_2^2) = 7{\cdot}2 \times 10^{-6}\,\text{ft}^{-2}.$$

By the time the waves have reached water of depth 10 ft. the amplitudes of the swell and the local sea are increased by 1·35 and 1·01 respectively, and we find

$$N^2 = 6{\cdot}3 \times 10^{-6}\,\text{ft}^{-2}.$$

Hence the mean crest-length is multiplied by 1·07, i.e. increased by 7%.

8. Conclusions

We have shown that, when a band of waves which has a fairly narrow spectrum in both wavelength and direction enters shallow water, the following changes occur.

(1) The mean wavelength decreases and the direction of the crests becomes more nearly parallel to the shore.

(2) The crests become 'staggered', i.e. the envelope of the waves is in a different direction to the direction of the crests.

(3) The mean crest-length may either increase or decrease, usually the former: if the waves are incident normally, the average crest-length remains unaltered. The ratio of crest-length to wavelength almost always increases.

(4) The number of waves in a group is increased, being multiplied by 2 when the waves reach shallow water.

(5) The amplitude of the waves first diminishes and then increases, being proportional to $h^{-1/4}$ in shallow water. The increase is less for waves approaching obliquely.

If the spectrum of the waves is not narrow, or if more than one narrow band is present, we may expect that the longer waves will eventually be amplified more than the shorter ones. Since the longer waves usually have a much greater crest-length than the shorter waves, this leads to an increase in the crest-length.

The above conclusions suggest two possible reasons for the frequently observed change in crest-length as the waves approach the shore. The first is the simple effect of refraction, as described in § 4 and § 5. The second is the relative amplification of a long band of swell, which might be hidden in deeper water off-shore.

Our quantitative analysis is applicable only so long as the waves are fairly low (see equation (5.14)), and does not apply to waves in shallow water

which have steepened at their crests, still less to breaking waves. For these, some of the effects described may still be true qualitatively, but non-linear effects such as those pointed out by Jeffreys (1924) must also be taken into account.

Appendix

Some of the effects described in the present paper are clearly illustrated by the aerial photograph shown in plate 1, for which I am indebted to Mr W. W. Williams. This shows a very regular swell approaching a coastline in a gradually diminishing depth of water. Not only do the mean wavelength and direction vary, but it will be seen that the wave crests arrange themselves in an échelon pa.tern with an angle of skewness that becomes very pronounced inshore. Lines of low wave amplitude may be traced visually over limited distances, and are not unlike those in figure 3 (*a*).

References

Barber, N. F. 1950 Ocean waves and swell. Lecture published by Institution of Civil Engineers, London.

Burnside, W. 1915 On the modification of a train of waves as it advances into shallow water, *Proc. Lond. Math. Soc.* (2), **14,** 131.

Green, G. 1838 On the motion of waves in a variable canal of small depth and width, *Trans. Camb. Phil. Soc.* **6,** 457.

Jeffreys, H. 1924 On water waves near the shore, *Phil. Mag.* (6), **48,** 44.

Lamb, H. 1932 *Hydrodynamics,* 6th ed. Cambridge University Press.

Longuet-Higgins, M. S. 1956 a The statistical analysis of a random moving surface, *Phil. Trans.* A (in press).

Longuet-Higgins, M. S. 1956 b On the transformation of a continuous spectrum by refraction, *Proc. Camb. Phil. Soc.* (in press).

Stokes, G. G. 1847 On the theory of oscillatory waves, *Trans. Camb. Phil. Soc.* **8,** 441. *Mathematical and Physical Papers,* **1,** 197. Cambridge University Press.

Stoneley, R. 1935 The refraction of a wave group, *Proc. Camb. Phil. Soc.* **31,** 360.

Ursell, F. 1953 The long-wave paradox in the theory of gravity waves, *Proc. Camb. Phil. Soc.* **49,** 685.

Plate 1. Aerial photograph of regular swell approaching a coastline obliquely.

On steady laminar flow with closed streamlines at large Reynolds number

By G. K. BATCHELOR
Cavendish Laboratory, Cambridge

(*Received* 19 *December* 1955)

SUMMARY

Frictionless flows with finite vorticity are usually made determinate by the imposition of boundary conditions specifying the distribution of vorticity 'at infinity'. No such boundary conditions are available in the case of flows with closed streamlines, and the velocity distributions in regions where viscous forces are small (the Reynolds number of the flow being assumed large) cannot be made determinate by considerations of the fluid as inviscid. It is shown that if the motion is to be exactly steady there is an integral condition, arising from the existence of viscous forces, which must be satisfied by the vorticity distribution no matter how small the viscosity may be. This condition states that the contribution from viscous forces to the rate of change of circulation round any streamline must be identically zero. (In cases in which the vortex lines are also closed, there is a similar condition concerning the circulation round vortex lines.)

The inviscid flow equations are then combined with this integral condition in cases for which typical streamlines lie entirely in the region of small viscous forces. In two-dimensional closed flows, the vorticity is found to be uniform in a connected region of small viscous forces, with a value which remains to be determined—as is done explicitly in one simple case—by the condition that the viscous boundary layer surrounding this region must also be in steady motion. Analogous results are obtained for rotationally symmetric flows without azimuthal swirl, and for a certain class of flows with swirl having no interior boundary to the streamlines in an axial plane, the latter case requiring use of the fact that the vortex lines are also closed. In all these cases, the results are such that the Bernoulli constant, or 'total head', varies linearly with the appropriate stream function, and the effect of viscosity on the rate of change of vorticity at any point vanishes identically.

1. GENERAL REMARKS

The work described herein concerns the steady laminar motion of fluids of small viscosity, and is based on the generally accepted premise that, when the Reynolds number of a flow field is very large, viscous forces acting on the

fluid are small everywhere, except perhaps in the neighbourhood of certain surfaces in the fluid. 'Small viscous forces' here means forces that are small compared with unity when made non-dimensional using a length and a velocity typical of the flow as a whole (those used in the definition of Reynolds number would be suitable). It will usually happen that pressure forces on the fluid are of order unity when made non-dimensional in this same way, and the above premise is then equivalent to the statement that viscous forces are small compared with pressure forces nearly everywhere.

It is well known, partly as a matter of observation and partly from mathematical analysis, that, for certain steady flow fields amenable to study, the above premise is undoubtedly true. It seems that, if the Reynolds number of the flow is allowed to approach infinity, without any other change in the conditions of these flow fields, the region of the fluid in which viscous forces are not small becomes smaller and smaller, and ultimately reduces, at most, to a number of thin layers, usually in the form of boundary layers and wakes. In the limit of infinite Reynolds number, the region in which viscous forces are not small either disappears altogether or becomes a number of stream-surfaces (i.e. surfaces whose tangent planes everywhere contain the local velocity vector), which usually coincide with, or are connected with, rigid boundaries in the fluid. Across such singular stream-surfaces there may be a discontinuity in velocity, as for instance at a rigid boundary where the presence of a singular stream-surface ensures that the no-slip condition is satisfied even in the limit of zero viscosity. In what follows, the above-mentioned premise will simply be accepted as valid generally.

We shall consider those steady flows that take place in a confined region, the motion of the fluid being generated by steady tangential motion of the surrounding boundaries (which need not all be rigid). It will be assumed that the Reynolds number is large enough for the thicknesses of the associated viscous layers to be small compared with the linear dimensions of the region of fluid under consideration. It will also be assumed that the motion of the fluid is laminar, despite the high Reynolds number (which clearly will correspond with reality only if the velocity distribution happens to have strong inherent stability). Most of the flows of this type that are capable of practical reproduction involve plane rigid boundaries moving in their own planes, or rigid surfaces of revolution rotating about their axes. Cases in which part of the boundary is rigid and stationary, the remaining part of the boundary of the region of closed streamlines being a 'free boundary layer' —for example, the motion in a cavity opening off a plane wall over which fluid is streaming—are of interest in a wide range of practical problems in aerodynamics and hydraulics. Examples of steady flow in a closed region are not common, but they perhaps occur often enough in practice to warrant notice of their peculiar features.

The equations governing the steady laminar motion of a uniform incompressible fluid are

$$\nabla.\mathbf{u} = 0, \tag{1.1}$$

$$\mathbf{u}\times\boldsymbol{\omega} - \nabla(p/\rho + \tfrac{1}{2}q^2) + \nu\nabla^2\mathbf{u} = \partial\mathbf{u}/\partial t = 0, \tag{1.2}$$

where $\boldsymbol{\omega} = \nabla \times \mathbf{u}$, $q = |\mathbf{u}|$, and the other symbols have their usual meanings. When the Reynolds number of the motion is large, viscous forces, according to our premise, are small everywhere except in the neighbourhood of certain singular surfaces, and equation (1.2) reduces approximately to

$$\mathbf{u} \times \boldsymbol{\omega} = \nabla H, \tag{1.3}$$

where $H = p/\rho + \frac{1}{2}q^2$ is the local 'total head' in the fluid. H is here constant over stream-vortex surfaces, or 'Bernoulli surfaces', each such surface containing the local vectors $\mathbf{u}$ and $\boldsymbol{\omega}$ in its tangent plane everywhere and being swept out by a material vortex line. When $\nu = 0$, stream-vortex surfaces will not exist, in general, because $\mathbf{u} \times \boldsymbol{\omega}$ is then (see (1.2)) not necessarily parallel everywhere to the gradient of some scalar function.

It is well known that equation (1.3), which is approximately valid everywhere except in the neighbourhood of the singular surfaces, is not sufficient to allow the velocity distribution to be determined from the condition of zero normal velocity at specified boundaries in the field. In the case of two-dimensional steady motion, the indeterminacy takes a form such that the vorticity—which is constant along a streamline—may vary arbitrarily from one streamline to another. It often happens that the inviscid flow equations can be made sufficient to determine $\mathbf{u}$ with the help of additional information, for instance about the variation of $\boldsymbol{\omega}$ from one streamline to another far upstream (most often in the form of a statement that the velocity is uniform at infinity).

However, in the case of flow in a confined region, for which all the streamlines are necessarily closed, the possibility of making equation (1.3) sufficient to determine $\mathbf{u}$ in the region of small viscous forces, by introducing boundary conditions which specify $\boldsymbol{\omega}$ everywhere in a region 'far upstream', no longer exists. Other means of making the velocity distribution determinate must be found, and it is apparent that there is no further information to be found from considerations of the fluid as inviscid; this is the feature that makes the study of flow with closed streamlines novel and interesting. It will be shown that the action of viscosity imposes certainly one, and, when the vortex lines also are closed, two, integral conditions on the distribution of $\boldsymbol{\omega}$, and that in the cases of two-dimensional flow and of rotationally symmetric flow (with suitable restrictions) these integral conditions render the distributions of $\boldsymbol{\omega}$ and $\mathbf{u}$ determinate in the region of small viscous forces. The question of what further conditions are needed to make the distributions of $\boldsymbol{\omega}$ and $\mathbf{u}$ determinate in general three-dimensional flow with closed streamlines is left unresolved. We begin with a derivation of the integral conditions in the general three-dimensional case.

2. Integral conditions arising from the effect of viscosity

To obtain a condition which arises from the effect of viscosity and which is valid no matter how small the value of ν may be, we operate on the complete equation of motion (1.2) in such a way that the contributions from all terms other than the term containing ν vanish identically. Such an

operation is to take the line integral around a closed contour (in space) of certain shape, with line element $d\mathbf{l}$, giving

$$\oint (\mathbf{u}\times\boldsymbol{\omega}).d\mathbf{l} - \oint dl.\nabla H - \nu \oint (\nabla\times\boldsymbol{\omega}).d\mathbf{l} = \frac{\partial}{\partial t}\oint \mathbf{u}.d\mathbf{l}. \qquad (2.1)$$

The term on the right-hand side vanishes in view of the steadiness of the motion. (It is important to notice that the motion is regarded as exactly steady, even though the value of ν will later be taken as very small and even though steady motion would take a long time to develop from arbitrary initial conditions. In other words, we are considering flows subject to the double limiting operation $t \to \infty$, $\nu \to 0$, *in that order*, corresponding in effect, to the procedure that would be used in a real observation of the forms of the steady flows set up at several different large values of the Reynolds number.) The second term on the left-hand side vanishes since H is a single-valued function of position. We now make the first term on the left-hand side zero by choosing the closed contour to coincide with a streamline, of which a line element will be donated by $d\mathbf{s}$. Then, since ν is non-zero (although it will later be assumed to be small), we have the exact integral condition

$$\oint (\nabla\times\boldsymbol{\omega}).d\mathbf{s} = 0, \qquad (2.2)$$

to be satisfied for every closed streamline.

It is natural to enquire if there are any other choices of the closed contour for which the integral $\oint (\mathbf{u}\times\boldsymbol{\omega}).d\mathbf{l}$ vanishes identically. If there existed a family of surfaces such that their normals were everywhere parallel to $\mathbf{u}\times\boldsymbol{\omega}$, we could make the integral zero by choosing the contour as any closed curve on one of these surfaces. However, as already remarked, such a family of surfaces does not exist in general; the surface formed by all the streamlines passing through a given vortex line will in general be intersected by other vortex lines (except when $\nu = 0$, which is irrelevant, since we are seeking an integral condition which is exact for small but non-zero values of ν). For reasons related to the symmetry, surfaces which everywhere contain the local vectors $\mathbf{u}$ and $\boldsymbol{\omega}$ exist in cases of two-dimensional motion and of rotationally symmetric motion without azimuthal swirl when $\nu \neq 0$, but we shall see that the condition (2.2) alone is then sufficient to make the distributions of $\boldsymbol{\omega}$ and $\mathbf{u}$ determinate and no other choice of closed contour is needed.

There exists the possibility that vortex lines are closed and that the integral $\oint (\mathbf{u}\times\boldsymbol{\omega}).d\mathbf{l}$ may be made zero by choosing the contour to coincide with a closed vortex line. Vortex lines may end at a rigid boundary, but there is no reason why at least some of the vortex lines in a confined flow should not be closed; for such lines we have the additional exact integral condition

$$\oint (\nabla\times\boldsymbol{\omega}).d\mathbf{v} = 0, \qquad (2.3)$$

where $d\mathbf{v}$ is an element of a vortex line. It appears to be difficult to decide whether vortex lines are, or are not, closed in any given flow field, but in one case, described in § 4, this is possible and the condition (2.3) is utilized.

Other contours which are closed, and which are such that each line element is orthogonal to $\mathbf{u} \times \boldsymbol{\omega}$, may be imagined (one natural choice is a contour which consists of four segments, of which the first and third coincide with streamlines, and the second and fourth with vortex lines); however, their existence depends on the particular properties of the flow, and in any case it is not clear how the corresponding integral condition could be made use of.

The integral condition (2.2) (and likewise (2.3), where it is applicable) is valid independently of the Reynolds number of the flow. If now the Reynolds number is assumed to be large, the equation of inviscid flow, (1.3), is approximately valid over nearly all the flow field, and there exists the possibility of making use of *both* equation (1.3) and the condition (2.2). Provided the streamline, around which the integral in (2.2) is taken, lies entirely in the region of small viscous forces, the integrand in (2.2) may be evaluated with the aid of (1.3). It will be shown that, in this way, the form of the velocity distribution in the region of small viscous forces may be determined in certain cases.

The proviso of the penultimate sentence is equivalent to the requirement that the shortest distance from the streamline to any singular surface does not tend to zero as $\nu \to 0$. Now the velocity in the region of small viscous forces will in general be of the same order of magnitude as the tangential velocity of the boundaries (as can be verified experimentally in certain simple cases, and can in any case be examined *a posteriori*). Consequently, in cases of two-dimensional flow and of rotationally symmetric flow without azimuthal swirl, a typical streamline passing through the region of small viscous forces, on which the value of the appropriate stream function ψ differs from that for the outer enclosing boundary or singular surface by a finite amount, cannot come close to the boundary of this region without the velocity there being infinite. The above proviso is therefore satisfied for typical streamlines in these two cases. However, in more general types of flow, it is not certain that streamlines lying entirely in the region of small viscous forces exist; indeed, there are some closed flows for which *all* the closed streamlines pass through a boundary layer region.

3. Steady two-dimensional flow with closed streamlines

When the flow is two-dimensional, we can introduce the stream function ψ, and use (ψ, ξ) as orthogonal curvilinear coordinates, the lines $\xi = \text{const.}$ being everywhere normal to the streamlines. The displacements corresponding to increments in ψ and ξ are $d\psi/q$ and $hd\xi$, where h is an unknown function of ψ and ξ. The inviscid flow equation (1.3) can then be written as

$$\omega(\psi) = \frac{dH(\psi)}{d\psi}. \tag{3.1}$$

This equation will be approximately valid, when the Reynolds number is large, everywhere except in the neighbourhood of certain singular curves (in the plane of motion) which are themselves members of the family of

streamlines. Even when the shapes of outer and inner streamlines (perhaps given by the shape of enclosing rigid boundaries) bounding a region in which (3.1) holds is given, there will in general be a solution of this equation for any choice of function $\omega(\psi)$, and the flow in the region of small viscous forces can be made determinate only with the aid of further conditions. The considerations given in § 2 supply the integral condition (2.2), which we proceed to apply.

When evaluating the integral in (2.2) for streamlines lying wholly in the region of small viscous forces, we can make use of the approximation (3.1), whence $\nabla \times \boldsymbol{\omega}$ becomes a vector parallel to the local streamline, and (2.2) takes the form

$$\frac{d\omega}{d\psi} \oint q \, ds = 0. \tag{3.2}$$

Hence

$$\omega(\psi) = \frac{dH(\psi)}{d\psi} = \omega_0(\text{const.}) \tag{3.3}$$

everywhere in a connected region of small viscous forces. (The possibility of there being an exception to (3.3) on a streamline for which $\oint q \, ds = 0$ —which is possible only if the velocity is zero at all points on the streamline —with a possible discontinuity in ω across such a streamline, is irrelevant since the viscous forces would then be large at such a streamline). The distribution of velocity in the region of small viscous forces can be determined from (3.3) without difficulty when the shape of the streamline bounding this region is known*.

The argument leading to the simple result (3.3) may be summarized as follows. In view of the fact that ν is small, convection of vorticity will dominate viscous diffusion of vorticity when both processes occur, so that ω is approximately constant *along* streamlines. But, in exactly steady motion, the net viscous diffusion of vorticity across a closed streamline must be exactly zero (even when the streamline encloses a rigid boundary), and this is then possible only if ω is also approximately constant *across* streamlines. It seems that two-dimensional flows with closed streamlines cannot be exactly steady until the slow but persistent effect of viscous diffusion of vorticity across streamlines has evened out any variation of vorticity that may have been present initially; the time required for this asymptotic steady state to be set up will of course increase as ν decreases.

* The notion of a two-dimensional ' inviscid ' core with uniform vorticity has already been inferred from arguments rather less general or rigorous than those given above, and has been applied to some problems of two-dimensional free convection in closed regions. Pillow (in a dissertation submitted for the degree of Ph.D. at the University of Cambridge, 1952) and Batchelor (1954) have used it to calculate the heat transfer across rectangular cavities, and Carrier (1953) has done so for a circular cavity. The temperature in the core was shown to be uniform in all these cases from an argument based on symmetry of the streamlines, but in fact this result is true generally in a simply-connected ' non-conducting ' closed region in two dimensions, as may be seen from a proof like that used above.

The value of the constant ω_0 is undetermined as yet, and since the distribution (3.3) is such that $\nu\nabla^2\mathbf{u}$ is identically zero there is no further information to be gained from considerations of the region in which viscous forces are small. Surrounding the region in which (3.3) is valid there is a singular streamline, in the neighbourhood of which viscous forces are not small, and the value of ω_0 will presumably be determined by the need for steady motion to be possible near this singular streamline. The situation can be illustrated by reference to the simple case of flow inside a circular cylinder of radius a which rotates steadily with angular velocity $\frac{1}{2}\omega_1$, an inner sleeve of length $2\pi a\sigma$ being held stationary (figure 1). It is evident here that, when the Reynolds number is large, viscous forces will be small everywhere except near the outer circular boundary, so that the region of 'inviscid' flow is circular and in it the fluid rotates as a rigid body with angular velocity $\frac{1}{2}\omega_0$. The motion in the 'inviscid' core can be regarded as a standing eddy, which is driven by the motion of part of the outer boundary, the exact speed of rotation of the eddy being determined by the need for steadiness in the viscous boundary layer surrounding the eddy.

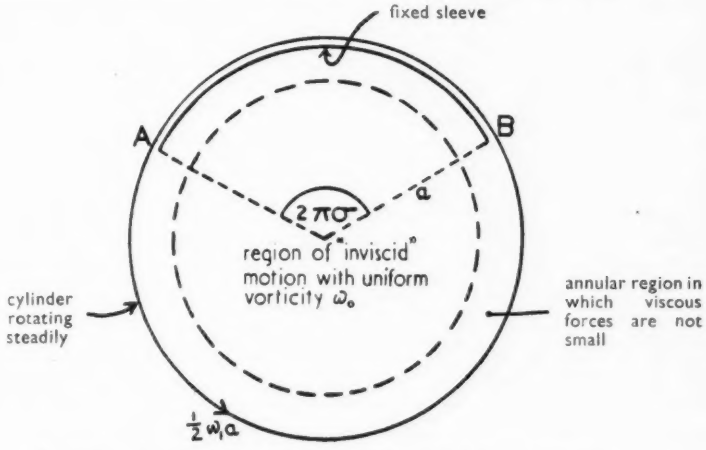

Figure 1. A case of two-dimensional flow in a closed region.

The present paper is concerned with general results rather than solutions for particular configurations of the boundaries, but it may be found illuminating to present some consideration of the boundary layer problem associated with the simple system shown in figure 1. Being unable to solve the boundary layer equation exactly, I at first solved the problem by linearizing it in the manner of Oseen* (which is equivalent to converting it to a time-dependent problem as Rayleigh did for a flat plate). However, it was

* Professor H. B. Squire has also conceived this simple boundary layer problem and has solved it in this same way, in a paper to be published in the *Journal of the Royal Aeronautical Society*.

later pointed out to me by Mr W. W. Wood that so far as the relation between ω_0 and ω_1 is concerned the problem may be solved exactly by using the von Mises form of the boundary layer equation. This form (see *Modern Developments in Fluid Dynamics*, Oxford University Press, 1938, Vol. 1, § 50) becomes

$$\frac{1}{h}\frac{\partial q}{\partial \xi} = \tfrac{1}{2}\nu\frac{\partial^2(q^2)}{\partial \psi^2} \tag{3.4}$$

in cases in which the velocity outside the boundary layer is uniform, where $hd\xi$ represents a displacement along the streamline $\psi = \text{const.}$, as before, and q is the velocity in this same direction. Then, since the streamlines here are closed and q is single-valued, we have

$$0 = \oint \frac{\partial^2(q^2)}{\partial \psi^2}\, qh\, d\xi \doteq \frac{\partial^2}{\partial \psi^2}\oint q^2 h\, d\xi, \tag{3.5}$$

since the mesh parameter h is approximately constant across the boundary layer. The total variation of ψ across the boundary layer tends to zero as $\nu \to 0$, so that the solution of (3.5) is effectively

$$\oint q^2 h\, d\xi = \text{const.} \tag{3.6}$$

throughout the boundary layer. On evaluating the integral for the streamline at the wall and for one just outside the boundary layer, we find the required relation to be

$$\omega_0/\omega_1 = (1-\sigma)^{1/2}. \tag{3.7}$$

It is still necessary to rely on some approximate procedure like the Oseen linearization for details of the velocity distribution in the boundary layer at different values of ξ, but (3.7) represents the crucial piece of information. It should be noted that the basic assumption that the velocity in the region of small viscous forces does not tend to zero as $\nu \to 0$ is confirmed in this case.

Another problem whose examination involves a consideration of the exact shape of the boundaries, and which will not be attempted here, concerns the position of the singular streamlines. The location of these viscous layers will sometimes be evident from the nature of the conditions at the outer boundary, as in the very simple case represented in figure 1. Cases in which their location is not evident will clearly present great difficulties in any detailed analysis, akin to those in problems in which a boundary layer separates from a rigid wall. The natural assumption that the singular surfaces coincide everywhere with rigid boundaries (except where the contrary is evident) needs particularly careful scrutiny. For instance, in a case of flow in a region bounded externally by a rigid wall which has a 90° corner, a viscous boundary layer would not flow along the wall right up to the corner, in general, because there would then be a stagnation point of the inviscid flow at the corner; it is probable that a singular surface exists to divide the main body of the fluid from a secondary 'standing eddy' in the corner, and indeed there may be even a whole sequence of such singular surfaces and 'standing eddies' of diminishing size as the corner is approached.

Finally, it is worth noting that steady two-dimensional motion of a fluid relative to given boundaries is unaffected by steady rotation of the whole system about an axis normal to the plane of motion (Taylor 1921). Consequently, all the above remarks and results apply not only to two-dimensional flows enclosed by outer boundaries whose positions are fixed and whose velocities are steady, but also to flows enclosed by boundaries whose positions and velocities are steady relative to suitably chosen uniformly rotating axes.

4. Steady rotationally symmetric flow in a closed region

It is convenient here to introduce orthogonal curvilinear coordinates (ξ, η, ψ), where the ξ-lines (on which η and ψ are constant) are everywhere parallel to the component of $\mathbf{u}$ lying in an axial plane, the η-lines are azimuthal

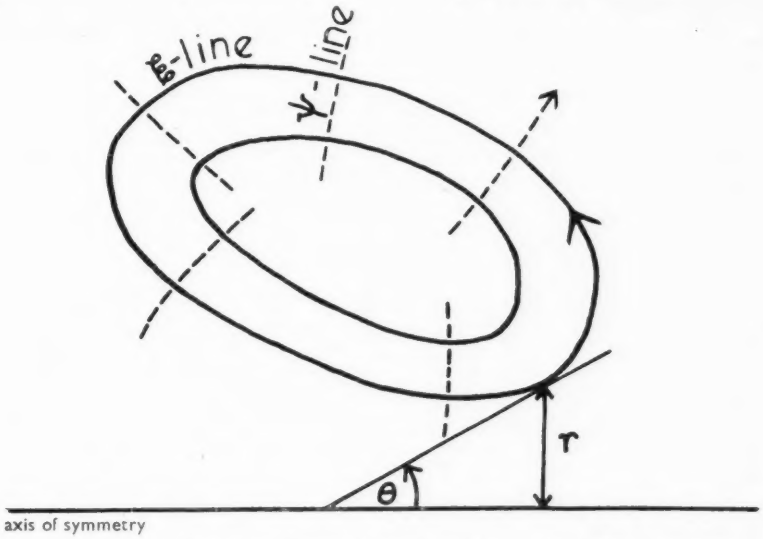

Figure 2. Coordinate system for rotationally symmetric flow.

circles, and the ψ-lines (ψ being the Stokes stream function of the component of the motion in an axial plane) lie in axial planes and are orthogonal to the ξ-lines (figure 2). The displacements corresponding to increments in ξ, η, ψ are

$$h_1\, d\xi, \qquad r\, d\eta, \qquad h_3\, d\psi,$$

where $h_1(\xi, \eta)$ is unknown, r is the distance from the axis of symmetry, and the definition of ψ supplies the relation

$$h_3 = (ru_1)^{-1}, \tag{4.1}$$

where $(u_1, u_2, 0)$ are the velocity components.

The ξ-lines, or streamlines of the components of velocity in an axial plane, are bounded externally, and perhaps internally also, by a singular

curve which is itself a member of the family of ξ-lines. Provided the velocity component u_1 in the region of small viscous forces remains of order unity as $\nu \to 0$ —which is evident in the case of flow without swirl, since the 'inviscid' core would not otherwise be responding to the motion of the boundaries, but is not necessarily true in the case of flow with swirl since the motion generated in the 'inviscid' core may here be primarily an azimuthal swirl—a typical streamline will lie in the region of small viscous forces over the whole of its length. It will thus be possible to combine the exact integral condition (2.2) with the approximate inviscid flow equation (1.3). However, only in the case in which the azimuthal component of velocity is zero are these two equations sufficient to determine the form of the distributions of $\boldsymbol{\omega}$ and $\mathbf{u}$ in the region of small viscous forces.

(a) *Flow without azimuthal swirl*

The velocity here has components $(u_1, 0, 0)$, and the components of the vorticity are $(0, \omega_2, 0)$ where

$$\omega_2 = \frac{1}{h_1 h_3} \frac{\partial (h_1 u_1)}{\partial \psi}.$$

Everywhere in the region of small viscous forces, (1.3) is satisfied approximately, whence

$$u_1 \omega_2 = \frac{1}{h_3} \frac{dH(\psi)}{d\psi},$$

that is,

$$\frac{\omega_2}{r} = \frac{dH(\psi)}{d\psi}. \tag{4.2}$$

This last relation describes the known proportionality, in inviscid flow, between the vorticity and the length of a material element of a vortex line. This is as far as one can go, making use only of the equations for inviscid motion, and (4.3) is the counterpart of (3.1) in two-dimensional flow. For information about the function $H'(\psi)$, which describes the unknown variation of vorticity across the streamlines, we must take some account of the action of viscosity, and this will be done by applying the integral condition (2.2) to closed streamlines lying entirely within the region of small viscous forces.

The components of $\nabla \times \boldsymbol{\omega}$ are given by

$$\nabla \times \boldsymbol{\omega} = \left(-\frac{1}{r h_3} \frac{\partial (r\omega_2)}{\partial \psi}, 0, \frac{1}{r h_1} \frac{\partial (r\omega_2)}{\partial \xi} \right), \tag{4.3}$$

and the condition (2.2) becomes

$$\oint \frac{\partial (r\omega_2)}{\partial \psi} \frac{h_1}{r h_3} \, d\xi = 0,$$

or, in view of (4.1) and (4.2),

$$\begin{aligned} H''(\psi) \oint r^2 u_1 h_1 \, d\xi &= -H'(\psi) \oint \frac{\partial r}{\partial \psi} \frac{2h_1}{h_3} \, d\xi \\ &= 2H'(\psi) \oint \cos\theta \, ds \\ &= 0, \end{aligned} \tag{4.4}$$

where θ is the angle between the tangent to the streamline (ξ and s increasing) and the axis of symmetry (with regard for the sense). Hence, we require

$$H''(\psi) = 0, \qquad H(\psi) = \alpha\psi, \tag{4.5}$$

where α is a constant (the other constant of integration being absorbed in the definition of ψ), and

$$\omega_2/r = H'(\psi) = \alpha \tag{4.6}$$

everywhere in a connected region of small viscous forces (the possibility of a different result applying on certain exceptional streamlines again being irrelevant, since viscous forces would not be small at such streamlines).

The result (4.6) is an obvious counterpart of the result that the vorticity is uniform in the region of small viscous forces in two-dimensional flow, and it is also true of (4.6) that the net effect of viscosity on the rate of change of the vorticity at any point vanishes identically. (But note that in axisymmetric motion the vorticity does not satisfy a heat-conduction type of equation, and it does not seem possible here to arrive at the result (4.6) by an argument in terms of diffusion of vorticity across streamlines.) There is also the common linear dependence of H on ψ, although the meanings of ψ in the two cases are not the same. The result established for the region of small viscous forces in two-dimensional flow is such that the net viscous force on any element of fluid vanishes identically, but this is not true of (4.6). The local viscous force per unit mass of fluid is $-\nu\nabla\times\boldsymbol{\omega}$, and it is readily seen from (4.3) and (4.6) that this is a uniform vector, of magnitude -2α and directed along the axis of symmetry. Thus the local viscous force has a simple character, and does not require the velocity distribution to be different (by even a small amount) from that for an inviscid fluid, since the viscous force can be balanced exactly by a uniform pressure gradient.

When the shape of the singular surfaces bounding the region of small viscous forces is known, the velocity distribution can be found from (4.6). The constant α, like ω_0, then remains to be determined from the condition that the surrounding viscous boundary layer is steady.

(b) *The general case (flow with swirl)*

The velocity components are now $(u_1, u_2, 0)$, and the components of the vorticity are $(\omega_1, \omega_2, \omega_3)$, where

$$\omega_1 = -\frac{1}{rh_3}\frac{\partial(ru_2)}{\partial\psi}, \qquad \omega_2 = \frac{1}{h_1h_3}\frac{\partial(h_1u_1)}{\partial\psi}, \qquad \omega_3 = \frac{1}{rh_1}\frac{\partial(ru_2)}{\partial\xi}. \tag{4.7}$$

The approximate equation (1.3) then yields the three scalar relations

$$\frac{1}{h_1}\frac{\partial H}{\partial\xi} = \frac{u_2}{rh_1}\frac{\partial(ru_2)}{\partial\xi}, \tag{4.8}$$

$$\frac{1}{r}\frac{\partial H}{\partial\eta} = 0 = -\frac{u_1}{rh_1}\frac{\partial(ru_2)}{\partial\xi}, \tag{4.9}$$

$$\frac{1}{h_3}\frac{\partial H}{\partial\psi} = \frac{u_1}{h_1h_3}\frac{\partial(h_1u_1)}{\partial\psi} + \frac{u_2}{rh_3}\frac{\partial(ru_2)}{\partial\psi}. \tag{4.10}$$

From (4.9), we have

$$ru_2 = C(\psi) \quad (\text{and } \omega_3 = 0), \tag{4.11}$$

which describes the constancy of circulation around a material curve in the form of a circle about the axis of symmetry, and then (4.8) reduces to

$$H \equiv H(\psi). \tag{4.12}$$

The last scalar equation, (4.10), can be written as

$$\frac{\omega_2}{r} = \frac{dH}{d\psi} - \frac{1}{2r^2}\frac{dC^2}{d\psi}, \tag{4.13}$$

which is the generalization of (4.2).

These relations appropriate to purely inviscid flow are now combined with the exact relation (2.2) which arises from the existence of viscous forces. This can be done only if there exist streamlines which lie entirely in the region of small viscous forces. As before, it follows that such streamlines will exist provided u_1 does not tend to zero, as $\nu \to 0$, everywhere in the region of small viscous forces. However, whereas the possibility of u_1 tending to zero could be rejected in cases of two-dimensional motion and of rotationally symmetric flow without swirl, it cannot immediately be rejected in cases in which u_1 is not the only component of velocity that may be finite. The assumption that u_1 does not tend to zero as $\nu \to 0$ is here a genuine restriction, which places some cases of rotationally symmetric flow with swirl outside the scope of the theory.

We first find that the components of $\nabla \times \boldsymbol{\omega}$ are given by expressions like those on the right-hand sides of (4.7), with ω_1 and ω_2 replacing u_1 and u_2. All these components are independent of η, and the integral (2.2) round a streamline reduces to an integral round a closed ξ-line, giving

$$\oint [(\nabla \times \boldsymbol{\omega})_1 u_1 + (\nabla \times \boldsymbol{\omega})_2 u_2] \frac{h_1}{u_1} d\xi = 0. \tag{4.14}$$

When the inviscid relations (4.11) and (4.13) are employed, this condition reduces to

$$\oint \left[r^2 \frac{d^2H}{d\psi^2} - \left(\frac{dC}{d\psi}\right)^2 + C\frac{dC}{d\psi}\frac{1}{h_1 u_1}\frac{\partial(h_1 u_1)}{\partial \psi} \right] u_1 h_1 \, d\xi = 0, \tag{4.15}$$

which is a more general version of (4.4).

It is not possible to determine the unknown functions $H(\psi)$ and $C(\psi)$ from (4.15), and the inviscid flow equations together with the integral condition (2.2) are not sufficient here to determine the distributions of $\boldsymbol{\omega}$ and $\mathbf{u}$ in the region of small viscous forces. However, there is another condition that is applicable in this case of rotationally symmetric flow, at any rate provided the ξ-lines are not bounded internally by a solid boundary or a singular surface. Since $\omega_3 \to 0$ as $\nu \to 0$, the angle between the local components of $\mathbf{u}$ and $\boldsymbol{\omega}$ in the axial plane tends to zero as $\nu \to 0$, and the ξ-lines and the vector lines formed from the components of $\boldsymbol{\omega}$ in an axial plane (the latter being referred to as 'vortex lines in an axial plane') nearly coincide. This approximate coincidence of the two families of curves may take either

of two forms. The ξ-line and 'vortex line in an axial plane' that pass through any given point may intersect once more at some other point along their lengths (or, more generally, may intersect at an odd number of additional points) or they may not intersect again (even number of additional points.) In the former case the 'vortex lines in an axial plane' are necessarily closed when ν is small, whereas in the latter case they have one end at a point exterior to all the ξ-lines and another end at a point interior to all the ξ-lines—which is possible only if the area intercepted on an axial plane by the region of small viscous forces is bounded internally. Thus, provided the ξ-lines have no inner boundary, we conclude that the vortex lines are closed when ν is small, and hence that, as explained in § 2,

$$\oint (\nabla \times \boldsymbol{\omega}).d\mathbf{v} = 0. \tag{4.16}$$

For small values of ν, when $\omega_3 \neq 0$, this condition becomes

$$\oint \left[(\nabla \times \boldsymbol{\omega})_1 \omega_1 + (\nabla \times \boldsymbol{\omega})_2 \omega_2 \right] \frac{h_1}{\omega_1} \, d\xi = 0. \tag{4.17}$$

Combining (4.17) with (4.14), we have

$$\oint \left(\frac{u_2}{u_1} - \frac{\omega_2}{\omega_1} \right) \frac{1}{h_3} \frac{\partial (h_1 \omega_1)}{\partial \psi} \, d\xi = 0,$$

which, after some reduction using (4.11) and (4.13), becomes

$$\oint r^2 \frac{\partial}{\partial \psi} \left(u_1 h_1 \frac{dC}{d\psi} \right) d\xi = 0,$$

that is

$$\frac{d}{d\psi} \left[\frac{dC}{d\psi} \oint r^2 u_1 h_1 \, d\xi \right] = 0. \tag{4.18}$$

It has already been assumed that the ξ-lines are not bounded internally, so that there will exist an inner limiting ξ-line which is merely a point. On this degenerate ξ-line, $h_1 = 0$ and $u_1 \, dC/d\psi$ is finite, in general, so that the integral in (4.18) is zero; hence

$$\frac{dC}{d\psi} \oint r^2 u_1 h_1 \, d\xi = 0. \tag{4.19}$$

The integral cannot be zero, except perhaps on an isolated ξ-line (since we have already supposed that u_1 is not zero everywhere, even when $\nu \to 0$), and (4.19) becomes

$$C = r u_2 = \text{const.} \tag{4.20}$$

Equation (4.15) now reduces to the form appropriate to flow without swirl, and the solution is

$$\frac{\omega_2}{r} = \frac{dH}{d\psi} = \text{const.} \tag{4.21}$$

as before.

The solution represented by (4.20) and (4.21) is such that the vortex lines are circles about the axis of symmetry, as for flow without azimuthal

swirl. Moreover, the remarks of the preceding sub-section about the effect of viscosity on the rate of change of vorticity at any point, and on the acceleration of any fluid element, apply here also. When the azimuthal component of velocity is allowed to be non-zero, it seems that in truly steady motion this component is necessarily an irrotational velocity field corresponding to a circulation about the axis (provided, as above, that (*a*) u_1 does not tend to zero as $r \to 0$, and (*b*) there is a degenerate inner ξ-line). Note, however, that the result (4.20) does not apply in the neighbourhood of the axis of symmetry, since, in cases in which the region of flow does include part of the axis of symmetry, the axis is part of the streamline that bounds the whole flow (in the axial plane) and this streamline necessarily passes through a region in which viscous forces are appreciable.

In cases in which the area intercepted on an axial plane by the region of small viscous forces does have an inner boundary (as, for example, when the fluid lies between two anchor rings with a common axis of symmetry, one ring enclosing the other), it does not seem possible to deduce the distributions of $\boldsymbol{\omega}$ and $\mathbf{u}$ in the region of small viscous forces unless the vortex lines can first be shown to be closed.

I am grateful to Dr I. Proudman and to Mr W. W. Wood for their useful comments on certain parts of this paper.

References

Batchelor, G. K. 1954 *Quart. Appl. Math.* **12,** 209.

Carrier, G. F. 1953 *Advances in Applied Mechanics* **3,** 1, New York: Academic Press.

Taylor, G. I. 1921 *Proc. Roy. Soc.* A, **100,** 114.

The law of the wake in the turbulent boundary layer

By DONALD COLES
Guggenheim Aeronautical Laboratory, California Institute of Technology, Pasadena

(*Received* 14 *January* 1956)

SUMMARY

After an extensive survey of mean-velocity profile measurements in various two-dimensional incompressible turbulent boundary-layer flows, it is proposed to represent the profile by a linear combination of two universal functions. One is the well-known law of the wall. The other, called the law of the wake, is characterized by the profile at a point of separation or reattachment. These functions are considered to be established empirically, by a study of the mean-velocity profile, without reference to any hypothetical mechanism of turbulence. Using the resulting complete analytic representation for the mean-velocity field, the shearing-stress field for several flows is computed from the boundary-layer equations and compared with experimental data.

The development of a turbulent boundary layer is ultimately interpreted in terms of an equivalent wake profile, which supposedly represents the large-eddy structure and is a consequence of the constraint provided by inertia. This equivalent wake profile is modified by the presence of a wall, at which a further constraint is provided by viscosity. The wall constraint, although it penetrates the entire boundary layer, is manifested chiefly in the sublayer flow and in the logarithmic profile near the wall.

Finally, it is suggested that yawed or three-dimensional flows may be usefully represented by the same two universal functions, considered as vector rather than scalar quantities. If the wall component is defined to be in the direction of the surface shearing stress, then the wake component, at least in the few cases studied, is found to be very nearly parallel to the gradient of the pressure.

I. COMPENDIUM

A. The law of the wall

Consider a turbulent shear flow which is steady and two-dimensional on the average. Let $u(x, y)$ and $v(x, y)$ be the mean velocities in the direction of increasing rectangular coordinates x and y respectively. Suppose that the flow exerts a shearing stress $\tau_w(x)$ on a smooth impermeable wall at rest at $y = 0$. For a fluid of constant density, define a friction velocity $u_\tau(x)$ by

$$\rho u_\tau^2 = \tau_w. \tag{1}$$

Experience with turbulent shear flow has shown that, under these conditions the mean-velocity profile in a considerable region near the surface is described by a relationship called the 'law of the wall':

$$\frac{u}{u_\tau} = f\left(\frac{yu_\tau}{\nu}\right). \tag{2}$$

The earliest formulation of the law of the wall was based on observations of pipe flow. The current view, however, is one first suggested by Ludwieg & Tillmann (1949); the relationship (2) is taken for practical purposes as a unique and universal similarity law for every turbulent flow past a smooth surface.

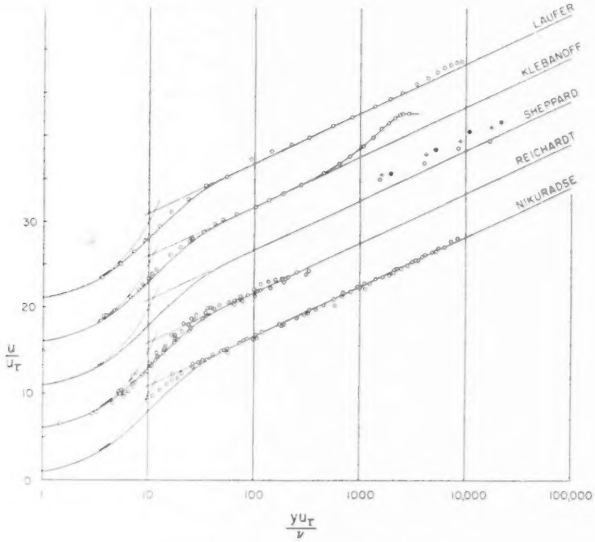

Figure 1. The law of the wall.

For the special case of steady two-dimensional mean flow of an incompressible fluid, the form of the universal law is well established. In particular, for values of yu_τ/ν greater than about 50, equation (2) takes the form

$$\frac{u}{u_\tau} = \frac{1}{\kappa}\ln\left(\frac{yu_\tau}{\nu}\right) + c, \tag{3}$$

in which κ and c are constants to be determined experimentally. On the other hand, the predominance of laminar shear very near the wall requires u/u_τ to approach yu_τ/ν as y approaches zero. To illustrate the presence of linear and logarithmic regions in the mean-velocity profile, experimental data from several sources are collected in figure 1. A brief discussion of these data will be found in Part II of the present paper.

B. The defect law and the equilibrium boundary layer

The description just given of the mean velocity profile in a turbulent shear flow may be summarized in the formula

$$\frac{u}{u_\tau} = f\left(\frac{yu_\tau}{\nu}\right) + h(x, y), \tag{4}$$

where the function h is arbitrary except that it is negligibly small in some finite region near the wall—say for y/δ less than about 0·1, where δ is the thickness of the shear flow.

For certain special cases frequently encountered (e.g. uniform pipe and channel flow and the boundary layer on a flat plate in a uniform stream), equation (4) is found experimentally to have the special form

$$\frac{u}{u_\tau} = f\left(\frac{yu_\tau}{\nu}\right) + g\left(\Pi, \frac{y}{\delta}\right), \tag{5}$$

where Π is a parameter which is independent of x and y. Profile similarity in terms of the argument y/δ is usually expressed by a relationship known as the velocity-defect law, or more properly the momentum-defect law. Outside the sublayer, it is an immediate consequence of the logarithmic variation of f in equation (5) that

$$\frac{u_1 - u}{u_\tau} = F\left(\Pi, \frac{y}{\delta}\right), \tag{6}$$

with $u = u_1$ at $y = \delta$.

Quite recently these contributions to the experimental definition of turbulent shear flows have been brilliantly extended by F. Clauser (1954), who generalized the idea of a defect law by showing experimentally the existence of boundary-layer flows for which the similarity laws (5) and (6) remain valid although the pressure gradient is positive.

Finally, the existence of a logarithmic region in the mean-velocity profile has been shown by Millikan (1938) to follow directly, without reference to any hypothetical mechanism of turbulent mixing, from the assumption of the simultaneous validity of the law of the wall in the form (2) and the defect law in the form (6).

C. The law of the wake

The relationships so far cited, especially the law of the wall, form the hard core of empirical knowledge of flow in turbulent boundary layers. Once they are accepted, it is natural to look for further inspiration in the inverse of Millikan's problem. That is, given a universal law of the wall which is logarithmic outside the sublayer, what other assumptions about the motion are necessary in order to establish a defect law? The most obvious answer is that the mean-velocity profile must have the form of equation (5). The purpose of the present paper, however, is to suggest a less superficial answer, one which has several immediately useful consequences and which at the same time appears to approach somewhat closer to the central problem of turbulence itself.

The essential element in this work is a study of the function $h(x, y)$ in the general mean-velocity formula (4). An extensive survey of experimental data at large Reynolds numbers, reported in Parts II and III, leads to the crucial conclusion that this function can be reduced directly to a second universal similarity law. Specifically, equation (4) may be written in the form

$$\frac{u}{u_\tau} = f\left(\frac{yu_\tau}{\nu}\right) + \frac{\Pi}{\kappa} w\left(\frac{y}{\delta}\right), \tag{7}$$

where Π is a profile parameter, as in equation (5), but the function $w(y/\delta)$ is now supposedly common to all two-dimensional turbulent boundary-layer flows.

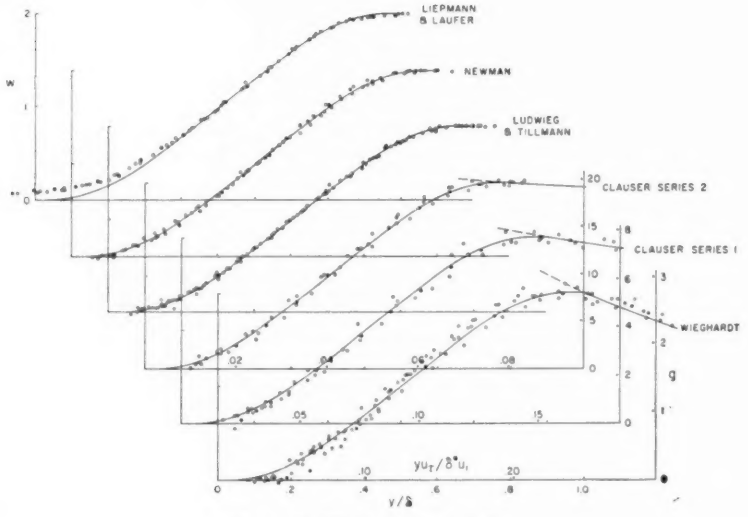

Figure 2. The law of the wake.

The introduction of a second universal function in the mean-velocity profile will be referred to as the wake hypothesis, and the function $w(y/\delta)$ in equation (7) will be referred to as the 'law of the wake'. Some experimental data which support the wake hypothesis are collected in figure 2. The measurements in question are included in the survey already mentioned, and the development leading to equation (7) and to figure 2 will be found in Part III.

In preparing figure 2 the wake function $w(y/\delta)$ in (7) has been subjected to the normalizing conditions $w(0) = 0$, $w(1) = 2$ and $\int_0^2 (y/\delta)\, dw = 1$. The parameter Π is then found to be related to the local friction coefficient $C_f = 2u_\tau^2/u_1^2$ by

$$\frac{u_1}{u_\tau} = \frac{1}{\kappa} \ln\left(\frac{\delta u_\tau}{\nu}\right) + c + \frac{2\Pi}{\kappa}, \tag{8}$$

to the displacement thickness δ^* by

$$\kappa \frac{\delta^* u_1}{\delta u_\tau} = 1 + \Pi, \tag{9}$$

and to the momentum thickness θ by

$$\frac{\kappa^2}{2}\left(\frac{\delta^* - \theta}{\delta}\right)\frac{u_1^2}{u_\tau^2} = 1 + \alpha\Pi + \beta\Pi^2, \tag{10}$$

where α and β are constants of order unity.

D. The equations of mean motion

To the extent that the similarity laws of the preceding sections are empirical, and not based on clear physical principles, these laws cannot be extended with confidence to conditions outside the range of observation. At the same time, these similarity laws go well beyond the usual limits of dimensional analysis.

In the first place, the thickness δ and the parameter Π are uniquely defined by equations (8) and (9), as is easily confirmed by eliminating either of these parameters between the equations in question. In the second place, the mean-velocity field, including the flow in the sublayer, is determined whenever the kinematic viscosity ν and three of the four parameters u_1, u_τ, δ and Π are known. But a complete analytic description of the mean-velocity field implies a complete knowledge (at least within the boundary-layer approximation) of the streamline pattern, of the shearing-stress field, and of the local rate of transfer of energy from the mean flow to the turbulent secondary flow. Some typical calculations based on the formula (7) are presented in Part IV.

E. Physical interpretation

It is instructive to examine the nature of the wake component in equation (7) by letting u_τ approach zero (i.e. $\tau_w \to 0$) after expressing Π in terms of δ, δ^*, u_1 and u_τ with the aid of equation (9). The result is

$$\frac{u}{u_1} = \tfrac{1}{2}w\left(\frac{y}{\delta}\right),$$

which does not involve either κ or ν. It follows, since $w(y/\delta)$ is by hypothesis a universal function, that the flow at a point of separation or reattachment is locally a pure wake flow.

This observation suggests a simple physical interpretation for the law of the wall and the law of the wake, as illustrated in figure 3. The figure shows the profile $u(y)$ for various values of x in a hypothetical boundary layer, which is proceeding from separation to separation through a region of attached flow. The dashed lines in the figure denote the wake-like structure represented in equation (7) by the function $w(y/\delta)$. The associated velocity defect $u_1 - u$ is given by $\Pi u_\tau(2-w)/\kappa$, and the intercept at $y = 0$ of the equivalent wake profile therefore differs from the velocity in the external stream by an amount $2\Pi u_\tau/\kappa$.

According to this interpretation, the law of the wake is to be viewed as a manifestation of a large-scale mixing process similar to flow in a wake, in that it is constrained primarily by inertia rather than by viscosity. When the flow is bounded by a wall, however, it is ultimately necessary to satisfy the boundary conditions of vanishing velocity and Newtonian friction at the surface. These conditions impose a further viscous constraint on the flow whose effect is to modify the mean-velocity distribution as shown by the solid lines in figure 3. Near the wall, where the wake mean velocity is nearly constant, the constraint provided by viscosity can be observed in the sublayer flow and in the similarity relationship known as the law of the wall.

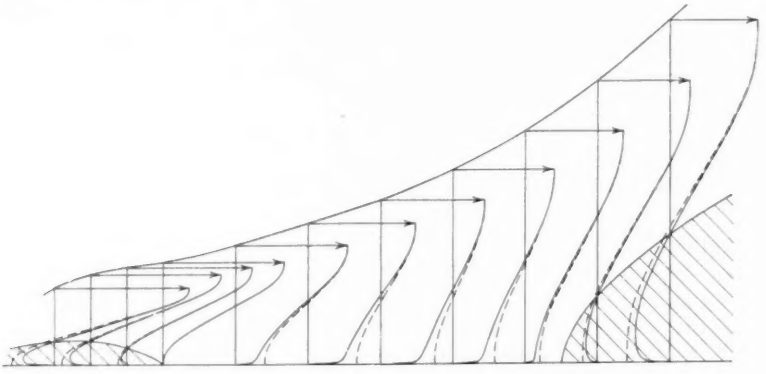

Figure 3. Mean-velocity field in a hypothetical boundary layer, including the equivalent wake.

II. The law of the wall

A. Historical development

1. *Evolution before* 1949. The early development of the law of the wall, in the hands of Prandtl, von Kármán and others, included a simple dimensional argument which has not lost its usefulness. Suppose that the mean-velocity profile in a turbulent shear flow is found to be adequately represented by a relationship $\phi(u, y, \delta, \tau_w, \mu, \rho) = 0$, in an obvious notation, and that this relationship is found in some region to be independent of the characteristic length δ. It follows from the principles of dimensional analysis, without any explicit assumptions about the nature of the turbulence, that in this region equation (2) must be valid.

Before the development of the mixing analogy, the function in equation (2) was sometimes taken as a power law, for lack of a better representation. The sublayer, that is, the region where viscous stress is predominant, was treated separately by means of the plausible assumption of a linear velocity profile very near the wall. In this approximation

$$\partial u/\partial y = u/y = \tau/\mu = \tau_w/\mu = u_\tau^2/\nu,$$

and therefore $u/u_\tau = yu_\tau/\nu$.

By 1930 the present general formulation of the law of the wall had been achieved, in the sense that no distinction was made in equation (2) between the sublayer and the fully turbulent flow. Nikuradse (1930), at the suggestion of Prandtl, expressed the law of the wall in the present form during an analysis of some measurements in pipe flow. Equation (2) also appears in articles by Tollmien and by Schiller in Volume IV of *Handbuch der Experimentalphysik*.

At about the same time, the mixing analogy of Prandtl (1926) and the similarity hypothesis of von Kármán (1932) had provided an equation $\partial u(x,y)/\partial y = u_\tau(x)/\kappa y$ for the mean velocity in the fully turbulent region, with the integral $u/u_\tau = (1/\kappa)\ln[y/y_0(x)] + \text{constant}$. It is clear, however, that the choice of ν/u_τ for the unspecified characteristic length $y_0(x)$ is not properly a part of the mixing analogy, but rather a part of the dimensional argument already mentioned.

2. *Recent developments.* Until quite recently, the three most important elements in the development of the law of the wall have been, first, the dimensional argument leading to equation (2); second, the stipulation that the function f is linear at the wall; and third, the recognition that, for whatever reason, the function f is very nearly logarithmic in a certain region outside the sublayer.

A fourth important element was added when Ludwieg & Tillmann (1949) found experimentally, using an ingenious heat-transfer technique for the indirect measurement of surface shearing stress, that for flow in a turbulent boundary layer the function f in equation (2) is apparently independent of pressure gradient. This result lies at the heart of the present study, virtually every part of which depends directly or indirectly on the hypothesis that the law of the wall is a unique and universal relationship for flow past a smooth surface.

As several writers in the field have pointed out, equation (2) is an implicit equation for u_τ (hence for τ_w) when ρ, μ, and $u(y)$ are given. The law of the wall thus provides a means for accurate determination of the elusive wall shearing stress, once the function f in (2) has been established by a survey of experimental data on flows for which τ_w is accurately known.

3. *Experimental data.* Nikuradse's classical pipe measurements (1930) confirmed the prediction of a logarithmic region in the mean-velocity profile. The lowest curve in figure 1 shows the data obtained, including a small correction for wall interference, in sixteen surveys at various Reynolds numbers of the region between the pipe wall and a value of y/δ of about 0·15, where δ is the pipe radius. Nikuradse did not obtain data on the sublayer, but inferred the validity of the general law of the wall from the argument already given in favour of the limiting form $u/u_\tau = yu_\tau/\nu$ at $y = 0$. This omission was partly repaired by Reichardt's measurements (1940) of mean velocity in the sublayer of a channel flow, and more completely repaired by the work of Laufer (1953) and Klebanoff (1954) on pipe flow and boundary-layer flow respectively.

The latter measurements, shown in figure 1, include data on the sublayer obtained in each instance with a hot-wire anemometer. For Laufer's experiments on pipe flow, the wall shearing stress has been derived from the observed axial pressure gradient. For Klebanoff's experiments on boundary layers, the wall shearing stress has been derived from the rate of momentum loss observed in other experiments with the same model (Klebanoff & Diehl 1951; see also Coles 1954). For Reichardt's experiments on channel flow, the wall shearing stress was not measured independently, as Reichardt's object was to interpolate experimentally in the region of the mean-velocity profile not studied by Nikuradse.

Finally, some measurements by Sheppard (1947) in a natural wind near the ground offer a striking example of a turbulent shear flow for which it would seem that no Reynolds number can be explicitly defined. However, difficulty in visualizing either an origin of coordinates or a second boundary does not prevent the presentation of these data in terms of the law of the wall. Sheppard observed the surface shearing stress directly, using the floating-element technique, together with the mean velocity at several points up to a height of two metres. The result of the measurements is given in figure 1. The agreement with wind-tunnel data is surprisingly good when it is considered that Sheppard's measurements were made over a concrete surface, and that the vertical temperature gradient may have differed significantly from the adiabatic lapse rate associated with neutral stability.

4. *Numerical evaluation.* Two empirical constants, κ and c, appear in equation (3). Throughout the present study, the numerical values given to these constants are

$$\kappa = 0{\cdot}40,$$

$$c = 5{\cdot}1.$$

A great variety of other values, especially for κ, can be found in the experimental literature. However, in practically all cases where equation (3) is explicitly taken as a definition, κ is found to lie between 0·39 and 0·41. Values outside this range are usually the result of operations or assumptions which change the definition of κ and c. In any event, it is clear in figure 1 that the data outside the sublayer are well represented by equation (3) when κ and c are given the values already mentioned.

Within the sublayer, on the other hand, large fluctuations in velocity and cramped quarters for experimentation usually combine to make measurements of mean velocity somewhat uncertain. The available data in figure 1, therefore, should not be said to establish conclusively the uniqueness of the law of the wall in the sublayer, although these data have been used elsewhere (Coles 1955) in forming a tentative estimate of the function $f(yu_\tau/\nu)$ and related functions.

B. Test of the wall law

1. *Momentum balance.* Except for a few applications of the floating-element technique in flows at constant pressure, values of surface stress in

turbulent boundary layers have usually been obtained indirectly from the observed pressure gradient and rate of momentum loss, using the momentum-integral equation of von Kármán (1921). For two-dimensional incompressible steady mean flow in a boundary layer, this equation is

$$\frac{\tau_w}{\rho} = \frac{d}{dx} u_1^2 \theta + u_1 \delta^* \frac{du_1}{dx}, \tag{11}$$

where $\tau_w(x)$ is the wall shearing stress, $u_1(x)$ is the velocity of the free stream outside the boundary layer, and $\delta^*(x)$ and $\theta(x)$ are the displacement and momentum thicknesses, defined respectively by

$$\delta^* = \int_0^\delta \left(1 - \frac{u}{u_1}\right) dy, \tag{12}$$

and

$$\theta = \int_0^\delta \frac{u}{u_1}\left(1 - \frac{u}{u_1}\right) dy. \tag{13}$$

Experience in applying equation (11) to flows with positive pressure gradient has usually been that the values obtained for τ_w appear to increase rapidly when separation is imminent, contrary to the behaviour which is intuitively expected. In fact, the experiments of Ludwieg & Tillmann (1949) were originally designed not to study the law of the wall, but rather to investigate the validity of the momentum-integral equation (11) by providing an independent estimate for τ_w.

It is therefore instructive to compare, for various experimental studies of flow in turbulent boundary layers, the values of wall shearing stress obtained from equation (11) with those inferred from the law of the wall. In order to avoid differentiation of measured quantities, equation (11) may be integrated with respect to x between two stations x_0 and x. Replacing τ_w by ρu^2, the result of the integration can be expressed by the two equations

$$\Phi(x) = \frac{u_1^2 \theta}{u_0^2 \theta_0} - 1 + \tfrac{1}{2} \int_{x_0}^{x} \frac{\delta^*}{\theta_0} d\left(\frac{u_1^2}{u_0^2}\right), \tag{14}$$

and

$$\Phi(x) = \int_{x_0}^{x} \frac{u_\tau^2}{u_0^2} d\left(\frac{x}{\theta_0}\right), \tag{15}$$

where $u_0 = u_1(x_0)$ and $\theta_0 = \theta(x_0)$.

The dimensionless function $\Phi(x)$ may be evaluated experimentally from equation (14) if δ^*, θ, and u_1 are known as functions of x. Quite independently, the same function $\Phi(x)$ may be evaluated from equation (15) if the friction velocity u_τ is obtained by fitting the velocity profile to the hypothetical law of the wall. Agreement between the slopes of the two functions $\Phi(x)$ shows that the flow in question is not inconsistent with the logarithmic law of the wall displayed in figure 1.

2. *Presentation of data.* The discussion will be limited to data obtained at reasonably large Reynolds numbers in experiments at reasonably large

scale.* The experimental point of departure is flow at constant pressure, for which some mean-velocity measurements of Wieghardt (1943) for a free-stream velocity of 33 m/sec are shown in figure 4. Here and in the fifteen following figures, the mean-velocity profiles shown are typical of the measurements, although some of the profile data have occasionally been omitted for reasons of economy in the graphical presentation.

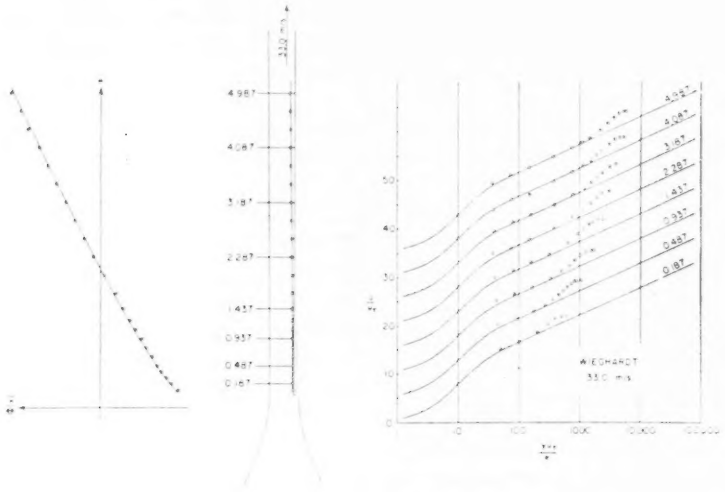

Figure 4. Data of Wieghardt (1943) for constant stream velocity; stations in metres

All of the profiles, whether shown in the figures or not, have first been individually fitted to the logarithmic region of the law of the wall, i.e. to the formula $u/u_\tau = 5{\cdot}75 \log_{10}(yu_\tau/\nu) + 5{\cdot}10$, and the resulting values of u_1/u_τ have then been smoothed where necessary. In the fitting operation it has generally been assumed that the measurements for values of yu_τ/ν less than about 200 may be unreliable as a result of large fluctuations in velocity, wall interference, poor probe sensitivity at small mean velocities, probe position error, or uncertainty in the static pressure. For consistency, therefore, the contribution of the sublayer and of the logarithmic region to δ^* and θ have been computed for the function f of figure 1, i.e. for the solid lines in figures 4 to 19, rather than for the actual measurements.

* This survey of experimental data includes certain material which has not previously been reported in detail in the literature. For their courtesy in providing this material I am indebted to F. Clauser of the Johns Hopkins University, Baltimore; Smith J. DeFrance of the NACA Ames Aeronautical Laboratory, Moffett Field; W. Tillmann of the Max-Planck-Institut für Strömungsforschung, Göttingen; K. Wieghardt of the Institut für Schiffbau, Hamburg; and A. Kuethe of the University of Michigan, Ann Arbor. I am also indebted to F. Goddard of the Jet Propulsion Laboratory, Pasadena, for making available the services of the JPL computing section.

Each of figures 4 to 19 includes a sketch showing both the geometry of the experiment and the physical extent $\delta(x)$ of the shear flow. Finally, each of the figures includes a comparison of the two functions $\Phi(x)$ of equations (14) and (15), represented by open points and by a solid line respectively.

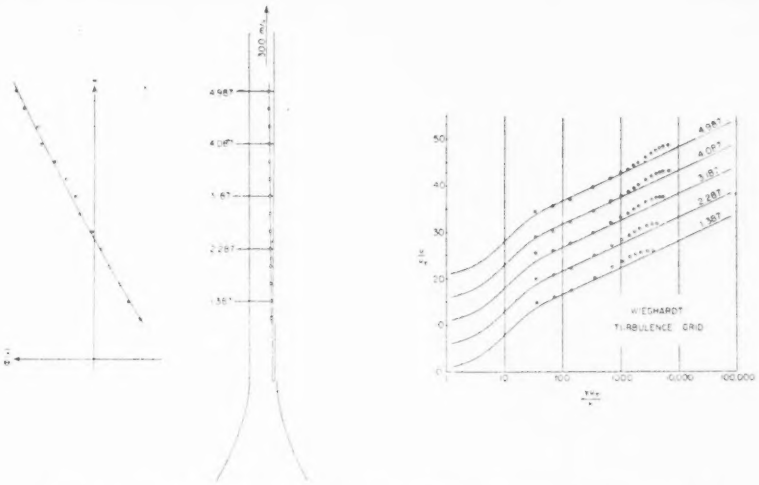

Figure 5. Data of Wieghardt (1944) with turbulence grid; stations in metres.

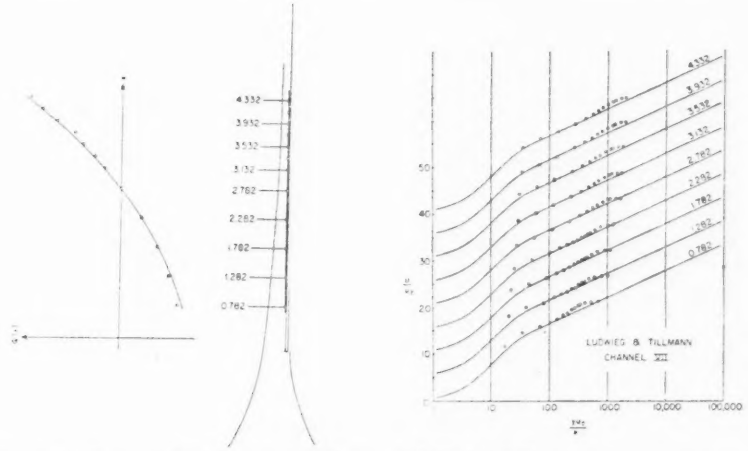

Figure 6. Data of Ludwieg and Tillmann (1949) for falling pressure; stations in metres.

3. *Unseparated flows.* Wieghardt's measurements (1943) of boundary-layer growth for a uniform external stream have already been presented in figure 4. Wieghardt (1944) also investigated the effect of increasing the

tunnel turbulence level by means of a coarse screen, obtaining the mean-velocity profiles shown in figure 5. Using the same channel and instrumentation, Ludwieg & Tillmann (1949) observed a turbulent boundary-layer flow in a region of a negative pressure gradient, with the result shown in figure 6. These particular profile measurements, and those of figures 13 and 14 below, are the ones originally cited by Ludwieg & Tillmann in their cogent paper on the law of the wall.

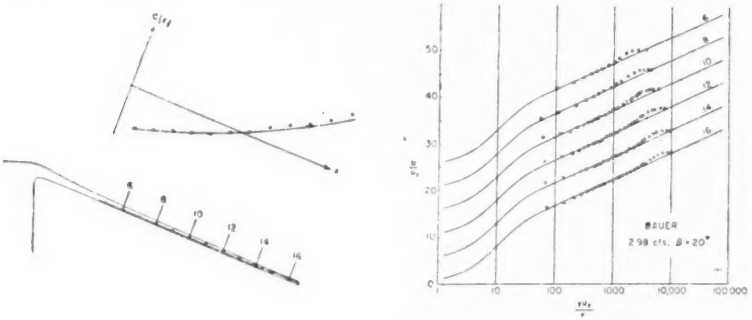

Figure 7. Data of Bauer (1951) for 20° slope; stations in feet.

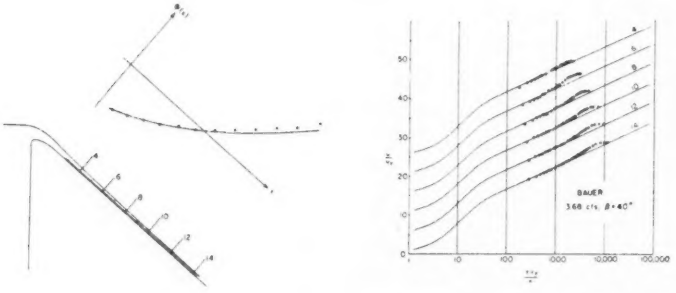

Figure 8. Data of Bauer (1951) for 40° slope; stations in feet.

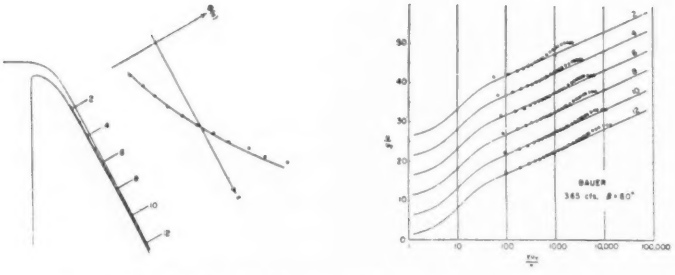

Figure 9. Data of Bauer (1951) for 60° slope; stations in feet.

Some measurements of flow near the lower boundary of a stream accelerating under the force of gravity at essentially constant pressure have been reported by Bauer (1951). The fluid is water traversing the face of a model spillway; data for flow over a smooth plane surface at angles of 20°, 40°, and 60° to the horizontal are reproduced in figures 7, 8, and 9. In each case the body force per unit volume $\rho g \sin \beta$ is independent of x and y and so plays the same role as a constant pressure force per unit volume dp/dx.

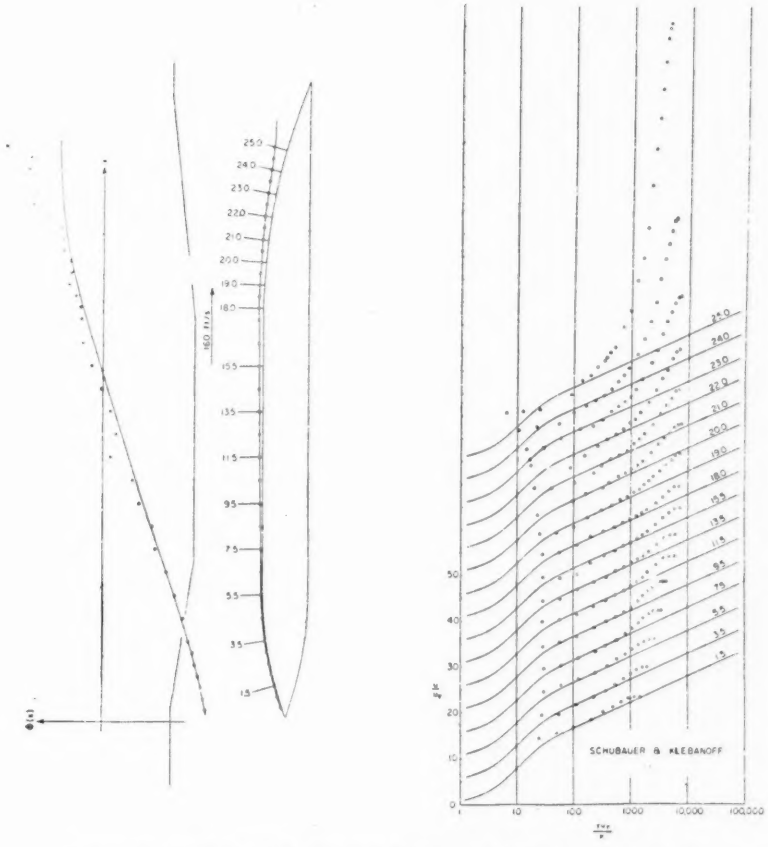

Figure 10. Data of Schubauer and Klebanoff (1950); stations in feet.

4. *Flows approaching separation.* Extensive measurements in a flow approaching separation have been made by Schubauer & Klebanoff (1950) on a large airfoil at the National Bureau of Standards. Typical mean-velocity profiles are shown in figure 10. Upstream of the 7 ft. station, the surface shearing stress and free-stream dynamic pressure both increase

in the direction of flow. Between $x = 7$ ft. and $x = 17{\cdot}5$ ft. the stress at the wall and the pressure are nearly constant. The region of rising pressure begins at about $x = 18$ ft., and separation occurs at about $x = 25{\cdot}7$ ft.

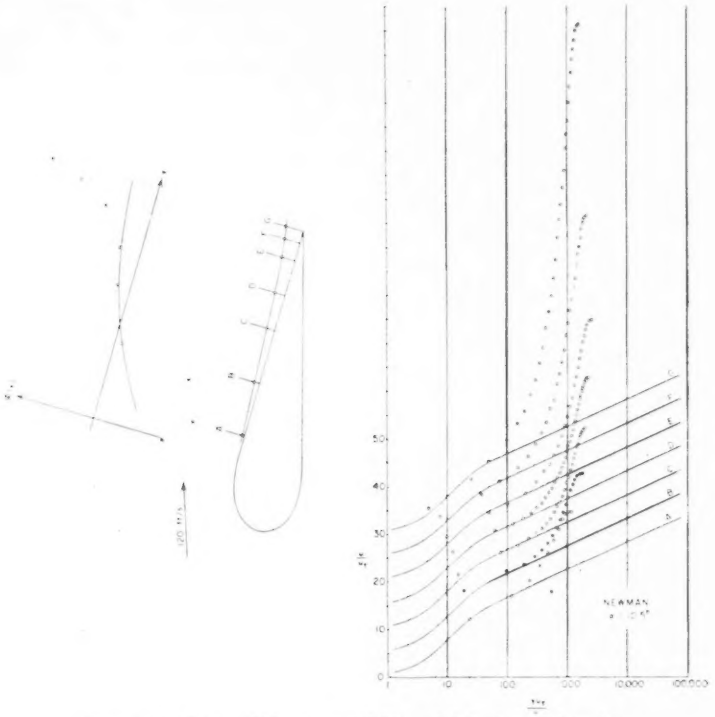

Figure 11. Data of Newman (1951); airfoil chord 50 inches.

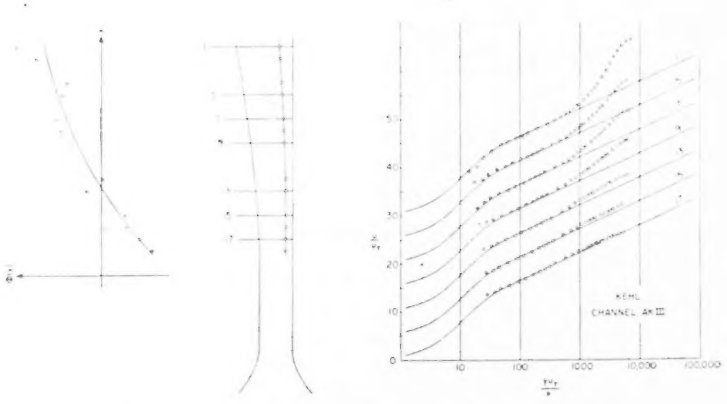

Figure 12. Data of Kehl (1943); stations in decimetres.

A similar study of a boundary layer near separation is available in some work of Newman (1951) for which the mean-velocity data are presented in figure 11. Because Newman measured the static-pressure variation within the boundary layer, and also made a plausible correction to his observed mean-velocity profiles for instrumental errors caused by turbulence, these data are among the most accurate and detailed which are available. Newman,

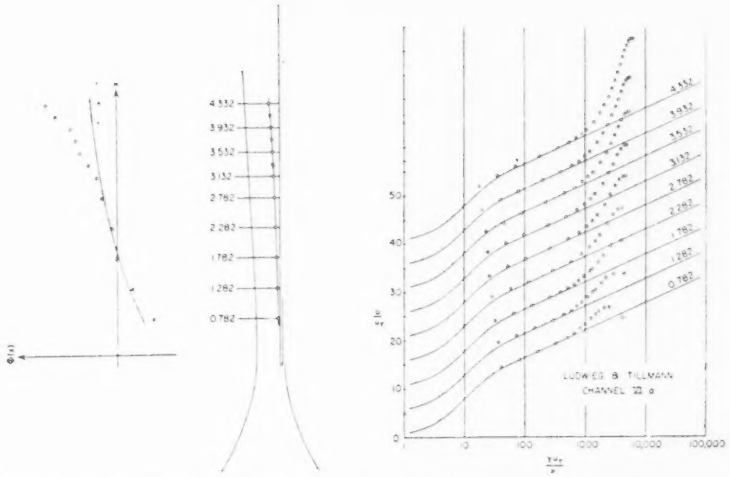

Figure 13. Data of Ludwieg and Tillmann (1949) for moderately rising pressure; stations in metres.

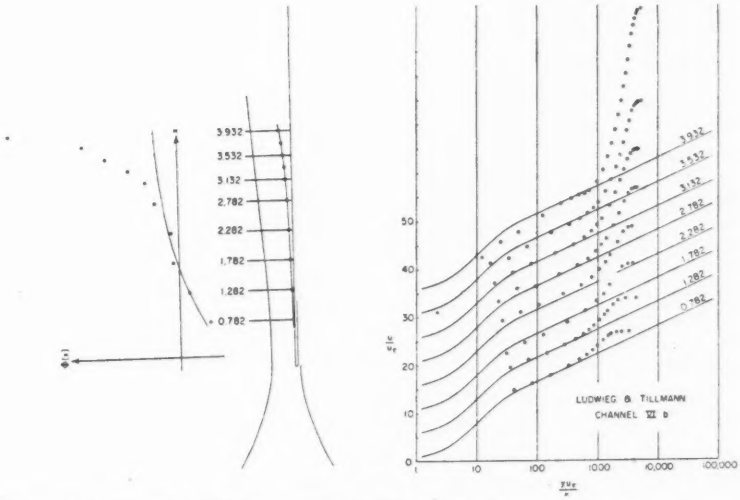

Figure 14. Data of Ludwieg and Tillmann (1949) for strongly rising pressure; stations in metres.

like Schubauer & Klebanoff, also measured turbulence intensities and turbulent shearing stress within the shear flow.

Boundary-layer flow in diffusers of constant width and rectangular section has been studied by Kehl (1943), by Ludwieg & Tillmann (1949), and by Clauser (1954), with the results shown in figures 12 to 16. In none of these five experiments did separation actually occur, and in the last two it was deliberately prevented.

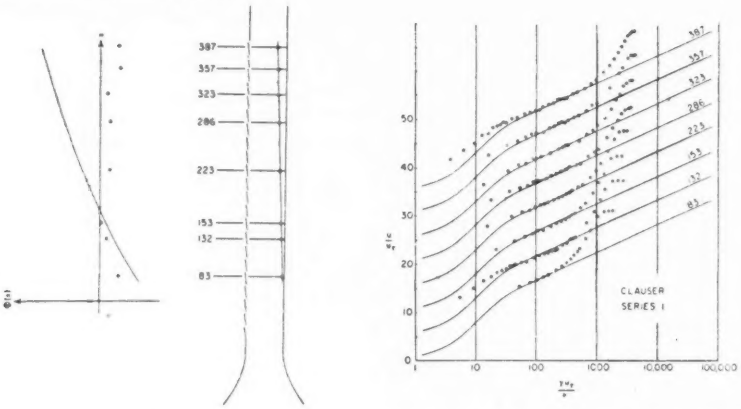

Figure 15. Data of Clauser (1954) for moderately rising pressure; stations in inches.

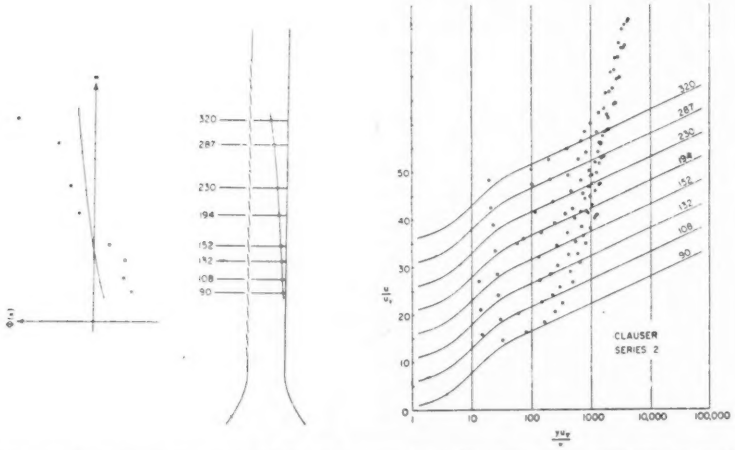

Figure 16. Data of Clauser (1954) for strongly rising pressure; stations in inches.

5. *Flows following reattachment.* Turbulent boundary-layer flow following reattachment downstream of a separation bubble has been investigated by McCullough & Gault (1949). Data for the upper surface of an NACA 64A006 airfoil section at an angle of attack of 5° are reproduced in figure 17.

Reattachment of separated flow downstream of a tripping device or spoiler, in flow with nominally constant pressure, is illustrated in figures 18 and 19 with some measurements of Klebanoff & Diehl (1951) and of Tillmann (1945). In the experiment of Klebanoff & Diehl transition occurred at the spoiler, which was a 1/4-in. diameter rod at the 4 ft. station of the plate.

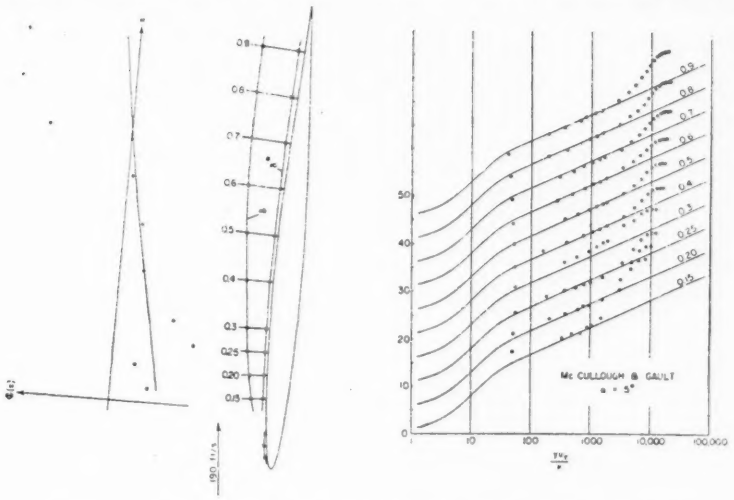

Figure 17. Data of McCullough and Gault (1949) for 5° angle of attack; airfoil chord 5 feet.

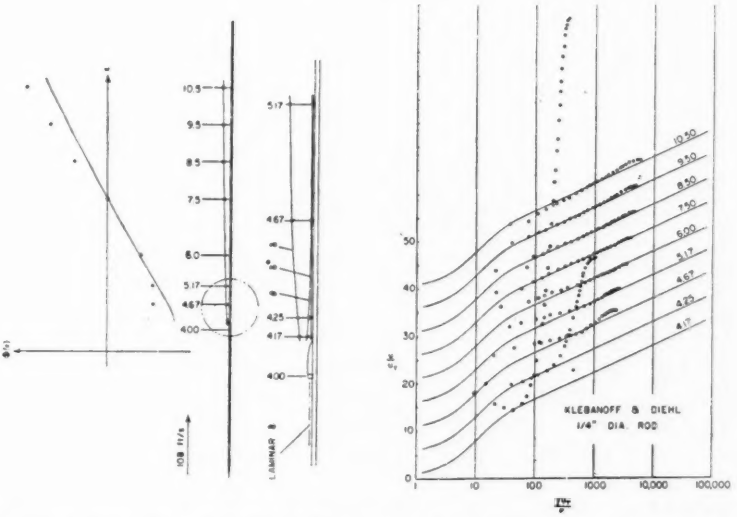

Figure 18. Data of Klebanoff and Diehl (1951) for 1/4-inch rod; stations in feet.

In the experiment of Tillmann the boundary layer was turbulent well upstream of the spoiler, which was a rectangular ledge 1·2 cm square at the 2·02 m station. In both cases it may be noted that the flow far downstream has apparently not recovered from the effects of the enforced separation, as the mean-velocity profiles do not resemble the profiles for flow at constant pressure shown in figure 4.

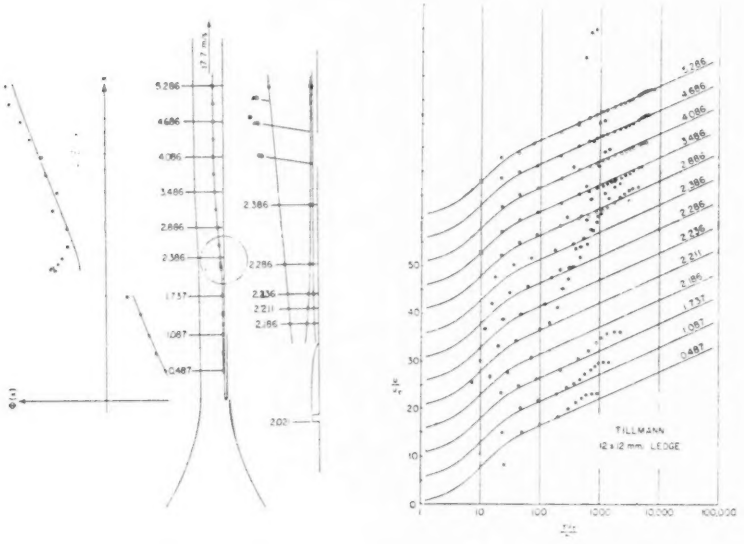

Figure 19. Data of Tillmann (1945) for 12 mm ledge; stations in metres.

6. *Evaluation.* The data cited in the previous section obviously do not provide a test of the hypothetical law of the wall alone, but provide a joint test of the law of the wall together with the turbulent boundary-layer approximation and the assumption of two-dimensional mean flow.

These data confirm that the momentum-integral equation (11) cannot be relied upon to give accurate values of surface shearing stress in the neighbourhood of separation, for the reason that the left side of (11) is then equal to a small difference between two large quantities on the right. Consequently, large errors in τ_w may be encountered, either as a result of inconspicuous departures from two-dimensional mean flow or as a result of the omission from the boundary-layer approximation of certain terms involving the Reynolds normal stresses and the pressure variation normal to the wall.

Both Ludwieg & Tillmann (1949), using a surface heat-transfer technique, and Schubauer & Klebanoff (1950), using extrapolated values of the measured

turbulent stress, have found experimentally that the surface shearing stress decreases monotonically toward zero on approaching a point of separation. Consequently, whether or not the hypothesis of a universal similarity law is correct for the flows in question, it is certain from the evidence, for example, of figures 10, 13 and 14 that the momentum-integral equation in the form (11) is seriously in error.

Besides the work of Ludwieg & Tillmann, perhaps the most convincing evidence for a universal law of the wall is simply that a distinct logarithmic region occurs in each of several hundred mean-velocity profiles examined here, with very few exceptions; a definite estimate for the wall shearing stress is readily obtained, and this estimate is entirely plausible.

At the same time, it is known (Coles 1955) that a necessary and sufficient condition for a universal law of the wall, given the boundary conditions of vanishing velocity and Newtonian friction at the surface, is that the ratio u/u_τ is constant on streamlines of the mean flow. The edge of the sublayer, as usually defined, is therefore a mean streamline. This result must surely be considered in any search for a fundamental order and unity in the description of turbulent shear flows.

It should also be noted that the concept of a universal similarity law has recently been reinforced by work of Preston (1954), using an experimental technique which depends on the general validity of equation (2) in essentially the same way that the use of a Stanton tube depends on the existence of a linear profile very near the wall.

In view of these remarks, the hypothesis of a universal law of the wall will be accepted for the purposes of the present paper. In fact, it will eventually be suggested that the similarity laws of this and the next section may be concepts sufficiently powerful to allow a quantitative treatment not only of flows approaching or recovering from separation, but also of yawed flows and flows which are actually separated from the adjacent wall.

III. The law of the wake

A. The defect law

1. *Historical development.* A special form of the defect law (6) was proposed by Darcy nearly a hundred years ago, and again by Stanton in 1911, to describe the mean-velocity profile in turbulent pipe flow. The defect law in the general form (6) was formulated independently by von Kármán (1932), who derived an approximate friction law involving two empirical constants for the turbulent boundary layer with constant pressure. According to experimental evidence from many sources, the defect function $F(\Pi, y/\delta)$ in a given flow is insensitive to roughness at the wall, provided that the origin for the normal coordinate y is properly chosen. On the other hand, it appears from a comparison of figures 4 and 5 that there is a small dependence of the defect law on the turbulence level in the external stream.

One well known and useful property of the defect law is that it avoids the awkward problem of defining the thickness δ for a boundary layer.

For, if the displacement thickness δ^* is computed from equation (12) for the profile (6), neglecting the departure of the flow in the sublayer from the logarithmic law,* there is obtained

$$\frac{\delta^* u_1}{\delta u_\tau} = \int_0^1 F\left(\Pi, \frac{y}{\delta}\right) d\left(\frac{y}{\delta}\right) = C(\Pi),$$

so that δ is proportional to $\delta^* u_1/u_\tau$. This implicit notation for the parameter Π will eventually be replaced by an explicit formula.

2. *The equilibrium boundary layer.* The concept of a defect law has recently been generalized by F. Clauser (1954), who constructed experimentally two boundary-layer flows with positive pressure gradient, such that equations (5) and (6) remained valid. The flows in question have already been described in figures 15 and 16. Clauser used the term 'equilibrium flow' to denote a flow with a defect law, that is, in the present notation, a flow for which the parameter Π is constant.

Examination of figures 7, 8 and 9 suggests that the three spillway flows studied by Bauer may be equilibrium flows in the sense of Clauser's definition. So, at least approximately, is the flow with falling pressure studied by Ludwieg & Tillmann and reported in figure 6.

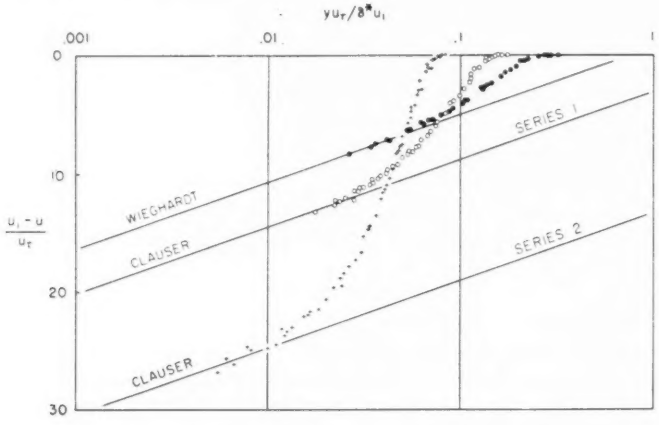

Figure 20. The defect law.

A comparison of the velocity-defect function F for three equilibrium flows can be found in figure 18 of Clauser's paper, and is repeated here in figure 20. This figure, unfortunately, sheds little light on the way in which the argument y/δ and the parameter Π are involved in the function $F(\Pi, y/\delta)$ of equation (6), and therefore does not immediately suggest any useful generalization of the defect law to non-equilibrium flows.

* This remark implies that, for example, $\int f\,dz$ is written $fz - \int z\,df$, and df is replaced by $dz/\kappa z$ as if the function f were logarithmic everywhere.

3. *The logarithmic region.* At this point a further important consequence of the defect law in equilibrium flow should be mentioned. In the first instance, the mixing analogy of Prandtl or von Kármán implies a logarithmic variation of the function $f(yu_\tau/\nu)$ in flows for which τ does not depend on y. However, if the law of the wall is universally valid, then the velocity distribution $u(y)$ can be expressed independently of the shear distribution $\tau(y)$; thus the argument based on the mixing analogy in favour of a logarithmic mean-velocity distribution is seriously weakened.

It is therefore instructive to consider another argument, first proposed by Millikan (1938) and based on the wall and defect laws, which also leads to a logarithmic function f in equation (2). From the law of the wall, $u/u_\tau = f(yu_\tau/\nu)$, it follows that

$$\frac{y}{u_\tau}\frac{\partial u}{\partial y} = \frac{yu_\tau}{\nu} f'\left(\frac{yu_\tau}{\nu}\right).$$

From the defect law, $(u_1-u)/u_\tau = F(\Pi, y/\delta)$, the corresponding expression is

$$\frac{y}{u_\tau}\frac{\partial u}{\partial y} = -\frac{y}{\delta} F'\left(\frac{y}{\delta}\right),$$

where the constant parameter Π has been suppressed for an equilibrium flow. Now suppose that there is a finite region in which the wall and defect laws are simultaneously valid. In this region, the last two equations require that

$$\frac{yu_\tau}{\nu} f'\left(\frac{yu_\tau}{\nu}\right) = -\frac{y}{\delta} F'\left(\frac{y}{\delta}\right) = \frac{y}{u_\tau}\frac{\partial u}{\partial y} = \frac{1}{\kappa(x,y)},$$

say. Obviously, $\kappa(x,y)$ is fixed when either of the two variables yu_τ/ν or y/δ is specified. But these variables are formally independent of each other, since their ratio $\delta u_\tau/\nu$ may be chosen arbitrarily. It follows that κ must be a constant. Furthermore, on integrating the expression for $\partial u/\partial y$ over the region in question, it is found that

$$f\left(\frac{yu_\tau}{\nu}\right) = \frac{1}{\kappa}\ln\frac{yu_\tau}{\nu} + \text{const.},$$

in agreement with equation (3).

B. The wake hypothesis

1. *The wake function.* The defect law (6) has at least a limited physical interpretation, in that the loss of momentum is expressed independently of the viscosity. This property, being consistent with the idea of a turbulent rather than a viscous transport process, can reasonably be assumed, as in Millikan's argument, to apply everywhere outside the sublayer. Furthermore, the observed sensitivity of the momentum defect to external turbulence level and the observed insensitivity to wall roughness are not surprising.

On the other hand, the various mean-velocity profiles so far studied are quite systematic in coordinates $(u/u_\tau, yu_\tau/\nu)$ which involve the viscosity

of the fluid. In fact, once the universal law of the wall is accepted, it is difficult to escape the conviction that an arbitrarily chosen profile is completely determined when the free-stream point $(u_1/u_\tau, \delta u_\tau/\nu)$ is specified. To illustrate this remark, figure 21 shows several mean-velocity profiles selected from various boundary-layer flows described earlier.* These profiles have essentially the same defect law (that is to say, the same value of the parameter Π) in spite of wide variations in environment.

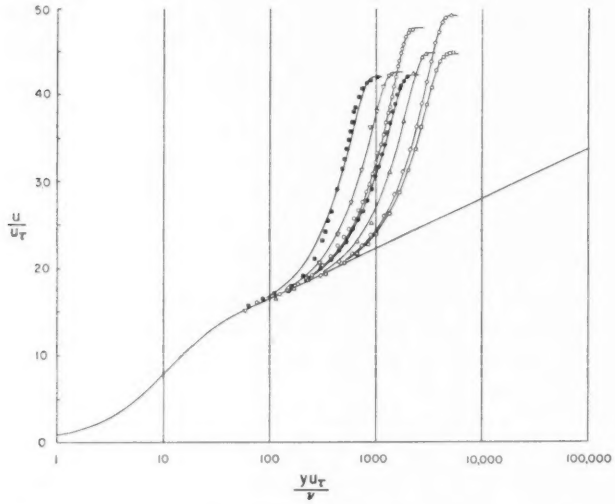

Figure 21. Two-parameter similarity in the mean-velocity profile.

Taking these properties together, it is something of an anticlimax to discover that the puzzle of the defect law is apparently a simple one. The key lies not in a study of the defect function F of equation (6), but in a study of the original function $g(\Pi, y/\delta)$ of equation (5), which gives the departure of the mean-velocity profile from the logarithmic law of the wall. For the three equilibrium flows of figure 20, this departure is shown in figure 2, using a linear scale for $yu_\tau/\delta^* u_1$. There is a striking resemblance between the three curves, including a common anti-symmetry about a midpoint. But this resemblance is obviously not confined to equilibrium flows if, as has just been suggested in figure 21, an arbitrary profile in non-equilibrium flow coincides in the coordinate system $(u/u_\tau, yu_0/\nu)$ with a profile from some member of the one-parameter family of equilibrium flows.

* Reading from left to right, the profiles are taken from figure 18 (Klebanoff & Diehl 1951, station 4.25), figure 16 (Clauser 1954, Series 2, station 108), figure 11 (Newman 1951, stations D and C), figure 16 (Clauser 1954, Series 2, station 230), and figure 14 (Ludwieg & Tillmann 1949, Channel VI b, stations 3.73 and 3.53).

In view of these remarks and especially in view of figure 2, the mean-velocity profile may tentatively be written in the form already presented as equation (7),

$$\frac{u}{u_\tau} = f\left(\frac{yu_\tau}{\nu}\right) + \frac{\Pi(x)}{\kappa} w\left(\frac{y}{\delta}\right),$$

where the function $w(y/\delta)$, for reasons which will become apparent, will be called the law of the wake. If Π does not depend on x, then both $g(\Pi, y/\delta)$ in equation (5) and $\Pi w(y/\delta)$ in equation (7) are functions of y/δ only. This is the property assigned to equilibrium flows by Clauser. The present formulation of the mean-velocity profile is, however, more general than equation (5), in the sense that the law of the wake, although it occurs as a restricted form of (5) which is itself a special form of equation (4), is here assumed to apply for non-equilibrium flows.

2. *Normalizing conditions.* In order to test the hypothesis of a universal wake function in equation (7), it is necessary first to define the thickness δ and to specify some normalizing factor for w. To this end, the displacement thickness δ^* may be computed from the definition, equation (12), for the particular profile given by (7). Neglecting the departure of the flow in the sublayer from the logarithmic wall law, we obtain

$$\delta^* = \delta \frac{u_\tau}{u_1}\left(\frac{1}{\kappa} + \frac{\Pi}{\kappa}\int_0^{w_1} \frac{y}{\delta}\, dw\right),$$

where w_1 is tentatively defined as the maximum value of w. It is therefore convenient to take as a first normalizing condition

$$\int_0^{w_1} \frac{y}{\delta}\, dw = 1. \tag{16}$$

A second normalizing condition is suggested by the nearly anti-symmetric form of the curves in figure 2. The maximum value of w will occur very nearly at $y/\delta = 1$, provided that

$$w_1 = w(1) = 2. \tag{17}$$

Now $w(y/\delta)$ is by hypothesis a universal function, so that the boundary-layer thickness δ is uniquely defined in terms of δ^* by the integral condition (16) and the maximum condition (17). That is, the two relationships (8) and (9), together with the identity

$$\left(\frac{\delta^*}{\delta}\right)\left(\frac{u_1}{u_\tau}\right) = \left(\frac{\delta^* u_1}{\nu}\right)\Big/\left(\frac{\delta u_\tau}{\nu}\right),$$

are sufficient to determine all five of the dimensionless parameters u_1/u_τ, δ^*/δ, $\delta u_\tau/\nu$, $\delta^* u_1/\nu$, and Π (or $\delta^* u_1/\delta u_\tau$) when any two are given. For example, if the two known quantities are u_1/u_τ and $\delta^* u_1/\nu$, as is supposedly the case for the data cited in Part II of this study, then equations (8) and (9) lead to a simple transcendental equation for Π;

$$2\Pi - \ln(1+\Pi) = \kappa \frac{u_1}{u_\tau} - \ln \frac{\delta^* u_1}{\nu} - \kappa c - \ln \kappa. \tag{18}$$

3. *Profile at separation.* Equation (7) as originally written is not in a convenient form for use near a point of separation or reattachment. However, on multiplication by u_τ/u_1 and the elimination of Π by means of (9), equation (7) leads to

$$\frac{u}{u_1} = \frac{u_\tau}{u_1} f\left(\frac{yu_\tau}{\nu}\right) + \left(\frac{\delta^*}{\delta} - \frac{1}{\kappa}\frac{u_\tau}{u_1}\right) w\left(\frac{y}{\delta}\right).$$

If u_τ is put equal to zero in this expression, the result is evidently

$$\frac{u}{u_1} = \frac{\delta^*}{\delta}\, w\left(\frac{y}{\delta}\right) = \tfrac{1}{2} w\left(\frac{y}{\delta}\right).$$

Moreover, certain numerical values can be assigned in advance to the ratios δ^*/δ, θ/δ and δ^*/θ at separation or reattachment. For example, the definition of δ adopted here takes account of the nearly anti-symmetric variation of w by requiring that $\delta^*/\delta = \frac{1}{2}$ at separation. A corollary, anticipating numerical values of the next section, is $\theta/\delta = 0{\cdot}12$ (approximately). On the other hand, the prediction $\delta^*/\theta = 4{\cdot}2$ (approximately) at separation or reattachment is a result which is relatively free of preconceptions about the form of the wake function w. It should also be noted that this prediction is based on examination of the mean-velocity profile in flows which need not be close to separation.

Table 1. The wake function $w(\zeta)$ and related functions.

ζ	$w(\zeta)$	$\int_0^w \zeta\, dw$	$\omega_1(\Pi, \zeta)$	$\omega_2(\Pi, \zeta)$
0	0	0	$1 - 0{\cdot}000\Pi$	$1 - 0{\cdot}000\Pi - 0{\cdot}000\Pi^2$
0·05	0·004	0	$1 - 0{\cdot}002\Pi$	
0·10	0·029	0·002	$1 - 0{\cdot}022\Pi$	$1 - 0{\cdot}027\Pi - 0{\cdot}000\Pi^2$
0·15	0·084	0·009	$1 - 0{\cdot}062\Pi$	
0·20	0·168	0·024	$1 - 0{\cdot}119\Pi$	$1 - 0{\cdot}154\Pi - 0{\cdot}008\Pi^2$
0·25	0·272	0·047	$1 - 0{\cdot}190\Pi$	
0·30	0·396	0·082	$1 - 0{\cdot}272\Pi$	$1 - 0{\cdot}360\Pi - 0{\cdot}044\Pi^2$
0·35	0·535	0·127	$1 - 0{\cdot}363\Pi$	
0·40	0·685	0·183	$1 - 0{\cdot}458\Pi$	$1 - 0{\cdot}614\Pi - 0{\cdot}127\Pi^2$
0·45	0·838	0·248	$1 - 0{\cdot}552\Pi$	
0·50	0·994	0·322	$1 - 0{\cdot}645\Pi$	$1 - 0{\cdot}880\Pi - 0{\cdot}257\Pi^2$
0·55	1·152	0·405	$1 - 0{\cdot}737\Pi$	
0·60	1·307	0·495	$1 - 0{\cdot}824\Pi$	$1 - 1{\cdot}143\Pi - 0{\cdot}426\Pi^2$
0·65	1·458	0·589	$1 - 0{\cdot}906\Pi$	
0·70	1·600	0·685	$1 - 0{\cdot}978\Pi$	$1 - 1{\cdot}380\Pi - 0{\cdot}610\Pi^2$
0·75	1·729	0·778	$1 - 1{\cdot}037\Pi$	
0·80	1·840	0·863	$1 - 1{\cdot}079\Pi$	$1 - 1{\cdot}561\Pi - 0{\cdot}765\Pi^2$
0·85	1·926	0·935	$1 - 1{\cdot}100\Pi$	
0·90	1·980	0·981	$1 - 1{\cdot}090\Pi$	$1 - 1{\cdot}640\Pi - 0{\cdot}823\Pi^2$
0·95	1·999	0·999	$1 - 1{\cdot}051\Pi$	
1·00	2·000	1·000	$1 - 1{\cdot}000\Pi$	$1 - 1{\cdot}600\Pi - 0{\cdot}761\Pi^2$

4. *Test of the hypothesis.* For obvious reasons, the existence and form of the hypothetical wake function $w(y/\delta)$ are most readily investigated in flows with a large wake component. Figure 2 shows the function in question,

subject to the normalizing conditions (16) and (17), for several mean-velocity profiles taken from the present survey. The difference in apparent scatter between the non-equilibrium and equilibrium data is the result of applying the normalizing conditions to individual profiles in the first case, but to the average of several profiles in the second. For unseparated flows at least, the wake hypothesis appears to be a useful concept, and a tentative determination of the wake function $w(y/\delta)$ is therefore tabulated in table 1 and plotted in figures 2 and 21.

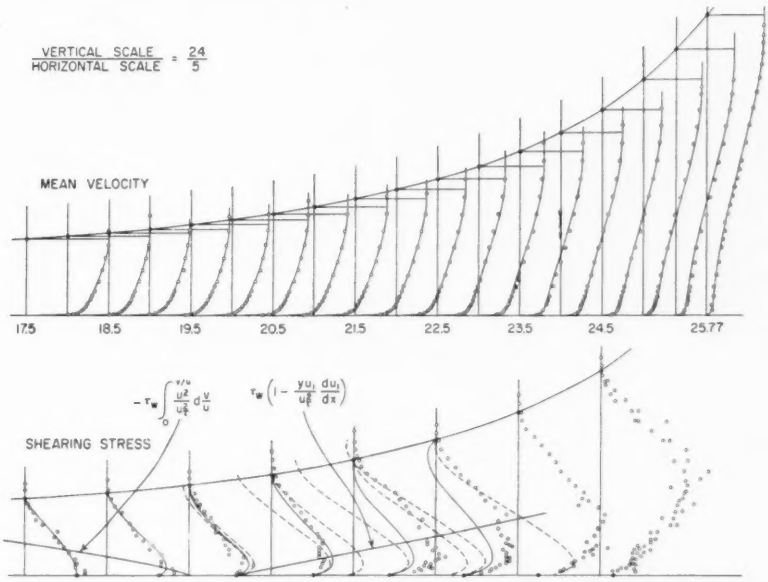

Figure 22. The separating flow of Schubauer and Klebanoff (1950) (measured values of shearing stress have been reduced by 31 percent).

The two-component profile, equation (7), can be made to represent quite well the data of Schubauer & Klebanoff, as shown in figure 22; of Newman, as shown in figure 23; of Kehl; of Clauser; of Ludwieg & Tillmann; of McCullough & Gault at 5° angle of attack, as shown in figure 24; and of Tillmann for reattaching flow, as shown in figure 25. The solid lines in these figures are computed from equation (7), using values for u_1, u_τ, δ, and Π which vary smoothly with x. Occasionally it has been found desirable to make slight revisions in the original values for the profile parameters obtained from consideration of the law of the wall alone.

A few exceptions to the law of the wake can be found among the numerous profiles presented here. For example, it is impossible to find satisfactory values for the parameters u_1, u_τ, δ, and Π in the general formula (7) such that the profile at the left in figure 21 can be represented within the apparent

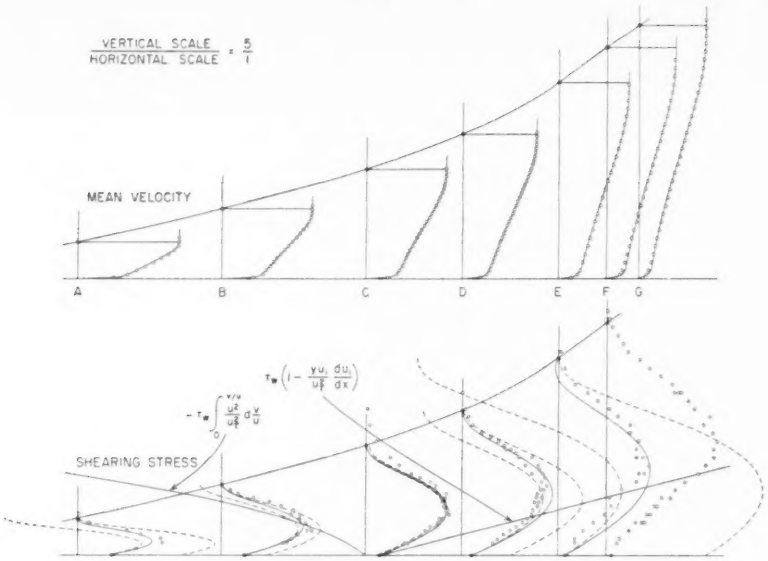

Figure 23. The separating flow of Newman (1951).

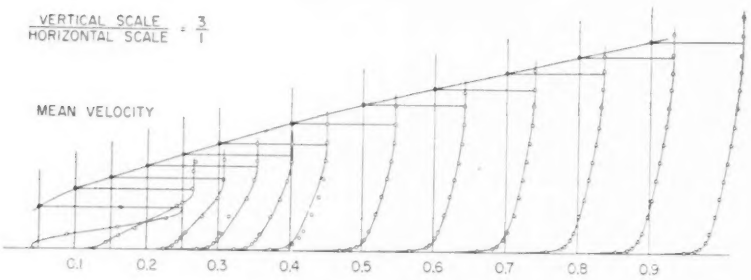

Figure 24. The reattaching flow of McCullough and Gault (1949).

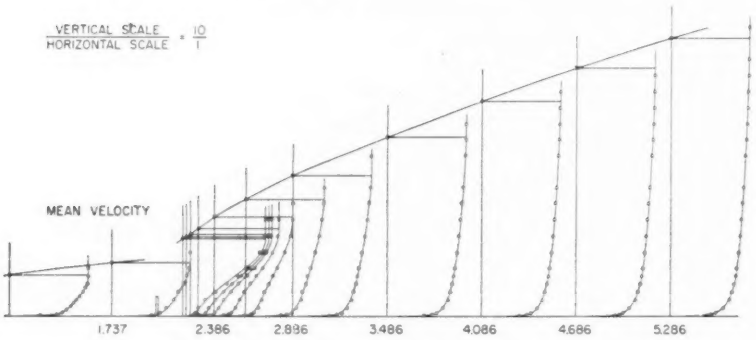

Figure 25. The reattaching flow of Tillmann (1945).

experimental accuracy. This profile, however, was obtained about two boundary-layer thicknesses downstream of reattachment, in a region where the real accuracy of the profile measurements is unknown.

Finally, it may be remarked that Wieghardt's experiments in figure 5 indicate that there is a definite change in the shape as well as the amplitude of the wake component in flow at constant pressure when the free-stream turbulence level is increased. The term 'universal function' applied to the law of the wake therefore implies that the external turbulence level is low, much as the same term applied to the law of the wall implies negligible surface roughness.

IV. Discussion

A. The equations of mean motion

1. *The turbulent shearing stress.* In the past an important aim of phenomenological theories of turbulent shear flow has usually been to develop *a priori* some relationship connecting shearing stress and mean velocity, by analogy with the relationship $\tau = \mu \partial u/\partial y$ for laminar flow. It is now generally accepted that such a relationship probably does not exist in any practical sense. However, the same purpose is ultimately served by the equations of mean motion, which provide a valid relationship between shearing stress and mean velocity. In this respect the present analytic representation (7) of the mean-velocity profile may be exploited immediately.

The continuity equation may first be satisfied by introducing a stream function $\psi(x,y)$ such that $u = \partial\psi/\partial y$ and $v = -\partial\psi/\partial x$; ψ is then constant on streamlines of the mean flow. But, if the departure of the profile in the sublayer from the logarithmic law of the wall is neglected, equation (7) requires that

$$\frac{\psi}{\nu} = \frac{1}{\nu}\int_0^y u\,dy = \frac{yu_\tau}{\nu}\left(\frac{u}{u_\tau} - \frac{1}{\kappa}\right) - \frac{\Pi}{\kappa}\frac{\delta u_\tau}{\nu}\int_0^w \frac{y}{\delta}\,dw. \tag{19}$$

A formula for the normal component of velocity may be obtained from $v = -\partial\psi/\partial x$, using equation (19) for $\psi(x,y)$, or directly from the continuity equation $\partial u/\partial x + \partial v/\partial y = 0$, using equation (7) for $u(x,y)$. In either case it is found that

$$\frac{v}{u} = -\frac{y}{u_\tau}\frac{du_\tau}{dx} - \frac{yu_\tau}{\kappa}\frac{w}{u}\frac{d\Pi}{dx} + \frac{1}{\kappa u}\frac{d(\Pi\delta u_\tau)}{dx}\int_0^w \frac{y}{\delta}\,dw. \tag{20}$$

This expression is an exact consequence of equation (7), in the sublayer as elsewhere. Its application in the calculation of the shearing-stress profile is most easily shown by putting $-\partial v/\partial y$ for $\partial u/\partial x$ in the boundary-layer momentum equation

$$\tau = \tau_w - y\rho u_1\frac{du_1}{dx} + \rho\int_0^y \left(u\frac{\partial u}{\partial x} + v\frac{\partial u}{\partial y}\right)dy,$$

thereby obtaining

$$\frac{\tau}{\tau_w} = 1 - \frac{yu_1}{u_\tau^2}\frac{du_1}{dx} - \int_0^{v/u}\frac{u^2}{u_\tau^2}\,d\left(\frac{v}{u}\right). \tag{21}$$

2. *Flow at constant pressure.* For flow at constant pressure, i.e. for Π and u_1 constant, the expression (21) will be evaluated explicitly for the profile given by equation (7). Making the usual approximation in the sublayer, the result can be written in the form

$$\kappa^2\left(1-\frac{\tau}{\tau_w}\right) = -\frac{y}{u_\tau}\frac{du_\tau}{dx}\left[\left(\kappa\frac{u}{u_\tau}\right)^2 - 2\left(\kappa\frac{u}{u_\tau}\right)\omega_1 + \right.$$
$$\left. + \left(\kappa\frac{u}{u_\tau}\right)\left(\kappa\frac{u_1}{u_\tau}\right)(\omega_1-1) - 2\left(\kappa\frac{u_1}{u_\tau}\right)(\omega_2-\omega_1) + 2\omega_2\right], \quad (22)$$

where ω_1 and ω_2 are auxiliary functions which depend on an argument $\zeta = y/\delta$ and a parameter Π; that is,

$$\omega_1(\Pi,\zeta) = 1 + \frac{\Pi}{\zeta}\int_0^{w(\zeta)} \zeta'\,dw',$$

$$\omega_2(\Pi,\zeta) = \omega_1 + \frac{\Pi}{\zeta}\int_0^{w(\zeta)} \zeta' \ln\frac{\zeta}{\zeta'}\,dw' + \frac{\Pi^2}{\zeta}\int_0^{w(\zeta)} \zeta'(w-w')\,dw',$$

where $w(\zeta)$ is the wake function. The quantities $\omega_1(\Pi,\zeta)$ and $\omega_2(\Pi,\zeta)$ are tabulated together with w in table 1.

Finally, the derivative du_τ/dx in equation (22) may be disposed of by putting $y = \delta$ to obtain*

$$\kappa^2 = -\frac{\delta}{u_\tau}\frac{du_\tau}{dx}\left[\left(\kappa\frac{u_1}{u_\tau}\right)^2\Omega_1 - 2\left(\kappa\frac{u_1}{u_\tau}\right)\Omega_2 + 2\Omega_2\right]$$

with $$\Omega_1(\Pi) = \omega_1(\Pi,1) = 1+\Pi$$

and $$\Omega_2(\Pi) = \omega_2(\Pi,1) = 1+1{\cdot}600\Pi+0{\cdot}761\Pi^2.$$

Klebanoff (1954) has recently measured the turbulent shearing-stress distribution in a boundary layer with constant pressure such that

$$\delta^* u_1/\nu = 9{,}700,$$
$$\delta^* = 0{\cdot}400\text{ in.}$$

The experimental mean-velocity profile for this flow has already been shown in figure 1. However, in order to make the present calculation independent of Klebanoff's measurements, it is convenient to estimate the parameter Π from the data of Wieghardt in figure 4. Using either equation (7) and the observed maximum excursion from the logarithmic law, or equation (18) and the experimental values for u_1/u_τ and $\delta^* u_1/\nu$, it is found that Π is very nearly 0·55 for flow at constant pressure. Then, from equations (9) and (8), with $\delta^* u_1/\nu = 9{,}700$ and $\Pi = 0{\cdot}55$,

$$\delta u_\tau/\nu = 2{,}500, \quad u_1/u_\tau = 27{\cdot}4, \quad \delta^*/\delta = 0{\cdot}142.$$

Furthermore, with $\delta^* = 0{\cdot}400$ in., $\delta = 2{\cdot}83$ in.

The profile u/u_τ computed as a function of $yu_\tau/\nu = (\delta u_\tau/\nu)(y/\delta)$ from equation (7) is plotted in figure 1. The excellent agreement with Klebanoff's

* This expression, like equation (37) of a previous paper (Coles 1954), is a special form of the momentum-integral equation (11), and may be used to compute a length Reynolds number. The present definition of the thickness δ, however, requires the numerical constants $\phi(1) = 7{\cdot}90$, $C_1 = 4{\cdot}05$, and $C_2 = 29{\cdot}0$ of the cited paper to be replaced (anticipating the value $\Pi = 0{\cdot}55$) by $c + 2\Pi/\kappa = 7{\cdot}85$, $\Omega_1/\kappa = 3{\cdot}88$, and $2\Omega_2/\kappa^2 = 26{\cdot}4$.

measurements is to be expected in view of the efforts made at the National Bureau of Standards to insure that the flow in question would be typical of the fully-developed boundary layer.

The profile $\tau/q = (\tau/\tau_w)(2u_\tau^2/u_1^2) = -2\overline{u'v'}/u^2$ computed from equation (22) is plotted against y/δ in figure 26, together with measured data using the present estimate for δ of 2·83 in. Finally, to establish the extent of the region of intermittent turbulence in terms of the coordinate y/δ occurring in the law of the wake, figure 26 also shows Klebanoff's measurements of the intermittency factor γ, defined as the fraction of the time that the flow is turbulent. The mean position of the turbulent boundary, i.e. the point $\gamma = \frac{1}{2}$, is found to be at $y/\delta = 0{\cdot}825$, with a standard deviation of 0·148 about the mean.

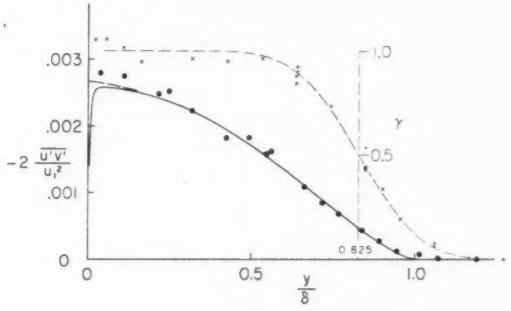

Figure 26. Shearing-stress profile in the flow of Klebanoff (1954).

3. *Flow approaching separation.* Schubauer & Klebanoff (1950) and Newman (1951) have recently carried out hot-wire measurements of turbulent shearing-stress in flows approaching separation. The representation of the mean-velocity field by the general profile equation (7) has already been illustrated in figures 22 and 23 for the flows in question. The corresponding shearing stress profiles, computed with the aid of equations (20) and (21), are shown in the same figures together with the profiles determined experimentally. As noted in the figure, the values of $\overline{u'v'}$ reported by Schubauer & Klebanoff have been reduced by 31% in view of the excessively large values obtained for τ_w when $\tau(y)$ is extrapolated to $y = 0$. It is likely that the hot-wire data are in fact too high, most probably as a result of over-compensation.

Unfortunately, these calculations of shearing stress can be attempted only for regions in which the mean-velocity field is in reasonable agreement with the momentum-integral condition expressed by equation (11). Elsewhere in the flow it is found to be possible to satisfy only one of the two boundary conditions $\tau = 0$ at $y = \delta$ or $\tau = \rho u_\tau^2$ at $y = 0$, u_τ being derived from a fit to the law of the wall. The alternative calculations are shown in figures 22 and 23 by the dashed lines. Because equation (21) is precisely

equivalent to equation (11), the values obtained for τ_w on putting $\tau = 0$ at $y = \delta$ are obviously the same as the values implied by the slope of the function $\Phi(x)$ which is defined by equation (14) and is denoted by the open points in figures 10 and 11 for the data of Schubauer & Klebanoff and of Newman respectively. The discrepancies encountered in τ_w appear to be too large to be caused entirely by the neglect in equation (21) of the Reynolds normal stresses and the pressure variation $\partial p/\partial y$, although this question is still open.

Another explanation for the failure of the two-dimensional momentum-integral equation (11) has been suggested on experimental grounds by several writers. The displacement of fluid in a boundary layer is assumed to be described by the streamline slope v/u, obtained by integrating the continuity equation $\partial u/\partial x + \partial v/\partial y = 0$. This displacement will certainly be affected by lateral convergence or divergence of the general flow, although the presence of three-dimensional effects would not necessarily be revealed by a study of the mean-velocity profile $u(y)$ measured at various lateral stations.

If τ_w is known but the values taken for v/u are even slightly in error, the right-hand side of equation (21) will not vanish at the outer edge of the boundary layer. Conversely, large errors in τ_w may be encountered on putting $\tau = 0$ at $y = \delta$. At one station in each of figures 22 and 23, the quantities

$$1 - \frac{yu_1}{u_\tau^2}\frac{du_1}{dx} \qquad \text{and} \qquad -\int_0^{v/u} \frac{u^2}{u_\tau^2}\, d\left(\frac{v}{u}\right)$$

are plotted separately in order to illustrate the extreme sensitivity of their sum τ/τ_w to small variations in v/u or in du_1/dx. Finally, as a tentative correction for three-dimensional flow the streamline slopes v/u have been multiplied by suitable constant factors close to unity in order to satisfy both boundary conditions on τ. The corrected shearing stress profiles are shown by the solid lines in figures 22 and 23.

B. Physical interpetation

1. *Two-dimensional flow.* In this paper the term 'wake function' has consistently been used to denote the function $w(y/\delta)$ in equation (7). The reason for this choice of terminology can be found in some measurements by Liepmann & Laufer (1947) of a plane half-wake or half-jet; that is, in the wedge-shaped region of turbulent mixing between a uniform flow and a fluid at rest.

The dimensionless mean-velocity profiles for the fully developed half-wake were originally reported by Liepmann & Laufer to satisfy a similarity law corresponding to a linear growth of the shear flow. These same profiles, after a further translation and change of scale for the coordinates,* are compared in figure 2 with the wake function w for flow

* The present variable $\zeta = y/\delta$ is related to the original variable $\sigma y/x$ in figure 13 of Liepmann & Laufer's paper by the expression $\zeta = 0{\cdot}505 + 0{\cdot}331\sigma y/x$. When $\zeta = 0$, $\sigma y/x = -1{\cdot}52$; and when $\zeta = 1$, $\sigma y/x = 1{\cdot}50$. Then $\sigma\delta/x = 3{\cdot}02$, and it follows that, if $\sigma = 12$, $\delta/x = 0{\cdot}252$ rads or $14{\cdot}4°$.

in a boundary layer. The residual velocity near $y/\delta = 0$ in the figure is the normal component of velocity associated with fluid entrainment, and agrees in magnitude with the value $v/u_1 = 0{\cdot}03$ implied at $y/\delta = 0$ by the equations of mean motion for the half-wake.

Although the motion represented by the upper curve in figure 2 is bounded on the low-velocity side by fluid at rest, rather than by a solid wall, there can be little doubt that the similarity between the various experimental curves in the figure is more than accidental, and that substantially the same physical phenomenon is involved. The interpretation of the wake component in a boundary layer as a large-scale mixing process has already been mentioned in Part I in connection with figure 3.

It goes without saying that if the streamwise mean-velocity distribution in a turbulent boundary layer can in fact be expressed as a linear combination of wall and wake components, as in equation (7), then so can the normal mean-velocity component v, the mean stream function ψ, and the displacement thickness δ^*, all of which are obtained from $u(x, y)$ by linear operations. This is not so, however, for the flow inclination v/u, the momentum thickness θ, or the shearing stress τ; and it is most emphatically not so for the turbulent fluctuations, except in so far as the wake and wall components might be expected to contribute more strongly to the small and large wave number regions of the spectrum respectively. On the other hand, a foundation has been laid in the present paper for the comparison, at corresponding points in various free and bound shear layers, of measurements of intermittency factor as well as of spectra and intensity of various fluctuating quantities.

Finally, in the event that the parameter Π is constant in a turbulent boundary layer, a certain balance is implied between the constraints imposed by inertia and by viscosity, and between the large-scale and small-scale mixing processes. This balance is precisely measured in equation (9) by the magnitude of the parameter Π or alternatively of the combination $\delta^* u_1/\delta u_\tau$. From the point of view adopted in these paragraphs, therefore, Clauser's choice of the term 'equilibrium flow' to describe the situation when Π is constant may well be regarded as inspired.

It should be noted that Lees & Crocco (1952) have recently attempted a qualitative analysis of turbulent shear flows in which they visualize a continuous spectrum of mixing processes having both wake-like and boundary-layer-like properties. The concept of two flow components, one depending on friction and the other on the cumulative effect of pressure gradient, has also been independently advanced by Ross & Robertson (1951) and by Rotta (1950), both of whom used a term linear in y to represent what is called here the wake function $w(y/\delta)$. These authors did not give any interpretation for either of the mean-velocity functions, and were therefore able to recommend their formulation of the problem only as a useful engineering approach, although Rotta obtained relationships which anticipate the present work. As a matter of historical interest, it should also be noted that a much earlier attempt by Millikan (1938) to

examine the function denoted by $h(x, y)$ in equation (4) was unsuccessful because the experimental data studied were not sufficiently precise. These efforts have certainly contributed, if not to the specific concept called the law of the wake, at least to the atmosphere in which this concept was evolved.

2. *Yawed flow.* The present interpretation of the wake and wall components in a turbulent boundary layer, as manifestations of the constraints provided by inertia and viscosity respectively, is not necessarily restricted to two-dimensional flows, provided the two flow components are viewed as vector rather than scalar functions of position. Specifically, suppose that the general profile equation (7) is rewritten in the form

$$\mathbf{q} = \mathbf{q}_f + \mathbf{q}_w,$$

where

$$\mathbf{q}_f = \mathbf{q}_\tau f\left(\frac{yq_\tau}{\nu}\right),$$

and

$$\mathbf{q}_w = \frac{\Pi \mathbf{q}_\tau}{\kappa} w\left(\frac{y}{\delta}\right).$$

In these expressions, $f(yq_\tau/\nu)$ and $w(y/\delta)$ are to be identified with the scalar functions previously described for two-dimensional flow, and q_τ is defined as the magnitude of a friction velocity vector $\mathbf{q}_\tau$ taken parallel to the surface shearing stress $\boldsymbol{\tau}_w$, i.e.

$$\boldsymbol{\tau}_w = \rho q_\tau \mathbf{q}_\tau.$$

Furthermore, both $\mathbf{q}_\tau$ and Π are assumed to depend on two space coordinates, say x and z. Then, if $\mathbf{q}_f$ and $\mathbf{q}_w$ are not parallel vectors, the parameter $\Pi(x, z)$ should presumably be interpreted as a linear operator having the properties of a square matrix, i.e. as a tensor. It also follows that the generalized vector friction law is

$$\mathbf{q}_1 = \mathbf{q}_\tau f\left(\frac{\delta q_\tau}{\nu}\right) + \frac{2\Pi \mathbf{q}_\tau}{\kappa}.$$

This notation is highly tentative, and may have to be revised after more data on yawed flows become available. In particular, the present definition for q_τ is not perfectly consistent with the streamline hypothesis (Coles 1955) if $\boldsymbol{\tau}_w$ is an arbitrary continuous function of two coordinates on the surface. However, the notation does allow the interpretation already proposed, that the flow near the surface where the wake component is small should have the same direction and sense as the surface shearing stress. Thus the concept of a constraint provided by friction is a vector concept.

Given a mean-velocity profile in yawed flow, the vector nature of the wall and wake components can be tested in five steps. First, the direction of the mean flow near the surface, which is also by assumption the direction of the shearing-stress vector $\boldsymbol{\tau}_w$ and of the wall component $\mathbf{q}_f$, is noted. Second, the component of mean velocity in this direction is plotted in coordinates $(\mathbf{q} \cdot \mathbf{q}_\tau/q_\tau^2,\ yq_\tau/\nu)$ appropriate to the law of the wall; a fit to the function f then yields a value for q_τ. Third, the thickness δ is estimated

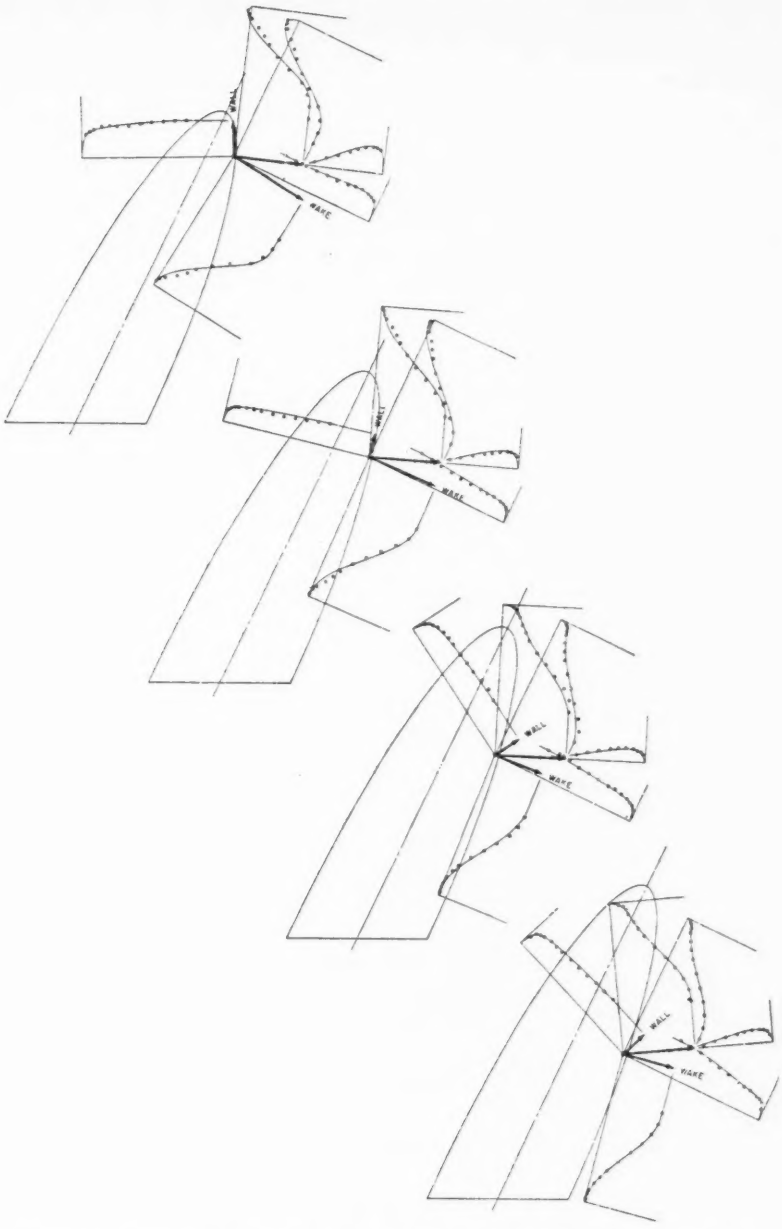

Figure 27. Vector resolution of the yawed flow of Kuethe, McKee, & Curry (1949).

from this same plot, for example as twice the value of y for which the profile reaches half of its maximum excursion from the law of the wall. Fourth, the 'wall' vector $\mathbf{q}_{f_1} = \mathbf{q}_\tau f(\delta q_\tau/\nu)$ is computed and subtracted from the free-stream vector $\mathbf{q}_1$ to obtain the 'wake' vector $\mathbf{q}_{w_1} = 2\Pi\mathbf{q}_\tau/\kappa$. Finally, the profile is resolved in oblique coordinates determined by the direction of the wall and wake vectors.

An examination of the experimental data of Gruschwitz (1935) in a curved channel suggests that serious errors were introduced in the mean-velocity measurements near the surface by the use of a periscope probe. In particular, the profiles in the straight portion of the channel differ from the concensus of data obtained by other investigators under similar conditions. Fortunately, the hot-wire measurements of Kuethe, McKee & Curry (1949) on a swept airfoil, although carried out at relatively small Reynolds number, involve large angles of yaw within the boundary layer and therefore provide a useful test for the concept of vector similarity. In treating these data, incidentally, it has been assumed that the indication in some of the profiles of a sudden change in flow direction within the sublayer is fictitious.

The airfoil of Kuethe, McKee & Curry was of elliptical planform, of 18 in. chord and 96·5 in. span, with the major axis swept back at an angle of 25°. Four profiles obtained near the trailing edge of the airfoil at an angle of attack of 14° are plotted in figure 27 in terms of spanwise and chordwise components of mean velocity; in terms of streamwise and crossflow components; and finally in terms of wall and wake components.

The data in figure 27 can be fairly well represented by the characteristic wall and wake functions defined previously for unyawed flows, and it is difficult to say whether or not there is any systematic discrepancy. A more stimulating result, which may be coincidental or may illustrate an important intrinsic property of strongly wake-like yawed flows, is that the direction of the wake component is found in each case to be nearly the same as the direction of the gradient of the pressure field over the airfoil surface. That is, the final resolution is for practical purposes along the directions defined by the two vectors $\boldsymbol{\tau}_w$ and $-\operatorname{grad} p$, so that $(\operatorname{grad} p) \times (\Pi\boldsymbol{\tau}_w)$ vanishes everywhere. The inference that the constraint provided by inertia is also a vector constraint is potentially useful in investigating the nature of the tensor parameter Π when more suitable data become available from experiments carried out at larger Reynolds numbers in flow on a larger scale.

References

Bauer, W. 1951 The development of the turbulent boundary layer on steep slopes, Thesis: State Univ. of Iowa; abridged in *Proc. Amer. Soc. Civ. Engrs.*, *Separate* no. 281, 1953.

Clauser, F. 1954 Turbulent boundary layers in adverse pressure gradients, *J. Aero. Sci.* **21**, 91–108.

Coles, D. 1954 The problem of the turbulent boundary layer, *Z. angew. Math. Phys.* **5**, 181–203.

COLES, D. 1955 The law of the wall in turbulent shear flow, 50 *Jahre Grenzschicht-forschung* (Ed. H. Görtler & W. Tollmien), pp. 153–163. Braunschweig: F. Vieweg und Sohn.

GRUSCHWITZ, E. 1935 Turbulente Reibungsschichten mit Sekundärströmung, *Ing.-Arch.* **6,** 355–365.

KÁRMÁN, T. v. 1921 Über laminare und turbulente Reibung, *Z. angew. Math. Mech.* **1,** 233–252; *translated as* On laminar and turbulent friction, *Nat. Adv. Comm. Aero., Wash., Tech. Mem.* no. 1092, 1946.

KÁRMÁN, T. v. 1932 Theorie des Reibungswiderstandes, *Hydromechanische Probleme des Schiffsantriebs, Hamburg.*

KEHL, A. 1943 Untersuchungen über konvergente und divergente turbulente Reibungsschichten, *Ing.-Arch.* **13,** 293–329; *translated as* Investigations on convergent and divergent turbulent boundary layers, *British Ministry of Supply R.T.P.* no. 2035, 1946.

KLEBANOFF, P. & DIEHL, Z. 1951 Some features of artificially thickened fully developed turbulent boundary layers with zero pressure gradient, *Nat. Adv. Comm. Aero., Wash., Tech. Note* no. 2475.

KLEBANOFF, P. 1954 Characteristics of turbulence in a boundary layer with zero pressure gradient, *Nat. Adv. Comm. Aero., Wash., Tech. Note* no. 3178.

KUETHE, A., MCKEE, P. & CURRY, W. 1949 Measurements in the boundary layer of a yawed wing, *Nat. Adv. Comm. Aero., Wash., Tech. Note* no. 1946.

LAUFER, J. 1953 The structure of turbulence in fully developed pipe flow, *Nat. Adv. Comm. Aero., Wash., Tech. Note* no. 2954.

LEES, L. & CROCCO, L. 1952 A mixing theory for the interaction between dissipative flows and nearly isentropic streams, *J. Aero. Sci.* **19,** 649–676.

LIEPMANN, H. & LAUFER, J. 1947 Investigations of free turbulent mixing, *Nat. Adv. Comm. Aero., Wash., Tech. Note* no. 1257.

LUDWIEG, H. & TILLMANN, W. 1949 Untersuchungen über die Wandschubspannung in turbulenten Reibungsschichten, *Ing.-Arch.* **17,** 288–299; *translated as* Investigations of the wall shearing stress in turbulent boundary layers, *Nat. Adv. Comm. Aero., Wash., Tech. Mem.* no. 1285, 1950.

MCCULLOUGH, G. & GAULT, D. 1949 Boundary-layer and stalling characteristics of the N.A.C.A. 64A006 airfoil section, *Nat. Adv. Comm. Aero., Wash., Tech. Note* no. 1923.

MILLIKAN, C. 1938 A critical discussion of turbulent flows in channels and circular tubes, *Proc. 5th Int. Cong. Appl. Mech., Cambridge*, 386–392.

NEWMAN, B. 1951 Some contributions to the study of the turbulent boundary layer near separation, *Aust. Dept. Supply, Rep.* no. *ACA*-53.

NIKURADSE, J. 1930 Widerstandsgesetz und Geschwindigkeitsverteilung von turbulenten Wasserströmung in glatten und rauhen Rohren, *Proc. 3rd Int. Cong. Appl. Mech., Stockholm*, 239–248.

PRANDTL, L. 1926 Über die ausgebildete Turbulenz, *Proc. 2nd Int. Cong. Appl. Mech., Zürich*, 62–74; *translated as* Turbulent flow, *Nat. Adv. Comm. Aero., Wash., Tech. Mem.* no. 435, 1927.

PRESTON, J. 1954 The determination of turbulent skin friction by means of pitot tubes, *J. R. Aero. Soc.* **58,** 109–121.

REICHARDT, H. 1940 Die Wärmeübertragung in turbulenten Reibungsschichten, *Z. angew. Math. Mech.* **20,** 297–328; *translated as* Heat transfer through turbulent friction layers, *Nat. Adv. Comm. Aero., Wash., Tech. Mem.* no. 1047, 1943.

Ross, D. & Robertson, J. 1951 A superposition analysis of the turbulent boundary layer in an adverse pressure gradient, *J. Appl. Mech.* **18,** 95–100.

Rotta, J. 1950 Über die Theorie der turbulenten Grenzschichten, *Mitt. Max-Planck-Inst., Göttingen, No.* 1; *translated as* On the theory of the turbulent boundary layer, *Nat. Adv. Comm. Aero., Wash., Tech. Mem.* no. 1344, 1953.

Schubauer, G. & Klebanoff, P. 1950 Investigation of separation of the turbulent boundary layer, *Nat. Adv. Comm. Aero., Wash., Tech. Note* no. 2133.

Sheppard, P. 1947 The aerodynamic drag of the earth's surface and the value of von Kármán's constant in the lower atmosphere, *Proc. Roy. Soc.* A, **188,** 208–222.

Tillmann, W. 1945 Untersuchungen über Besonderheiten bei turbulenten Reibungsschichten an Platten, *Z.W.B., K.W.I., Göttingen, U. & M.* 6627; *translated as* Investigations of some particularities of turbulent boundary layers on plates *British R. & T. MAP-VG*-34, 1946.

Wieghardt, K. 1943 Über die Wandschubspannung in turbulenten Reibungsschichten bei veränderlichem Aussendruck, *Z.W.B., K.W.I., Göttingen, U. & M.* 6603. *See also* Wieghardt, K. & Tillmann, W., Zur turbulenten Reibungsschicht bei Druckanstieg, *Z.W.B., K.W.I., Göttingen, U. & M.* 6617, 1944; *translated as* On the turbulent friction layer for rising pressure, *Nat. Adv. Comm. Aero., Wash., Tech. Mem.* no. 1314, 1951.

Wieghardt, K. 1944 Zum Reibungswiderstand rauher Platten, *Z.W.B., K.W.I., Göttingen, U. & M.* 6612.

On the flow in channels when rigid obstacles are placed in the stream

By T. BROOKE BENJAMIN
Department of Engineering, University of Cambridge

(*Received* 23 *December* 1955)

SUMMARY

A previous paper drew attention to the collective importance of three physical quantities Q, R, S associated with ideal fluid flow in a horizontal channel. Invariability of these quantities at different cross-sections of the flow implies respectively conservation of flow rate, energy and momentum; and their values determine a wave-train uniquely. The properties of Q, R, S are recalled in the present paper to account for the various effects of lowering a rigid obstacle into a stream. The conditions giving rise to dissimilar types of flow are examined; in particular, the circumstances causing stationary waves on the downstream side are clearly distinguished from those under which the receding stream assumes a uniform 'supercritical' state. A well-known result in the theory of the solitary wave is shown to apply to the receding stream even when the extreme conditions for the wave are exceeded; although it fails to account for a region close to the obstacle where the curvature of the streamlines becomes large. In passing, a feature of the theory is shown to bear on the practical problem of producing a uniform stream. Precise calculations are made for the flow under a vertical sluice-gate and under an inclined plane. To account for the region near the bottom edge of the sluice-gate, a method based on conformal transformation is used whereby an unknown curve in the hodograph plane is approximated by an arc of an ellipse. The accuracy of the results is more than sufficient for practical purposes, and they compare favourably with solutions previously obtained by relaxation methods. A number of experiments with water streams are described.

1. INTRODUCTION

When the stream in an open horizontal channel is spanned by a fixed cylindrical obstacle, the effects of the obstruction may extend to great distances both upstream and downstream. Furthermore, each part of the stream may take several distinct forms depending on the cross-sections of the cylinder, the extent of its immersion, and the nature of the undisturbed stream. Kelvin (1886) demonstrated that a train of periodic waves may form downstream, whose amplitude increases with the drag on the obstacle

(i.e. with the 'wave resistance'). His theoretical treatment was limited to cases where the waves are small in both amplitude and length; but Benjamin & Lighthill (1954) have shown in general that the wave resistance may take any value up to a certain maximum. If the obstacle is lowered sufficiently far into the stream, energy losses may occur due to breaking of waves, and further immersion may lead to the formation of a fully turbulent 'bore or' 'hydraulic jump' behind which waves appear to be absent. The action of a fixed obstacle can also bring about a transition from a uniform subcritical stream (of which the speed is less than $\sqrt{(g \times \text{depth})}$) to a supercritical one. This effect is best known through the example of a vertical sluice-gate, which is discussed in many text-books on hydraulics. The conditions under which waves can form ahead or in the rear of a sluice-gate have not, up to the present time, been satisfactorily explained.

The first object of this paper is to present a unified account of these various effects, and to make clear the relation amongst them. A general method for calculating the form of the receding stream when waves are absent will also be outlined, and will be illustrated by applications to the flow under a sluice-gate and under a planing surface. The treatment is based on ideal-fluid theory, but a number of experiments have been made on water streams in order to test the theoretical results; these experiments will be described in the concluding part of the paper. A fact emerging incidentally from the discussion appears to have an important bearing on the practical problem of producing a uniform horizontal stream of water. Such streams are often desired for tests on ship models, and for this reason they were made the subject of numerous experiments by Binnie, Davies & Orkney (1955). These authors found it possible to produce a satisfactory subcritical stream without measurable waves, provided the Froude number ($F = \text{speed}/\sqrt{(g \times \text{depth})}$) was less than about 0·5. At Froude numbers exceeding this value waves always appeared, despite a variety of measures aimed at avoiding them. In agreement with this result, the present theory indicates that flows converging towards a uniform stream are impossible at Froude numbers somewhat less than unity. This fact might be relevant to the design of a channel for model tests over a range of speeds.

In the course of examining the asymptotic properties of a disturbed stream, we shall show that a formula known in the theory of the solitary wave also applies to flows beyond the extreme conditions for the wave. It is subsequently used to calculate the form of the converging stream which issues from under a sluice-gate. The flow in the immediate neighbourhood of the gate has to be treated in another way; but when suitably combined, the two methods account satisfactorily for the whole stream. The results of the calculations demonstrate the variation of the contraction ratio with Froude number, and hence establish the relation between the sluice-opening and the total discharge. They are apparently more accurate than previous estimates, notably those due to Pajer (1937), and the single result which Southwell & Vaisey (1946) calculated by relaxation methods. The latter authors drew attention to the difficulties which confront their methods

when applied to flow near points of separation from solid boundaries (p. 160 in their paper). These difficulties appear to be responsible for most of the discrepancy (about 1·5%) between their computed value of the sluice-opening and the value according to the present theory. From a practical point of view there is admittedly little justification for carrying the calculations to high orders of approximation, since the theory does not apply with precision to real fluids. In the experiments described later, for instance, the thickness of the boundary layer on the channel bottom was observed to be about one-fifteenth of the sluice-opening, thus indicating that frictional effects were far more significant than the final error in the ideal-fluid calculations. An accurate form of the theory is nevertheless desirable, for at least it gives assurance that the discrepancies observed in real flows are due to friction alone.

The problem to be considered is indicated in figure 1. We shall assume that the motion is steady, and that both far upstream and far downstream

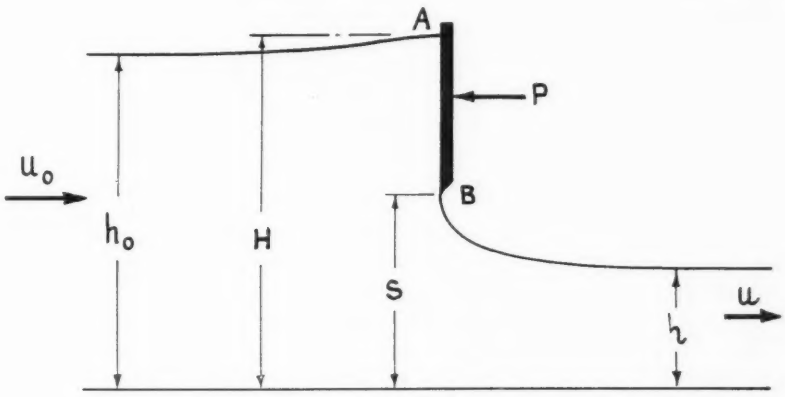

Figure 1. Side elevation of sluice-gate.

the flow is uniform and horizontal, having depth and velocity h_0, u_0 and h, u respectively. In the paper already cited, Southwell & Vaisey noted the existence of a symmetrical solution in which the free surface regains its original level after passing the sluice; but flow of this kind does not occur in practice unless there is some severe obstruction downstream. The free surface usually falls to a lower level, and Binnie (1952) has shown that the approaching stream must then be subcritical ($F < 1$) and the receding stream supercritical. The condition of continuity is

$$u_0 h_0 = uh = Q, \tag{1.1}$$

where Q is the discharge per unit span; and Bernoulli's equation may be written

$$gh_0 + \tfrac{1}{2}u_0^2 = gh + \tfrac{1}{2}u^2 = gH, \tag{1.2}$$

where H is the total head measured above the bottom of the channel. If both Q and H are given, h_0, h, u_0 and u can be calculated from (1.1) and (1.2), but there is no simple way of finding the sluice-opening s. Alternatively, if s is specified together with either Q or H, as is usual in a practical example, elementary methods fail to give any of the other quantities. In addition to (1.1) and (1.2) a third simple relation may be written down equating the reduction in flux of momentum to the resultant of horizontal forces, which include the force P on unit span of the gate and the pressure forces in the oncoming and receding streams; thus, denoting density by ρ, we have

$$\rho(u_0^2 h_0 - u^2 h) = P - \tfrac{1}{2}\rho g(h_0^2 - h^2). \tag{1.3}$$

However, since P is unknown, this equation is of no assistance in the main problem.

At point A in figure 1 the free surface rises to stagnation level, and the velocity there is zero. At point B it must slope vertically, since otherwise the bounding streamline would make a sharp corner there and the velocity would become infinite, which is clearly impossible if the surface is free. One may nevertheless expect that the free surface has infinite curvature at B, for this property has been established in many similar instances when gravity is absent (see, for example, Southwell & Vaisey, p. 160).

2. General theory of the flow

The investigation is conveniently begun by considering the different types of flow which may exist at points far removed from the obstacle. In other words, we shall first examine the possible asymptotic forms of the flow upstream and downstream. At the outset it is necessary to emphasize that the stream cannot be *perfectly* uniform at any finite distance from the obstacle. This fact becomes obvious when one considers that the hodograph variable $\zeta = qe^{-i\theta}$ (where q and θ are the magnitude and direction of the velocity) is analytic within the stream; therefore, by virtue of an elementary property of analytic functions, ζ cannot be constant throughout any finite region unless it is constant everywhere. Having thus dismissed the case of a uniform stream, there remain only two types of flow capable of extension to indefinitely large distances upstream or downstream. The first possibility is a train of periodic waves, and the second a steadily converging stream resembling the outskirts of a solitary wave. In practice, flow of the latter sort may be indistinguishable from a uniform stream except in a region close to the obstacle; strictly speaking, however, they become uniform only at infinity. Although this distinction is a trivial one in some respects, it will assume importance in the subsequent argument.

It is now desirable to recall some of the ideas put forward by Benjamin & Lighthill (1954) in connection with the theory of gravity waves of finite amplitude. They pointed out that for any two-dimensional steady flow in a horizontal channel, there are three important physical quantities which

in the absence of friction and horizontal external forces, have the same value at every cross-section of the flow. These are Q the volume flow per unit span, R the energy per unit mass (i.e. g times the total head as measured above the channel bottom), and S the resultant of momentum flux and pressure force per unit span divided by the density. A train of long waves was shown to be determined uniquely by the values of Q, R and S, and there is reason for believing that this property is common to all wave-trains in parts distant from their origin and termination. This view is supported by the recent work of De (1955), who calculated numerical values of the quantities in question for a wide range of wavelengths. The former authors also demonstrated that the physically realizable combinations of Q, R and S are confined within certain limits. For instance, if Q and R are fixed, then S is restricted between a higher value corresponding to uniform subcritical flow and a lower value corresponding to uniform supercritical flow. Stationary wave-trains may occur for intermediate values of S; but the wave amplitude tends to zero as the upper limit is approached, whereas at the lower limit the wavelength becomes infinite, and the only possible wave is the solitary wave.

We proceed by extending a line of argument begun in the paper by Benjamin & Lighthill (p. 455). If a rigid obstacle is lowered gradually into a *slightly* subcritical stream, it experiences an increasing wave resistance (corresponding to a reduction of S on the downstream side) until the waves formed downstream become of great length, and their profile approaches that of the solitary wave. A different situation arises, however, if the Froude number of the respective supercritical flow (i.e. the flow with the same values of Q and R as the subcritical flow upstream) is greater than the value 1·25, at which, as McCowan (1894) showed, the solitary wave takes its extreme sharp-crested form. A gradual approach to the lower value of S is now impossible, since the extreme condition for the solitary wave is exceeded at the limit. In fact, as S is reduced from its upper limit, periodic ' waves of maximum height ' occur at a value of S in excess of the lower limit, and a further gradual reduction will result in energy losses due to breaking of waves. The obstacle must then be lowered by a finite amount, bringing S to the minimum value, before steady lossless flow is again possible. No wave can form on the supercritical stream under these circumstances; but it will be shown presently that the stream has some features in common with the solitary wave. Recognition of the lower limit to S also shows that any obstruction of a stream initially in a supercritical condition is bound to result in energy losses, since a reduction of S is otherwise impossible. In fact a bore will be formed upstream. A bore sometimes occurs in practice on the stream receding from a sluice-gate. It may be caused by some obstruction, or simply by friction if the channel is fairly long. The flow assumes a subcritical state behind the bore, but with a smaller value of R than the subcritical flow upstream from the gate. (The material of this paragraph may be made somewhat clearer by consulting figure 1 in the paper by De (1955).)

The condition $F > 1{\cdot}25$ noted above may be shown, by means of (1.1) and (1.2), to correspond to the condition $F_0 < 0{\cdot}792$ for the respective subcritical stream. Hence we can conclude that if $F_0 > 0{\cdot}792$ a transition from subcritical to supercritical uniform flow, in the manner indicated by figure 1 (present paper), cannot be achieved with R unchanged, since only wave-trains can result on the downstream side. Although such a transition is possible if $F_0 < 0{\cdot}792$, the obstacle must be immersed to a considerably greater extent than that which causes waves. Thus a clear distinction is made between the action of a sluice-gate and that of a slightly submerged obstacle causing a wave-train downstream. These considerations seem to supply a complete answer to the question whether waves can form on the downstream side of a sluice-gate. This matter was raised by Southwell & Vaisey (1946), who were led to expect waves in the course of their calculations, although none were found. It was also considered by Binnie (1952), who presented a tentative argument indicating that waves are impossible. The question whether waves can form on the upstream side is deferred to a later part of the discussion.

The special case of critical flow ($F = 1$) deserves separate attention. Let us therefore consider the flow in a channel which is supplied from a large reservoir, so that R is fixed, and which is initially free from obstruction of any sort. Such circumstances are well-known to give rise to critical flow, which makes the value of Q the maximum possible at the given total head. This fact may be established by various methods, a review of which was given by Binnie (1949). Suppose now that an obstacle is fixed in slight contact with the free surface at a point well down the channel, thereby causing a small reduction in S on the downstream side. The disturbed flow is clearly unstable; for the change in S necessitates a decrease in Q from its maximum value, since R cannot change, and hence an increase in depth on the upstream side. As the free surface rises upstream, a greater force is exerted against the obstacle, and the downstream value of S further decreases. Before steady conditions can be resumed, the free surface must rise to stagnation level on the front of the obstacle. The elevation of stagnation level above the channel bottom (i.e. the total head H) is easily shown to be 1·5 times the depth of critical flow. Thus the obstacle is ' wetted ' to a height $\frac{1}{2}H$ in the final steady state. The resistance experienced by an obstacle this far immersed is much too large to be ascribable to wave formation; and the flow is therefore of the kind illustrated in figure 1.

It is now proposed to examine the profile of the receding stream in the case where waves are absent. The work of Benjamin & Lighthill again provides a convenient starting point. In a new presentation of ' cnoidal wave ' theory, they demonstrated that the condition of constant Q and S leads to an approximate differential equation for the free surface (the condition of constant R being superfluous). In terms of coordinates (x, y) with the x-axis along the channel bottom, this may be written

$$\tfrac{1}{3}Q^2\left(\frac{dy}{dx}\right)^2 + gy^3 - 2Ry^2 + 2Sy - Q^2 = 0. \qquad (2.1)$$

The nature of the approximation on which (2.1) is based is noteworthy. The assumption was made that successive derivatives of the slope y' diminish fairly rapidly in order of magnitude, so that, for instance, y^2y^{iv} can reasonably be neglected in comparison with y''. The next stage of approximation was observed to contribute terms of the order of y'^4 to (2.1), and further stages would evidently contribute terms of the order of successively higher powers of y'^2. The trend of the coefficients in the early stages suggests that the method of approximation is rapidly convergent, provided y' is fairly small. There is accordingly some justification for assuming that an exact solution exists for any flow with constant Q, R and S, and that (2.1) will provide a close approximation to it in parts where y' is small. As will be explained in the next paragraph, this equation can lead to an approximation for the solitary wave. The mathematical existence of this wave has been proved by Friedrichs & Hyers (1954), and so the validity of (2.1) is confirmed in this one respect. Its validity in the present application, however, cannot be established by appeal to the work of Friedrichs & Hyers; for the solitary wave is impossible with the values of Q, R and S to be considered here. Nevertheless, it may be said that the physical aspects of the present problem, in which the flow-pattern is supposed to be stationary relative to the obstacle, are a good deal clearer than these aspects of the solitary wave, which is stationary only with respect to a hypothetical frame of reference.

If Q, R and S take the values

$$Q = uh, \qquad R = gh + \tfrac{1}{2}u^2, \qquad S = \tfrac{1}{2}gh^2 + u^2h, \tag{2.2}$$

which are appropriate to a uniform stream with depth h and velocity u, and whose Froude number is therefore $F = u/\sqrt{(gh)}$, the cubic expression in (2.1) factorizes and the whole equation can be arranged in the form

$$\left(\frac{dy}{dx}\right)^2 = \frac{3}{F^2}\left(\frac{y}{h} - 1\right)^2\left(F^2 - \frac{y}{h}\right). \tag{2.3}$$

With $F > 1$ this is identical with the equation for the solitary wave obtained by Rayleigh (1876a). Other than the uniform flow $y = h$, its only solution is

$$\frac{y}{h} = 1 + (F^2 - 1)\operatorname{sech}^2\left[\frac{\sqrt{(3F^2 - 3)}x}{2Fh}\right]. \tag{2.4}$$

The solitary wave is thus the only wave which can emerge from a uniform supercritical stream without loss of energy or momentum.

This approximation to the solitary wave is most accurate at the outskirts of the wave where the slope and curvature are small. When the wave approaches its extreme form (at $F = 1{\cdot}25$), the approximation is found to be no longer accurate over the whole wave, yet still holds at the outskirts. It is clear also that these results apply to the outlying parts of a stream with constant Q, R and S which converges towards uniform flow at $F > 1{\cdot}25$, although the solitary wave is then impossible. The streams of concern here are clearly included in this category. Accordingly, their free surfaces

must satisfy (2.4) approximately up to a region close to the obstacle where the slope or curvature becomes large. There is a simple way of testing this assertion; for, as Addison (1938) and Binnie (1952) have pointed out, the flow under a sluice-gate when the ratio s/H is small resembles a jet issuing under pressure in the absence of gravity. The latter example is illustrated in figure 2 (*a*), where the bottom line may be taken to represent either a plane wall or the centre-line of a symmetrical jet. Rayleigh (1876*b*) found the complete solution of this problem. The free surface satisfies the equation

$$\frac{y}{d} = 1 - \frac{2}{\pi}\sin\theta, \tag{2.5}$$

where θ is the angular slope $\tan^{-1}(dy/dx)$ which ranges between 0 and $-\frac{1}{2}\pi$, and d has the same meaning as h in figure 1. In the corresponding gravity problem F is very large, and (2.3) consequently gives

$$\frac{y}{h} = 1 - \frac{1}{\sqrt{3}}\tan\theta. \tag{2.6}$$

Agreement between the two results is partly attributable to the similarity of the numerical factors $1/\sqrt{3}$ and $2/\pi$ appearing in (2.5) and (2.6), but is in fact better than this alone would suggest. The Cartesian equations equivalent to (2.5) and (2.6) are easily found; hence the agreement can be checked very readily by plotting the two curves on tracing paper and fitting them together. They are found to fit closely in parts where the magnitude of θ is less than about 30°, the maximum discrepancy in y/h being about 1%. The curves diverge significantly in the higher region where the curvature of the first of them (from (2.5)) becomes large. Note that for smaller Froude numbers the accuracy of (2.4) is likely to improve, whereas (2.5) becomes inaccurate.

The approximation of (2.4) may be tested in one further instance by comparison with the solution for a sluice-gate which Southwell & Vaisey (1946) obtained by relaxation methods. In their example the assumed conditions were, in the notation of figure 1, $H = 12$ and $h_0 = 11$ length units. The depth and Froude number of the flow far downstream were not given explicitly, but from (1.1) and (1.2) they are easily calculated to be $h = 3{\cdot}854$ length units and $F = 2{\cdot}055$. When these values are put into (2.4), the curve obtained from this equation is found to coincide with the lower part of the profile given by Southwell & Vaisey (p. 151 in their paper), but begins to diverge perceptibly from it at a point where the slope is about $-30°$, a little way below the highest point.

We turn from the main argument for a moment in order to consider another matter explained by the differential equation (2.3). If $F < 1$ the equation has no real solution except $y = h$, the case of uniform flow. This fact demonstrates convincingly that non-uniform flow converging towards a uniform stream, as discussed previously, is impossible for values of F less than unity yet large enough for a long-wave approximation to apply. Any attempt to produce a uniform stream under these conditions is therefore

bound to fail, unless the flow can be made uniform on entry into the channel. Clearly, the result of any non-uniformity on entry will be a train of periodic waves, the values of Q, R and S being differently correlated than for uniform flow. The occurrence of waves as predicted here was observed experimentally by Binnie, Davies & Orkney (1955), who mentioned similar findings by other investigators.

This is a suitable place to raise the question of wave formation on the upstream side of an immersed obstacle. The situation at small Froude numbers, to which a short wavelength approximation can be applied, was discussed at length by Lamb (1932, §§ 242–5), whose treatment was restricted, however, to infinitesimal disturbances of the free surface. He noted that in the absence of dissipative forces the problem is to some extent indeterminate, since waves of small amplitude can always be superimposed on the stream without altering certain of the physical conditions (e.g. Q or S). There appears to be no simple way of extending Lamb's argument to account for waves of finite size: but the presence or absence of waves seems likely to depend only on conditions specified far upstream. Hence one is justified in assuming that the flow is uniform upstream, as is done in the following treatment of the sluice-gate problem.

3. Flow under a sluice-gate

Equation (2.4) has been shown to apply behind, but not too near, any obstacle adequately immersed. Other methods are needed, however, to deal with the rapidly curving portion of the free surface which is always to be expected near a ' trailing edge ', and which clearly depends on the shape of the obstacle. A sluice-gate and planing surface are the only examples treated in this paper, but similar calculations could undoubtedly be carried out for other boundary shapes.

It is reasonable to suppose that in the region of B in figure 1 the flow is little affected by gravity, since the acceleration of the fluid particles is large there. Although (2.5) will roughly give this part of the free surface, the solution of the problem indicated in figure 2 (*b*) is rather more accurate. Here the flow upstream from the jet is confined within parallel walls at a distance D from the centre-line; and, as a basis for comparison with the example in figure 1, we may take $D = H$ as a useful estimate. This problem was solved by Mises (1917), although a formula for the free surface was not given in his paper. Straightforward methods show, however, that the free surface satisfies the equation

$$y = d - \frac{2d}{\pi m} \tan^{-1}(m \sin \theta), \tag{3.1}$$

with

$$m = \frac{2Dd}{D^2 - d^2}, \quad \text{and} \quad \frac{s}{d} = 1 + \frac{2 \tan^{-1} m}{\pi m}. \tag{3.2}$$

This result can be combined with (2.3) to obtain a rough estimate of the complete free surface below the sluice. The two curves may be joined

at a point where $\theta = -30^\circ$, say, so that in (2.3) $y'^2 = (\tan 30^\circ)^2 = \frac{1}{3}$. To calculate the sluice-opening s for a given value of F, which specifies an appropriate value of D and also the height of the 'joining point' (y_0, say), the two equations (3.2) are used to eliminate k and d from the relation

$$s - y_0 = \frac{2d}{\pi m}(\tan^{-1} m - \tan^{-1} \tfrac{1}{2}m), \tag{3.3}$$

which follows from (3.1). In the example treated by Southwell & Vaisey this method leads to a value 0·602 for the contraction ratio h/s, whereas they

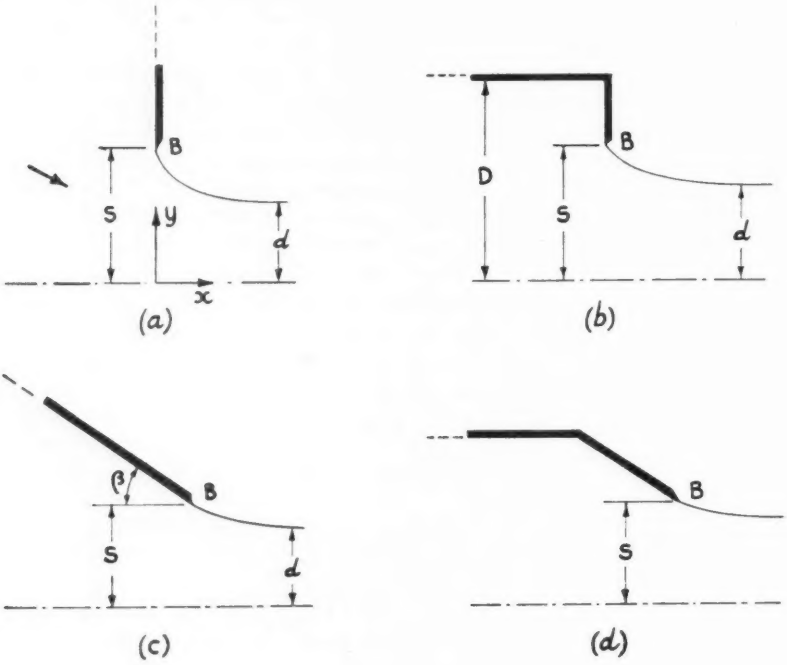

Figure 2. Free streamline problems not affected by gravity.

obtained 0·608.* The method takes no account of velocity changes over the upper portion of the free surface, although over all parts the resultant velocity q varies according to Bernoulli's equation

$$q^2 = 2g(H - y). \tag{3.4}$$

As the free surface falls between heights s and y_0, the velocity increases by a factor $\sqrt{(H-s)}/\sqrt{(H-y_0)}$, which is found to be significantly greater

* Their result was misprinted as 0·66; but Miss Vaisey has confirmed that the intented value is 0·608.

than unity in typical examples. We are therefore led to seek a more accurate method taking full account of gravity.

By the method now to be described, a solution is found which satisfies the boundary condition (3.4) exactly at the edge B and at a 'joining point' below which (2.3) can be applied accurately. The method is developed from one given by Pajer (1937), and so the present account is made fairly brief. Following the usual procedure in dealing with irrotational motions in the plane of a complex variable z, use is made of the fact that since the velocity potential ϕ and stream function ψ are harmonic, the variable $w = \phi + i\psi$ is a function of z only. The first aim of the method is to establish an approximate relation between w and the hodograph variable $\zeta = dw/dz = qe^{-i\theta}$. We consider a transformation to the plane of an auxilliary variable $f(z)$ defined by

$$\frac{p}{\zeta} = \frac{pe^{i\theta}}{q} = f - \frac{k}{f}, \tag{3.5}$$

where p and k are positive real constants. The separation of the real and imaginary parts of (3.5) leads to

$$\frac{p\cos\theta}{q} = \left(|f| - \frac{k}{|f|}\right)\cos\omega, \tag{3.6}$$

$$\frac{p\sin\theta}{q} = \left(|f| + \frac{k}{|f|}\right)\sin\omega, \tag{3.7}$$

where $\omega = \arg(f)$. We also make use of the transformation

$$f' = f^2 + 1/f^2. \tag{3.8}$$

It is now assumed that $\omega = \theta = -\frac{1}{2}\pi$ at the edge B, and that $|f| = 1$ along the free surface below this point. According to (3.5), the circle so defined in the f-plane is mapped in the hodograph as an ellipse, whose size and eccentricity depends on p and k. By a suitable choice of these constants, the points in the hodograph representing B and the 'joining point' may be linked by an arc of the ellipse.

From (3.8) we have that $f' = 2\cos 2\omega$ on the free surface below B. At B, $f' = -2$, since $\omega = -\frac{1}{2}\pi$; and at infinity downstream $f' = 2$, since $\omega = \theta = 0$. In other words, the free surface is mapped in the f'-plane between -2 and 2 along the real axis. On the straight line AB in figure 1, $\omega = \theta = -\frac{1}{2}\pi$; and $q = 0$ at A. Thus AB is mapped between infinity and -2 along the negative real axis of f'. If the free surface upstream from A is taken to be horizontal, we have $\omega = \theta = 0$, and so f' is real along this surface also. It is therefore mapped along the positive real axis between infinity and a value $f_0' = f_0^2 + 1/f_0^2$ representing the conditions far upstream. It is a simple step to show that the lower half of the f'-plane maps the entire flow-pattern.

The streamline $\psi = 0$ extends along the bed of the channel, and the streamline $\psi = Q$ (where Q is the volume flow rate) forms the upper boundary of the flow. As shown above, the latter streamline is mapped along the real axis in the f'-plane. The figure in the w-plane is an infinite strip of

width Q lying on the real (ϕ) axis, and is mapped in the lower half of the f'-plane by the Schwarz–Christoffel transformation

$$w = \phi + i\psi = \frac{Q}{\pi}\log\left(\frac{f'-f'_0}{2-f'}\right). \tag{3.9}$$

The relation between ζ and w is determined by (3.5), (3.8) and (3.9). The form of the free surface below B can hence be deduced by a standard method (see Lamb 1932, §74), details of which may be omitted here. We find for this surface

$$x = \frac{2cs}{\pi}\left[\operatorname{logtan}\left(\frac{\omega}{2}+\frac{\pi}{2}\right) - n\tanh^{-1}\left(\frac{\cos\omega}{n}\right)\right], \tag{3.10}$$

$$y = s - \frac{2cs}{m\pi}\frac{1+k}{1-k}[\tan^{-1}m + \tan^{-1}(m\sin\omega)], \tag{3.11}$$

where $n = \frac{1}{2}(f_0 + 1/f_0)$, $m = 2f_0/(f_0^2-1)$, and c is the value of y/s for $\omega = 0$.

If the boundary condition (3.4) is to be satisfied at B, we must have, by reason of (3.7),

$$\frac{p}{\sqrt{(2g[H-s])}} = 1+k.$$

If this condition is also to be satisfied at a point below B where $y = y_0$, $\theta = \theta_0$, and $\omega = \omega_0$, we must also have

$$\frac{p\sin\theta_0}{\sqrt{(2g[H-y_0])}} = (1+k)\sin\omega_0.$$

It follows that

$$\frac{H-y_0}{H-s} = \left(\frac{\sin\theta_0}{\sin\omega_0}\right)^2, \tag{3.12}$$

in which ω_0 is determined (from (3.6) and (3.7)) by

$$\tan\omega_0 = \frac{1-k}{1+k}\tan\theta_0. \tag{3.13}$$

There will be no need to consider further the constant p, which merely fixes the scale of the figure in the f-plane.

It is convenient to introduce a new constant $\alpha = \tan^{-1}m$ (hence $\cot\frac{1}{2}\alpha = f_0$), in terms of which (3.11) gives

$$y_0 = s - \frac{2cs}{\pi}\frac{1+k}{1-k}\cot\alpha\,[\alpha + \tan^{-1}(\tan\alpha\sin\omega_0)]. \tag{3.14}$$

We also find, by putting $\omega = 0$ in (3.11), that

$$\frac{1}{c} = 1 + \frac{2}{\pi}\frac{1+k}{1-k}\alpha\cot\alpha. \tag{3.15}$$

Furthermore, if h_1 is the value of the depth upstream consistent with the assumption of its being constant everywhere, the continuity condition (1.2) leads to

$$\frac{h_1}{cs} = (f_0-k)/(1-k) = (\cot\tfrac{1}{2}\alpha - k\tan\tfrac{1}{2}\alpha)/(1-k),$$

from which, if a substitution for c is made from (3.14), we obtain

$$k\left(\frac{h_1}{s} - \frac{2h_1}{\pi s}\alpha\cot\alpha - \tan\tfrac{1}{2}\alpha\right) = \frac{h_1}{s} + \frac{2h_1}{\pi s}\alpha\cot\alpha - \cot\tfrac{1}{2}\alpha. \tag{3.16}$$

These results represent a flow which closely resembles the true solution up to the cross-section where $y = y_0$; beyond this the methods described previously can be applied. Our main object is to calculate the contraction ratio h/s as a function of the ratio s/H, which defines the flow-pattern uniquely on the basis of Froude number scaling. It is first necessary to obtain a suitable estimate of the quantity h_1 appearing in (3.16). We have so far neglected the small difference between H and h_0 (see figure 1), but now tentatively take account of it by assigning to h_1 a value somewhere between the two. (Note that no continuity condition is violated by doing this, since we are merely seeking a flow particularly resembling the actual flow in the region just below the sluice.) Inspection of the flow-pattern obtained by Southwell & Vaisey (1946, figure 25) suggests that $\frac{1}{3}(H+2h_0)$ is a fair estimate for h_1, although the value of h_1 is not at all critical when s/H is fairly small. An initial estimate of h/s is required to calculate h_0 from the relation

$$H(h_0-h) = h_0^2+h_0h+h^2, \tag{3.17}$$

which follows from (1.2) and (1.3). When θ_0 is specified, y_0/s can be found by eliminating c, k, α and ω_0 amongst the five equations (3.12) to (3.16). The calculation has to be done by numerical methods, but the following procedure was found to give fairly quick results. The value of α is first guessed. This task is aided by extrapolation after solutions have been obtained for some values of s/H, and as a help in this respect we have $\alpha = 0$ for $s/H = 0$. Using this estimate of α, k is calculated directly from (3.16); then c is calculated from (3.15), and ω_0 from (3.13). Finally, y_0 is obtained both from (3.12) and from (3.14). This sequence is repeated with another estimate of α, and it is then possible to assess α more accurately by interpolation designed to bring the alternative estimates of y_0 together. Repetitions of the whole process with successively closer approximations to α lead rapidly to an accurate estimate of y_0. The method is helped by the fact that the value of y_0 given by (3.12) varies greatly with α, whereas the value from (3.14) varies very little with α.

θ	x (ft)	y (ft)	q_1 (f/s)	q_2 (f/s)	q_1-q_2 (f/s)
$-90°$	0	1·0	16·048	16·048	0
-75	0·0024	0·9863	16·085	16·075	0·010
-60	0·0197	0·9464	16·186	16·155	0·031
-45	0·0692	0·8835	16·318	16·280	0·038
-35	0·1324	0·8309	16·417	16·383	0·034
-25	0·2368	0·7719	16·499	16·499	0

Table 1

For example, with $s/H = 0{\cdot}2$ and $\theta_0 = -25°$ it is found that $y_0/s = 0{\cdot}7719$. Coordinates of the free surface in the region where $-90° \leqslant \theta \leqslant -25°$ are given in table 1, which also includes values of q given by (3.6) (q_1), and the correct values according to (3.4); s is taken as 1 ft, and g as 32·19 ft/sec^2. The largest error in q is seen to be slightly greater than 0·2%.

After the value of y_0 has been established in this way, the calculation is completed as follows. If (2.3) is applied at the 'joining point', it gives

$$\frac{3}{F^2}\left(\frac{y_0}{h}-1\right)^2\left(F^2-\frac{y_0}{h}\right)=\left(\frac{dy}{dx}\right)^2=\tan^2\theta_0.$$

From (1.3) we also have

$$\frac{H}{h}=1+\tfrac{1}{2}F^2.$$

The elimination of F^2 between these equations leads to

$$(y_0-h)^2(2H-2h-y_0)-\tfrac{2}{3}(H-h)h^2\tan^2\theta_0=0. \tag{3.18}$$

When divided by s^3, this equation becomes a cubic in h/s whose coefficients are functions of the known quantities H/s, y_0/s and θ_0; this can be solved in a straightforward manner.

Values of h/s calculated with $\theta_0=-25^\circ$ are tabulated as a function of s/H in table 2, which includes the Froude number according to (3.18). The table also shows the set of values obtained by Pajer (1937), who used

s/H	h/s	h/s (Pajer)	F
0	0·6110	0·6110	∞
0·1	0·6060	—	5·568
0·2	0·6022	0·6046	3·822
0·3	0·5995	0·6036	3·020
0·4	0·5980	0·6043	2·522
0·5	0·5981	0·6066	2·165

Table 2

a method similar to the first part of the present method but extended over the whole free surface. The errors in velocity were then considerably larger than at present, and were in fact largest in a region corresponding to $\theta\doteqdot-25^\circ$, where, by the present method, the error is deliberately reduced to zero. Moreover, no account was taken of the difference between H and h_0. The discrepancies between Pajer's results and the present ones are fairly small, although quite significant. A remarkable feature of table 2 is the smallness of the variation in h/s. This effect is mainly due to gravity; for in its absence (the case illustrated in figure 2 (*b*)) the contraction ratio increases quite rapidly as the flow is narrowed upstream, and is always greater than the extreme value for the case in figure 2 (*a*).

The present method requires slight modification when applied to the problem treated by Southwell & Vaisey, in which H, h and F are given and s remains to be found. First, an estimate of s/H is made, and then h/s is calculated as before. Since h/s varies quite slowly with s/H, this result leads to a much closer estimate and the approximation is then further improved by repetitions of the process. Starting with $h/H=0{\cdot}3212$ and

$F^2 = 4{\cdot}227$, which are the values appropriate to Southwell & Vaisey's example, the method gives finally $h/s = 0{\cdot}5991$. We recall that the value obtained by them was 0·608. The curves derived from the present theory and by Southwell & Vaisey are both shown in figure 3. The two are indistinguishable up to a region just below B, but diverge appreciably in this

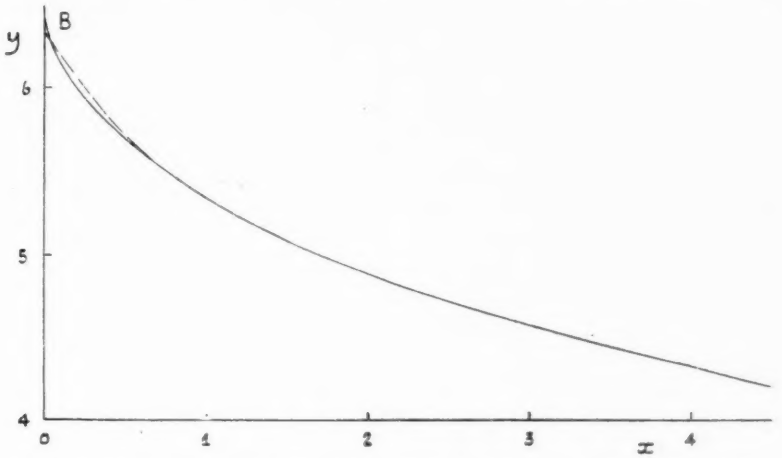

Figure 3. Comparison between free surface profiles given by Southwell & Vaisey (– – –) and by present method (——); $H = 12$ in the units of length used here.

region. The form of Southwell & Vaisey's curve very close to B seems unlikely to be correct, since it requires the streamline to undergo an unduly sudden change of direction at B. It should be noted, however, that figure 3 reproduces only a small part of their complete flow diagram. Even with the fine computational net which they employed in the vicinity of B, errors of the same order of magnitude as the discrepancy noted here are to be expected (the differences between their recorded values of $(H-y)$ and $q/\sqrt{(2g)}$ are of this order). The present method thus appears to be superior (in this one respect) to the relaxation method, even when the latter is applied with the high degree of precision achieved by Southwell & Vaisey.

4. Flow under a planing surface (hydroplane)

We now turn to the problem indicated in figure 4, where the obstacle is a plane inclined at an angle $\beta(< 90°)$ to the horizontal. The plane is assumed to have been lowered into the stream to an extent sufficient to avoid standing waves on the downstream side. This problem has received much attention in the past due to its bearing on hydroplanes and sea-plane floats. The scope of existing theories was discussed by Southwell & Vaisey (*loc. cit.*), who also treated an example by relaxation methods. They took $\beta = 30°$, and assumed the same initial conditions as in their sluice-gate

example. Their solution shows that the free surface curves very sharply just below the trailing edge B, but beyond this region follows the curve obtained in the previous example (figure 3).

To account for the region near B, we may use the solution of the problem indicated in figure 2(*c*). This was included in the series of jet problems solved by Mises (1917); but, as in the example previously mentioned, he did not give an expression for the free surface. It can be shown without difficulty, however, that the intrinsic equation of the surface is

$$l = \frac{2d}{\pi} \operatorname{logsec}\left(\frac{\theta+\beta}{2\beta/\pi}\right),$$

where l denotes the length of the arc. Hence, for $\beta = 30^\circ$, we find in the usual way that

$$\frac{y}{d} = 1 + \frac{6}{\pi}\left[\frac{1}{\sqrt{3}} \tanh^{-1}\left(\frac{2\sin\theta}{\sqrt{3}}\right) - \sin\theta\right], \tag{4.1}$$

$$= 1{\cdot}229 \quad \text{for} \quad \theta = -30^\circ.$$

The curves obtained from (2.3) and (4.1) are suitably linked at a point where $\theta = -20^\circ$. In the example treated by Southwell & Vaisey, this procedure leads to the value 0·777 for the contraction ratio. The same value is found from the coordinates given in their figure 26. The value in the absence of gravity is, from (4.1), $1/1{\cdot}229 = 0{\cdot}814$. For a refinement of the method, the solution of the problem in figure 2(*d*) may be used instead of (4.1).

5. Experimental tests

While in no respect being intended as a complete investigation, the following experiments serve to illustrate some of the matters considered in the preceding sections of this paper. The experiments were carried out in a horizontal channel previously used in the work of Binnie, Davies & Orkney (1955), whose paper can be consulted for full details of the equipment. After the completion of these authors' experiments, the wooden contraction connecting the channel with the supply tank was modified, with the result that uniform subcritical flow could be obtained at higher Froude numbers than before. The channel was 14 in. wide and 8 ft. long, with glass walls about 12 in. high. When necessary, the stream could be held up by means of an adjustable sharp-crested weir at the downstream end; but otherwise it fell freely into a sump after leaving the channel. A movable gantry supported a point gauge and Pitot tube, which provided accurate measurements of the stream depth and total head. Froude numbers were calculated from the formula $F^2 = 2(\text{total head/depth} - 1)$. The water supply was controlled in such a way that the flow rate Q was independent of any obstruction in the channel. This feature assumes significance when the theory of §2 is brought to bear on the experimental observations. The description of the experiments is suitably divided into three parts, as follows,

(i) *Experiments in which the obstacle was fixed*

A rectangular brass plate was contructed with a width slightly less than that of the channel. It was suspended from a horizontal axle mounted above the channel at about 1 ft. from the upstream end, so that it could be swung down broadside to the stream. A sharp edge was machined on the bottom of the plate, and the small gaps between the sides and the walls of the channel were made water-tight with rubber sleeving. Struts attached to the rear face of the plate held it in position at any desired inclination.

In the first experiment, the position of the plate was gradually adjusted until the bottom edge was brought into contact with the surface of a uniform subcritical stream. A large disturbance was always observed as soon as contact was made, provided the Froude number of the undisturbed stream was not too small. An appreciable increase in depth occurred on the upstream side, and a zone of eddying water was formed immediately in front on the obstacle. The latter effect evidently prevented the formation of a stagnation point in the manner indicated by figure 4. When steady conditions were resumed, the obstacle was well immersed in the stream

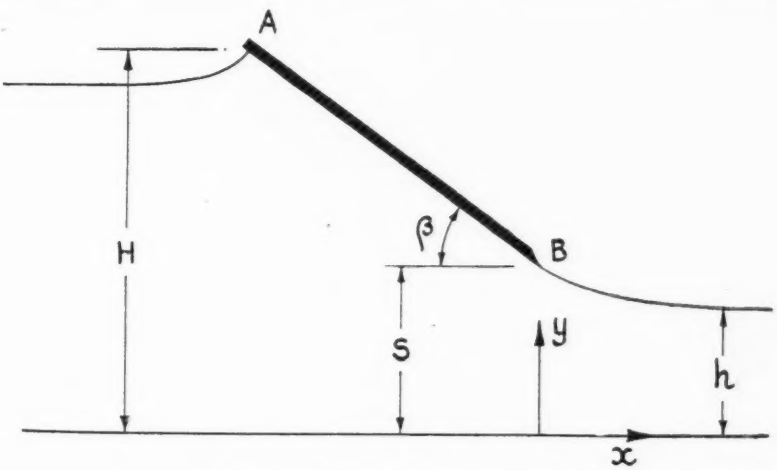

Figure 4. Side elevation of planing surface.

The result on the downstream side varied in character according to the initial Froude number and the inclination of the plate. If the Froude number was fairly small, say less than 0·3, and the plate sloped backwards as in figure 4, a stationary wave-train appeared, its surface being everywhere smooth. At rather higher Froude numbers the waves were larger both in amplitude and length, and the leading wave broke. At a Froude number about 0·7 and with the plate inclined slightly forward, a wave-train appeared immediately after contact but was then swept away, leaving the stream in a uniform supercritical state. The wave-train could be held in place, however, by slightly raising the weir at the channel exit.

The effects of lowering the plate further into the stream are most easily described in reverse, that is, we recount the results of gradually lifting the plate backwards from a vertical position as in figure 1. The adjustments to the plate were made slowly enough for the flow to approximate the steady state appropriate to each stage, and the weir was kept out of action. As the plate was raised, the water level fell upstream and rose downstream, so that the respective Froude numbers increased and decreased. Eventually a wave appeared near the end of the channel and moved upstream, thus causing other waves to form behind it. The leading wave then came to rest just behind the obstacle, and broke at its crest. This exemplified the type of weak undular bore (hydraulic jump) discussed theoretically by Benjamin & Lighthill (1954). By comparing the results of several experiments like this one, the Froude number at which the bore first occurred was found to vary with the depth of the stream. The critical value was about 1·5 for a depth of about 2·5 in., and increased for shallower streams. When the weir was not in use, the bore clearly resulted from the action of friction alone. By raising the weir it could, of course, be made to form at much higher Froude numbers. If the plate was lifted a little further, the turbulent zone at the crest of the leading wave became smaller, and in a few of the tests it vanished entirely. At this stage, however, some sort of instability evidently occurred, for the water level upstream began to rise and fall periodically, while the wave-train downstream began to oscillate longitudinally. The oscillations usually increased in amplitude until the surface of the water suddenly fell away from the bottom of the plate, whereupon the flow became uniform.

According to the theory of §2, a uniform supercritical stream cannot be formed by the action of an obstacle unless $F > 1{\cdot}25$, since a wave-train is bound to result from any attempt to reduce F below this value. The experiments indicated that, owing to the formation of bores which is not considered in the theory, the value of of F at which waves first appear is in practice somewhat higher than the theoretical limit. Nevertheless, when waves appear for $F > 1{\cdot}25$, a significant amount of energy must be dissipated in the bore; whereas in the range $1 < F < 1{\cdot}25$, a minute amount of dissipation, however small, is sufficient to precipitate a wave-train (see Benjamin & Lighthill, p. 452). It seems likely, therefore, that if measures were taken to reduce frictional effects and so inhibit the formation of a bore (by boundary layer suction, say), the critical value of F could be lowered, but could never be reduced below 1·25.

(ii) *Experiments in which the wave resistance was specified*

To obviate the confusing oscillations observed in the foregoing experiments, the following device was employed. As before, a planing plate was supported from a horizontal axle broadside to the stream. This time, however, the plate was delicately counter-balanced, and a small clearance was left open between each of its sides and the adjacent channel wall. The whole apparatus was of light construction, and the friction of

the support was extremely small; consequently a light finger-touch was sufficient to bring the bottom of the plate into contact with the stream. The plate could be immersed to any desired extent by loading the plate with suitable weights; hence it was a simple matter to estimate the horizontal force exerted against the stream. Disturbances arising from the sides of the plate tended to spoil the two-dimensional character of the flow, but were small enough to be unimportant.

By allowing the obstacle freedom of movement in this way, the resistance which it experienced on immersion was made independent of small changes in the level of the stream. This property was, of course, not possessed by the fixed obstacle in the previous experiments, and its absence then was evidently responsible for the instability accompanying slight immersions. No oscillation was observed with the second device in use.

A number of experiments were made in which the resistance was increased gradually from zero by the addition of weights to the plate. The waves first to appear were very small in amplitude, and their length λ was found to be in good agreement with the usual formula

$$F_0^2 = \frac{\lambda}{2\pi h_0} \tanh \frac{2\pi h_0}{\lambda}, \tag{5.1}$$

where h_0 and F_0 are the depth and Froude number upstream. The amplitude of the waves and the wavelength both became larger as the resistance was increased, although the proportional increase in the wavelength was quite small. Eventually the leading wave broke.

The reduction in the quantity S just sufficient to produce breaking waves was estimated for various values of F_0. These estimates were found to agree fairly well with the theoretical results of De (1955), the method of comparison being as follows. If the total drag on the obstacle is M grams weight, the reduction in S is obviously $S^* = Mg/(\rho b)$, where b is the breadth of the channel. In presenting his numerical results, De considers a dimensionless quantity $\mathbf{s} = S/S_c$, where S_c is the value of S for a critical stream with the given flow rate Q. It can easily be shown that

$$S_c = \tfrac{3}{2} g h_0^2 F_0^{4/3}. \tag{5.2}$$

Hence we have, for the reduction in $\mathbf{s}$,

$$\mathbf{s}^* = \frac{2MF_0^{-4/3}}{3\rho h_0^2 b}. \tag{5.3}$$

After specifying F_0, the required theoretical value of S^* can be measured on figure 2 in De's paper. Advantage was taken, however, of an enlarged and more detailed version of this figure kindly made available to the author. A typical set of measurements, made when the leading wave was on the point of breaking, was $h_0 = 14{\cdot}7$ cm, $F_0 = 0{\cdot}701$ and $M = 52$ gm. In addition we had $b = 35{\cdot}6$ cm and $\rho = 1$ gm/cm^3, and with these values (5.3) gives $\mathbf{s}^* = 0{\cdot}0072$. The value of $\mathbf{s}^*$ estimated from De's chart was $0{\cdot}0079$. The slight deficiency of the experimental estimate, which is a common feature in all similar tests, may have been due to the well-known fact that in practice

stationary waves break before their height reaches the theoretical limit. For the conditions quoted here the wavelength of breaking waves was estimated to be roughly 50 cm. The wave-number $2\pi h_0/\lambda$ was therefore about 1·8, which agrees fairly closely with the value indicated on the chart.

(iii) *Measurements of the contraction ratio for a sluice-gate*

These measurements were taken in order to check the theoretical values derived in § 3. The brass plate used in the first group of experiments was fixed in a vertical position, and careful adjustments were made to insure that the bottom edge was strictly horizontal. The opening s was 3·57 in. for one series of tests, and 1·02 in. for another. In each series, readings of the total head and depth were taken in mid-stream at a distance about $4{\cdot}5s$ downstream from the sluice. The value of H was varied over as wide a range as possible by adjusting the flow rate. The maximum useful value of H was that at which the water level in front of the sluice rose to the top of the channel walls. At the minimum value a bore formed on the downstream side.

Experimental values of the contraction ratio h/s are plotted as a function of s/H in figure 5, which includes the theoretical curve according to § 3.

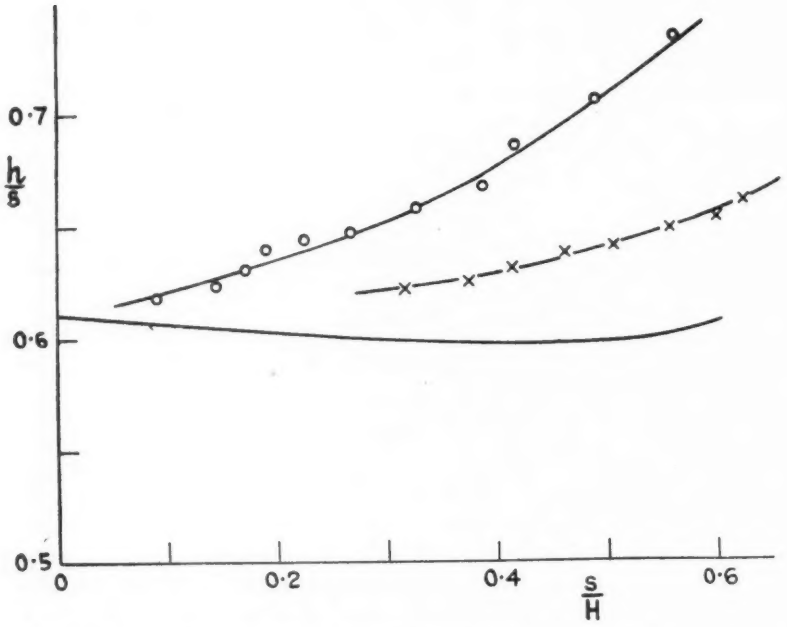

Figure 5. Comparison between theoretical values of contraction ratio (————) and experimental values for sluice-openings of 1·02 in. (——○——) and 3·57 in. (—— × ——).

Both series of tests specified above are represented in the figure. The two experimental curves are seen to lie above the theoretical curve, the discrepancy being larger for the smaller value of s. The three curves appear to converge for small values of s/H, that is, when the downstream Froude number is large. At first sight figure 5 tends to exaggerate the influence of friction on the flow; but the following interpetation casts a more favourable light on the comparison between theory and experiment.

Following the usual procedure in hydraulic experiments, traces of colouring matter were placed in the stream and their movements observed. In this way the flow-pattern was seen to be approximately as the theory predicts, except in an eddying region near the stagnation point and in the boundary layer on the channel bottom—which was apparently always in a laminar state in the vicinity of the sluice. The boundary layer on the face of the sluice appeared to have only local importance, probably because the velocity is small over most of this region. Let us therefore consider that the discharge under the sluice is affected by friction only in as far as the effective opening is reduced to a value $s-\delta$, where δ is a quantity roughly the same as the thickness of the boundary layer. The depth downstream is similarly reduced; hence the discrepancy Δ in the contraction ratio is approximately proportional to δ/s. If we now tentatively assume that s determines the length scale to be associated with the growth of the boundary layer, it follows that Δ is proportional to the Reynolds number based on the length s. Consequently, for two experiments at the same Froude number, we have $\Delta_1/\Delta_2 = (s_2/s_1)^{3/4}$. With $s_1 = 1{\cdot}02$ and $s_2 = 3{\cdot}57$, the values in inches for the tests in question, this ratio is 2·6. The discrepancy in s/H varies in the same way. Examination of figure 5 shows that the experimental values are roughly in agreement with this result over most of the range of s/H. The extent of the agreement is in fact quite surprising in view of the very rough and ready nature of the above calculation. By observing the drop in total head as the Pitot tube was brought near the channel bottom, the thickness of the boundary layer near the wider sluice ($s = 3{\cdot}57$ in.) was estimated to be of the order of $\frac{1}{4}$ in. Note that the corrections necessary to bring the experimental results into agreement with the theory are also of this order.

These three groups of experiments amply confirm the theory's usefulness in qualitatively assessing the flow. They suggest moreover that if allowance could be made for the boundary layer on the channel bottom, the theory would give accurate predictions of the drag on an obstacle and other physical quantities. The eddying zone in front of the obstacle was the most noticeable effect of friction in the experiments, but it appeared to have little influence on the flow downstream. Very complex phenomena, due to surface tension and shedding of the boundary layer, were to be expected in the region where the free surface first springs clear of the obstacle; but they did not appear to affect the overall characteristics of the flow.

Further experimental work is desirable, especially on the boundary layer. For instance, each of a series of measurements as in (iii) might

usefully be accompanied by careful estimates of the boundary layer thickness. This procedure might establish a close agreement with the theory of §2. Further, the method used in (ii) could probably be refined a good deal, and might profitably be extended to measurements of wave resistance over the entire range of De's theoretical results.

References

Addison, H. 1938 *J. Inst. Civ. Eng.* **9,** 53.

Benjamin, T. B. & Lighthill, M. H. 1954 *Proc. Roy. Soc.* A **224,** 448.

Binnie, A. M. 1949 *Proc. Roy. Soc.* A **197,** 545.

Binnie, A. M. 1952 *Quart. J. Mech. Appl. Math.* **5,** 395.

Binnie, A. M., Davies, P. A. O. L. & Orkney, J. C. 1955 *Proc. Roy. Soc.* A **230,** 225.

De, S. C. 1955 *Proc. Camb. Phil. Soc.* **51,** 713.

Friedrichs, K. O. & Hyers, D. H. 1954 *Comm. Pure Appl. Math.* **7,** 517.

Kelvin, Lord 1886 *Phil. Mag.* (5) **2,** 445; *Collected Papers* **4,** 275. Cambridge University Press.

Lamb, H. 1932 *Hydrodynamics,* 6th ed. Cambridge University Press.

McCowan, J. 1894 *Phil. Mag.* (5) **38,** 351.

Mises, R. v. 1917 *Z. ver. Deuts. Ing.* **61,** 447.

Pajer, H. 1937 *Z. angew. Math. Mech.* **17,** 259.

Rayleigh, Lord 1876 a *Phil. Mag.* (5) **1,** 257; *Collected Papers* **1,** 251. Cambridge University Press.

Rayleigh, Lord 1876 b *Phil. Mag.* (5) **2,** 441; *Collected Papers* **1,** 297. Cambridge University Press.

Southwell, R. V. & Vaisey, G. 1946 *Phil. Trans.* A **240,** 117.